Negative microfilm
received from university

61-6312

ALBRECHT, Robert William, 1935-
THE MEASUREMENT OF DYNAMIC NUCLEAR REACTOR PARAMETERS BY METHODS OF STOCHASTIC PROCESSES.

University of Michigan, Ph.D., 1961
Engineering, nuclear

University Microfilms, Inc., Ann Arbor, Michigan

THE MEASUREMENT OF DYNAMIC NUCLEAR REACTOR PARAMETERS BY METHODS OF STOCHASTIC PROCESSES

Robert William Albrecht

A dissertation submitted in partial fulfillment
of the requirements for the degree of
Doctor of Philosophy in the
University of Michigan
1961

Doctoral Committee:

Professor William Kerr, Chairman
Professor Donald Darling
Professor Henry Gomberg
Assistant Professor Geza Gyorey
Associate Professor John King
Professor Richard K. Osborn

ACKNOWLEDGMENTS

The guidance and assistance given the author by members of his doctoral committee was very helpful. The author is especially grateful to Professor William Kerr, chairman of the committee, who gave freely of his time and energy in all phases of this effort.

Aid in the understanding of the theoretical aspects of this effort was given by Professors R. K. Osborn and D. Darling.

Many people participated in the execution of the experiment. N. Barnett made the experiment possible by lending the author the tape recorder which is normally in his use. W. Dunbar and the members of the reactor operating staff were very cooperative throughout this experiment which required special effort on their part. P. Herman gave advice freely on the instrumentation requirements.

Assistance with the analytical work was given by the computing center staff, especially Greg Smith who worked with the author on the nonlinear estimation program.

For all of the above aid the author expresses his appreciation.

The opportunity for the author to participate in the Nuclear Engineering Program at the University of Michigan would not have been possible without the aid of three years financial support by the Oak Ridge Institute of Nuclear Studies. For this support the author is most grateful.

TABLE OF CONTENTS

		Page
ACKNOWLEDGMENT		ii
LIST OF FIGURES		v
LIST OF TABLES		vii
ABSTRACT		viii
I.	INTRODUCTION	1
	A. Introductory Remarks	1
	B. Organization of Text	3
II.	STOCHASTIC PROCESS THEORY	5
	A. Definition and Notation	5
	B. Relationships Between Stochastic Signals in Linear Systems	7
	C. White Noise	9
	D. System Driven by White Noise	11
	E. Relationship Between Variance to Mean Ratio Over an Interval and Auto-correlation Function	11
III.	MATHEMATICAL MODEL	14
	A. System Approach	14
	B. Physical Approach	22
IV.	EQUIPMENT	30
	A. Experimental Setup	30
	B. Description of Equipment	30
	C. Operating Characteristics	44
V.	EXPERIMENT	45
	A. Experimental Conditions	45
	B. Equipment Limitations	52
	C. Experimental Procedure	60
VI.	DATA ANALYSIS	66
	A. Data Handling	66
	B. Estimation	68
VII.	RESULTS	85
	A. Experimental Results	85
	B. Mathematical Model (General)	90

TABLE OF CONTENTS CONT'D

	Page
C. Mathematical Model (2-group)	93
D. Presentation of Results	95
E. Theory vs. Experiment	103
VIII. CONCLUSIONS	106
A. Introduction	106
B. Comparison of Conclusions with Preceding Authors	106
C. Independent Conclusions	108
D. Relevance to Future Experiments	109
APPENDICES	111
BIBLIOGRAPHY	120

LIST OF FIGURES

Figure		Page
2.1	Block Diagram of Linear System	7
3.1	Noise Source Only Signal and Noise	16
3.2	Noise Measurement Block Diagram	17
3.3	Possible Chains for an Accidental Pair of Counts	23
3.4	Possible Events Leading Up to a Coupled Pair of Counts	25
4.1	Data Taking Configuration	31
4.2	Data Transcription Configuration	32
4.3	Core Configuration for BF_3 Tube Experiments	33
4.4	Core Configuration for Fission Chamber Experiments	33
4.5	Circuit Diagram of Pulse Shaper	37
4.6	Simplified Block Diagram of Gate Scaler	39
4.7	Information Converter Parallel "Staircase" to Serial "Digital"	41
4.8	Power Supply for Converter	42
5.1	Gamma Background Measurement	49
5.2	Relationship of True Events to Registered Events in Paralyzable and Non-paralyzable Counters	53
5.3	Loss in Mean Count Rate Due to Dead Time Losses for Paralyzable and Non-paralyzable Cases	55
5.4	Ratio of Observed to True Variance Verses $\overline{N}\rho$ for Paralyzable and Non-paralyzable Counter	55
5.5	Ratio of Measured to True Variance to Mean Ratio Versus $\overline{N}\rho$	57

LIST OF FIGURES CONT'D

Figure		Page
5.6	Wow and Flutter Measurement on Ampex 307 Tape Recorder	59
5.7	Differential Rod Calibration	62
5.8	Integral Rod Calibration	63
6.1	Observation Space	69
6.2	Parameter Space	70
6.3	Observation Space	71
6.4	Observation Space	72
6.5	Parameter Space	72
6.6	Sum of Squares vs. Θ	73
6.7	Observation Space	75
6.8	Parameter Space	76
6.9	Linearized Parameter Space	76
6.10	Parametric Curves for $\phi^1(\gamma)$; $1 \leq \alpha \leq 350$	82
6.11	Parametric Curves for $\phi^1(\gamma)$; $0.1 \leq \alpha \leq 2$	83
7.1	Data and Curve Fit: Run BF_3-1	86
7.2	Data and Curve Fit: Run BF_3-2	87
7.3	Data and Curve Fit: Run BF_3-3	88
7.4	Data and Curve Fit: Run Fission Chamber	89
7.5	Comparison of BF_3 Experiments Fitted Curves	91
7.6	Confidence Contours BF_3-1	96
7.7	Confidence Contours BF_3-2	97
7.8	Confidence Contours BF_3-3	98

LIST OF TABLES

Table		Page
7.1	Physical Group Constants.....	99
7.2	Reduced Group Constants.....	99
7.3	Results BF_3-1.....	100
7.4	Results BF_3-2.....	101
7.5	Results BF_3-3.....	102

ABSTRACT

Mathematical models are developed for the statistic variance/mean of the number of neutrons detected in an interval of time in a point, unloaded reactor. An experiment which measured variance/mean for counting times between one millisecond and ten seconds was performed. Comparisons between the mathematical model and the experiment are made.

The experiment was performed by tape recording impulses from neutrons detected and transcribing the data to IBM cards using an automatic counting and card punching system. An IBM 704 was used for data reduction and for fitting the model to the experimental data in order to compare the measured parameters with parameters measured using other techniques.

The results show that the delayed neutron contribution to the measured variance/mean is significant, that these delayed neutron effects should be accounted for when using this method for determination of prompt neutron lifetime, and that these techniques may be used to measure dynamic reactor parameters without an external perturbation.

This experiment measured the prompt neutron lifetime of the Ford Reactor. It was found that the value agreed with measurements made using other techniques on similar reactors. This experiment is the first reactor noise experiment to be performed in such a way that delayed neutrons make a significant contribution to the measured quantities.

I. INTRODUCTION

A. Introductory Remarks

When a nuclear reactor is operating in steady-state its neutron population is not constant. When observed with a sensitive instrument, the neutron population is seen to fluctuate about some average value. These fluctuations reflect some of the characteristics of the reactor. In particular, the dynamic characteristics of the reactor are reflected in these fluctuations. This is as it should be since fluctuations are indeed dynamic phenomena.

Careful measurements of quantities which describe these fluctuations in neutron population should yield information about the dynamic reactor parameters which control the fluctuations. Obviously one must first formulate some mathematical model for fluctuations in terms of reactor parameters so that one can know what to expect from his measurements, over what regions to measure, and what is the required reactor configuration to yield optimum results.

One must also be sure to know how to distinguish "signal" from "noise." That is, when one is measuring in a reactor, the counting system may produce electrical impulses which are not caused by the detection of reactor neutrons and are not distinguishable from reactor neutrons. Possible sources of these impulses are source neutrons, gamma rays and electrical transients. It therefore becomes necessary for the theory to take the noise into account since it may well be a substantial part of the measured fluctuations.

Since flucuations in neutron population are by no means regular fluctuations such as a sine wave, it is necessary to take a large amount of data in order to distinguish the contribution of dynamic parameters with any accuracy. This dictates that a statistic which is amenable to data collection and data processing by automatic techniques should be measured.

In the following, mathematical models will be developed which describe neutron population fluctuations, the difference between "signal" and "noise" will be delineated, and an experiment which measures these fluctuations, and thus dynamic parameters, will be described.

One might ask, "Why measure dynamic parameters by stochastic process techniques?"

The answers to this question are many. Some of the most important reasons for making stochastic process measurements of nuclear reactor dynamic parameters are the disadvantages of making the measurements by other techniques. Other techniques employ some method of introducing a perturbation into the reactor and observing the resultant response of the mean neutron population. Disadvantages of these techniques are that a perturbation must be introduced which inevitably alters the dynamic parameters, the perturbation may have to be large so that the mean neutron population is easily observed over the fluctuations and may thereby drive the reactor beyond the applicability of the mathematical model, it may be very difficult to insert into the reactor the required perturbing mechanism, or it may be dangerous to drive the reactor through transients because of thermal shock or other possible damage.

Of course other, and more direct, reasons for making stochastic process measurements exist. One of these is to compare mathematical models with experiment. This is important since only a few stochastic process measurements have been made to date and the theoretical-experimental comparisons are as yet imcomplete. To the author's knowledge no experiments have, as yet, been performed for correlation times such that delayed neutrons are important.

In the following, delayed neutrons will be included in the mathematical model, measurements will be made over times for which delayed neutrons are important, and comparisons will be made between the observed and predicted effect of delayed neutrons.

Investigators who have preceded the author in this area have made fundamental contributions to the theory and experimental techniques of stochastic processes. Feynman, DeHoffman, and Serber[11] used these techniques to measure the distributions of the number of neutrons from fission. Luckow[16] measured prompt neutron lifetimes by measuring fluctuations as did Cohn.[8] Velez[23,24] developed an equation for the autocorrelation function and attempted measurements on the Ford Nuclear Reactor. Theoretical work in this area was done by Feynman, DeHoffman, and Serber[11], Brownrigg and Littler[7], Frisch and Littler[12], Feiner, Frost and Hurwitz[10], Moore[17,18,19] Bennett[1], Courant and Wallace[9], and several others.

B. Organization of Text

Chapters II and III deal with the development of the mathematical model for the statistic of interest here; the ratio of the variance

to mean number of neutron counts over an interval of time. Chapter III applies this theory to determining the mathematical model for stochastic processes in a nuclear reactor.

Chapters IV and V describe the experiment which was performed to test the models. Chapter IV describes the equipment which was used. Chapter V describes the experimental technique used to make the measurements.

Chapter VI describes the techniques employed to process and analyze the data.

Chapter VII discusses the results of the experiment with respect to the mathematical model.

Chapter VIII discusses the results and formulates conclusions based on these results.

The original contributions in this dissertation are contained mainly in the experiment. Here, the effects of delayed neutrons on the stochastic process measurements are shown clearly for the first time.

Some credit is also claimed for deriving the mathematical model in a way which is, in the author's opinion, more illuminating than those derivations which appear in the literature.

The techniques of nonlinear estimation developed for application to this problem represent a more powerful method of analyzing the results than has been used before.

II. STOCHASTIC PROCESS THEORY

This chapter will be devoted to illuminating the concepts of stochastic process theory. Several statistical functions will be defined. Notation will be adopted for these statistical functions which will be used consistently hereafter. The fundamental relationships between these statistical functions will be demonstrated. These relationships will be exploited to show the connection between stochastic processes and general system equations. For a more detailed description of this material see Laning and Battin[15] or Newton et al.[20]

A. Definition and Notation

In the following, consider $x(t)$ and $y(t)$ to be fluctuating functions of time and $x_i(t)$ and $y_i(t)$ to be the i-th member of an ensemble of fluctuating functions of time.

1. Mean of x(t)

The time average of $x(t) \equiv \overline{x(t)}$

$$= \lim_{T\to\infty} \frac{1}{2T} \int_{-T}^{T} x(t)\,dt \tag{2.1}$$

The ensemble average of $x(t) \equiv \overline{\overline{x(t)}}$

$$= \lim_{N\to\infty} \frac{1}{N} \sum_{i=1}^{N} x_i(t) \tag{2.2}$$

2. Mean Square Value of x(t)

The time average mean square value of $x(t) \equiv \overline{x^2(t)}$

$$= \lim_{T\to\infty} \frac{1}{2T} \int_{-T}^{T} x^2(t)\,dt \tag{2.3}$$

Ensemble average mean square value of $x(t) \equiv \overline{\overline{x^2(t)}}$

$$= \lim_{N\to\infty} \frac{1}{N} \sum_{i=1}^{N} x_i^2(t) \tag{2.4}$$

3. Variance of x(t)

The time average variance of $x(t) \equiv \mathrm{var}(x(t))$

$$= \overline{x^2(t)} - \overline{x(t)}^2 \tag{2.5}$$

The ensemble average variance of $x(t) \equiv \overline{\overline{\mathrm{var}}}(x(t))$

$$= \overline{\overline{x^2(t)}} - \overline{\overline{x(t)}}^2 \tag{2.6}$$

4. Autocorrelation Function of x(t)

The time averaged autocorrelation function of $x(t) \equiv \psi_{xx}(\tau)$

$$= \overline{x(t)x(t+\tau)} = \lim_{T\to\infty} \frac{1}{2T} \int_{-T}^{T} x(t)x(t+\tau)\,dt \tag{2.7}$$

The ensemble average autocorrelation function of $x(t) \equiv \psi_{xx}(t_1,\tau)$

$$= \overline{\overline{x(t_1)x(t_1+\tau)}} = \lim_{N\to\infty} \frac{1}{N} \sum_{i=1}^{N} x_i(t_1)x_i(t_1+\tau) \tag{2.8}$$

5. Cross Correlation Function of x(t) and y(t)

The time averaged cross correlation function of x(t) and y(t)

$\equiv \psi_{xy}(\tau)$

$$= \overline{x(t)y(t+\tau)} = \lim_{T\to\infty} \frac{1}{2T} \int_{-T}^{T} x(t)y(t+\tau)\,dt \tag{2.9}$$

The ensemble average cross correlation function of x(t) and y(t)

$\equiv \psi_{xy}(t_1,\tau)$

$$= \overline{\overline{x(t_1)y(t_1+\tau)}} = \lim_{N\to\infty} \frac{1}{N} \sum_{i=1}^{N} x_i(t_1)y_i(t_1+\tau) \tag{2.10}$$

6. Power Density Spectrum

It is useful to introduce a frequency function which is defined as $1/2\pi$ times the Fourier transform of the time-average correlation function in order to ultimately deal with transfer functions in the frequency domain. It can be shown[15,20] that this frequency function will be the power density spectrum. That is, it will be a function which will measure the power density of the signal as a function of frequency. The integral of this power density spectrum over all frequencies will then be the total power in the signal.

The power density spectrum corresponding to the time-averaged correlation function is denoted Ψ_{xx}, Ψ_{xy}, or Ψ_{yy} depending on which correlation function ψ_{xx}, ψ_{xy}, or ψ_{yy} is being considered.

For example, the power density spectrum corresponding to the cross correlation function defined in (2.9) is

$$\Psi_{xy}(\omega) = \frac{1}{2\pi}\int_{-\infty}^{\infty} \psi_{xy}(\tau) e^{-i\omega\tau} d\tau \qquad (2.11)$$

B. Relationships Between Stochastic Signals in Linear Systems

Consider a linear system which is described by a Green's function $g(t)$, and has a driving function $x(t)$ and a response $y(t)$. This system can be represented by the block diagram of Figure 2.1.

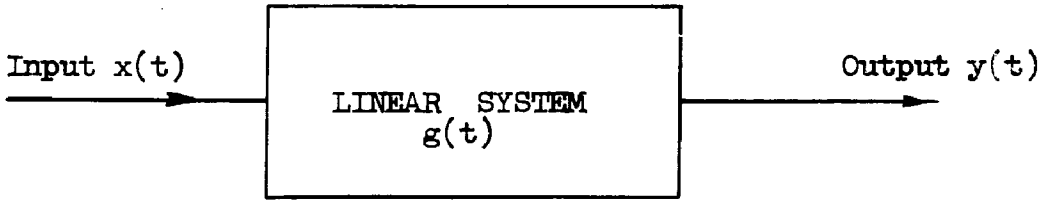


Figure 2.1 Block Diagram of Linear System

We seek the relationship between the autocorrelation function of the input and the autocorrelation function of the output. The relation between the input and the output is given by the convolution integral as

$$y(t) = \int_{-\infty}^{\infty} g(t_1) \times (t - t_1)\, dt_1 \tag{2.12}$$

and similarly,

$$y(t+\tau) = \int_{-\infty}^{\infty} g(t_2) \times (t + \tau - t_2)\, dt_2 \tag{2.13}$$

These two expressions can be substituted into the definition of the autocorrelation function to obtain

$$\begin{aligned} \psi_{yy}(\tau) &= \lim_{T\to\infty} \frac{1}{2T} \int_{-T}^{T} y(t)\, y(t+\tau)\, dt \\ &= \lim_{T\to\infty} \frac{1}{2T} \int_{-T}^{T} dt \int_{-\infty}^{\infty} dt_1\, g(t_1) \times (t - t_1) \int_{-\infty}^{\infty} dt_2\, g(t_2) \times (t + \tau - t_2) \end{aligned} \tag{2.14}$$

By interchanging the order of the limit process and the other integrations so that we integrate with respect to t first, we get

$$\psi_{yy}(\tau) = \int_{-\infty}^{\infty} dt_1\, g(t_1) \int_{-\infty}^{\infty} dt_2\, g(t_2) \lim_{T\to\infty} \frac{1}{2T} \int_{-T}^{T} dt \times (t - t_1) \times (t + \tau - t_2) \tag{2.15}$$

Recalling the definition of autocorrelation function, Equation (2.15) is written

$$\psi_{yy}(\tau) = \int_{-\infty}^{\infty} dt_1\, g(t_1) \int_{-\infty}^{\infty} dt_2\, g(t_2)\, \psi_{xx}(\tau + t_1 - t_2) \tag{2.16}$$

This is the relation between the autocorrelation function of the output and the autocorrelation function of the input.

In a similar way, an expression for the cross correlation function between input and output signals may be derived. Substitute the equation

$$y(t+\tau)=\int_{-\infty}^{\infty} dt_2\, g(t_2)\, x(t+\tau-t_2) \tag{2.17}$$

into the definition of cross correlation function,

$$\psi_{xy}(\tau)=\lim_{T\to\infty}\frac{1}{2T}\int_{-T}^{T} dt\, x(t)\, y(t+\tau) \tag{2.18}$$

to obtain

$$\psi_{xy}(\tau)=\lim_{T\to\infty}\frac{1}{2T}\int_{-T}^{T} dt\, x(t)\int_{-\infty}^{\infty} dt_2\, g(t_2)\, x(t+\tau-t_2) \tag{2.19}$$

Again interchange integration and the limit process to get

$$\psi_{xy}(\tau)=\int_{-\infty}^{\infty} dt_2\, g(t_2)\,\psi_{xx}(\tau-t_2) \tag{2.20}$$

The relation between the input and output power density spectra may be found by Fourier transforming both sides of the relationship between input and output autocorrelation functions. This leads to

$$\int_{-\infty}^{\infty}\psi_{yy}(\tau)e^{-i\omega\tau}d\tau=\int_{-\infty}^{\infty}e^{-i\omega\tau}d\tau\int_{-\infty}^{\infty}g(t_1)dt_1\int_{-\infty}^{\infty}g(t_2)\psi_{xx}(\tau+t_1-t_2)dt_2 \tag{2.21}$$

The order of integration may be changed and the arguments of the exponentials adjusted to give

$$\int_{-\infty}^{\infty}\psi_{yy}(\tau)e^{-i\omega\tau}d\tau=\int_{-\infty}^{\infty}g(t_1)e^{i\omega t_1}dt_1\int_{-\infty}^{\infty}g(t_2)e^{-i\omega t_2}dt_2\int_{-\infty}^{\infty}e^{-i\omega(\tau+t_1-t_2)}\psi_{xx}(\tau+t_1-t_2)d\tau \tag{2.22}$$

The system's transfer function is defined as the Fourier transform of the Green's function and denoted $T(i\omega)$. Substituting this into

Equation (2.22) and recalling the definition of the power density spectrum, Equation (2.22) may be written

$$\Psi_{yy}(\omega) = T(i\omega)T(-i\omega)\Psi_{xx}(\omega) \tag{2.23}$$

C. White Noise

A random process, x(t), possessing a constant power density spectrum is referred to as white noise. The physical origin of this term is in the concept of white light: a light that possesses all frequencies in equal amounts.

If x(t) is such that

$$\overline{x(t)} = 0 \quad ; \qquad \Psi_{xx}(\lambda) = 0, \quad \lambda >> \lambda_o \tag{2.24}$$

then, the process x(t) can be considered to be white noise in a range of frequencies $0 < \omega \ll \frac{1}{\lambda_o}$.

In this case, the autocorrelation function for white noise can be approximated by a delta function,

$$\Psi_{xx}(\lambda) \approx C\delta(\lambda) \tag{2.25}$$

so that the power density spectrum can be found by Fourier transforming to be

$$\Psi_{xx}(\omega) = C \tag{2.26}$$

It should be noted that, in a strict sense, white noise is a physically unrealizable phenomenon since it is a random process having

an infinite average power. This follows from the fact that the total power is given by

$$\int_0^\infty \Psi_{xx}(\omega)d\omega = \Psi_{xx}(0)\int_0^\infty d\omega = \infty \qquad (2.27)$$

In spite of this fact, white noise is a useful concept both for certain theoretical purposes and as a practical approximation to noise of a very broad bandwidth. In many problems a noise spectrum may be known to be substantially constant over the frequency range of interest. When this is true, the use of a constant power density spectrum for all frequencies often simplifies mathematical manipulation without introducing significant inaccuracy in the result.

D. System Driven by White Noise

A system driven by white noise has a constant input power density spectrum, C, so that the output power density spectrum will be proportional to the square of the modulus of the transfer function. This follows from substituting C for $\Psi_{xx}(\omega)$ in Equation (2.23) to get

$$\Psi_{yy}(\omega) = C\,T(i\omega)\,T(-i\omega) \qquad (2.28)$$

E. Relationship Between Variance to Mean Ratio Over an Interval and Autocorrelation Function

In certain systems, of which a nuclear reactor is an example, it may be more feasible experimentally to measure the accumulated value of y(t), the output noise, over an interval than to measure either the autocorrelation function or power density spectrum directly. The ratio of the variance to mean of this accumulated random process for intervals

of length τ is related to the autocorrelation function and thus the power density spectrum of $y(t)$.

To derive this relationship, consider $y(t)$ to be a stationary stochastic signal. The variance of the integral of $y(t)$ over an interval of length τ will be related to its autocorrelation function. Let $x(\tau)$ be the integral of $y(t)$ over the interval τ. The relationship between $x(\tau)$ and $y(t)$ is

$$x(\tau) \equiv \int_0^\tau y(t)\,dt \tag{2.29}$$

According to relation (2.7) the autocorrelation function of $y(t)$ is written

$$\psi_{yy}(t_1 - t_2) = \overline{y(t_1)\,y(t_2)} \tag{2.30}$$

Integrals of this autocorrelation function are investigated over the triangle $0 \le t_1 < t_2$, $0 \le t_2 \le \tau$.

Integrating once,

$$\int_0^{t_2} \psi_{yy}(t_1 - t_2)\,dt_1 = \overline{y(t_2)\int_0^{t_2} y(t_1)\,dt_1} = \overline{y(t_2)\,x(t_2)} \tag{2.31}$$

Integrating again (by parts)

$$\int_0^{\tau}\int_0^{t_2} \psi_{yy}(t_1-t_2)\,dt_1\,dt_2 = \overline{\int_0^{\tau} y(t_2)\,x(t_2)\,dt_2}$$

$$= \overline{x^2(\tau)} - \frac{\overline{x^2(\tau)}}{2} \qquad (2.32)$$

$$= \frac{\overline{x^2(\tau)}}{2}$$

The ratio of the variance to the mean of $x(\tau)$ is the quantity which is measured in the experiment to follow. This quantity can be formed from Equation (2.32) yielding

$$\frac{Var}{Mean}(\tau) = \frac{\overline{x^2(\tau)} - \overline{x(\tau)}^2}{\overline{x(\tau)}} = -\overline{x(\tau)} + \frac{2}{\overline{x(\tau)}}\int_0^{\tau}\int_0^{\tau'} \psi_{yy}(\tau'')\,d\tau''\,d\tau' \qquad (2.33)$$

It is to be noted that the variance/mean over an interval measures accumulated correlation. That is, it is related to the double integral of the autocorrelation function and hence to the system equations through Equation (2.16).

III. MATHEMATICAL MODEL

The mathematical model used here for stochastic processes in nuclear reactors operating at steady state is based upon a point reactor model. Two approaches to the derivation of this mathematical model are presented here. One approach will be termed the "system approach" which will use the results of the previous section to derive the power spectral density, autocorrelation function, and count-rate variance for a nuclear reactor by operations upon the square of the modulus of the sub-critical reactor transfer function. The other approach to be discussed will be the "physical approach" in which details of the multiplying processes in the reactor are followed showing the mechanisms which give rise to correlation.

The validity of this model will be examined in relation to an experiment in Chapter VII.

A. System Approach

In Chapter II it was shown that a linear system being driven by a white noise source has an output power density spectrum proportional to the square of the modulus of the system transfer function. In the system approach to the problem of predicting the characteristics of reactor noise we assume that a reactor operating in steady state is a linear system driven by a white noise source.

1. White Noise Source

According to definition (2.24) a white noise driving force must be such that if $x(t)$ is the white noise source, then $\overline{x(t)} = 0$

and $\psi_{xx}(\lambda) = \overline{x(t)x(t+\lambda)} = 0$ for λ's greater than some λ_o which is $\ll \tau_o$ the correlation time of interest in the system.

The assumption of white noise is used in the noise analysis of many systems when it can be argued that the possible origins of the noise are characterized by the conditions above.

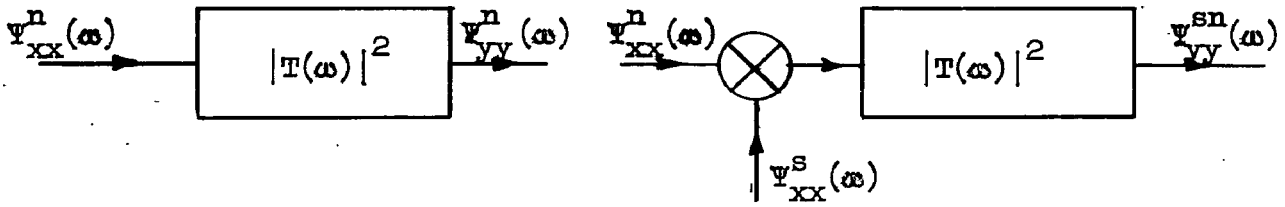
In a reactor, a possible origin of the noise is in the fluctuation of source neutrons from both external sources and the sources inherently existing in a reactor. Another possible source is in the fluctuations of the reactor parameters themselves.[17,18]

In the following, white noise will be assumed as the source noise for the derivation of the mathematical model by the system approach. The characteristics of the possible noise sources mentioned above are such that this assumption seems to be warranted.

It may be possible to investigate the character of the noise source by an experimental technique. By applying a known perturbation to the reactor and observing the output with and without this perturbation we may be able to gain information as to the characteristics of the inherent driving force.

For example, if $\Psi^{n}_{yy}(\omega)$ is the output power density spectrum due to the inerent noise alone and $\Psi^{sn}_{yy}(\omega)$ is the output power density spectrum due to signal plus noise (where signal is denoted $\Psi^{s}_{xx}(\omega)$ and the noise is $\Psi^{n}_{xx}(\omega)$. An experiment may be performed to measure $\Psi^{n}_{yy}(\omega)$ and $\Psi^{sn}_{yy}(\omega)$. Consider the systems depicted in Figure 3.1.

If the signal and the noise are uncorrelated, then



Noise Source Only Signal and Noise

Figure 3.1

$$\Psi^n_{yy}(\omega) = |T(\omega)|^2 \Psi^n_{xx}(\omega)$$

$$\Psi^{sn}_{yy}(\omega) = |T(\omega)|^2 \left[\Psi^n_{xx}(\omega) + \Psi^s_{xx}(\omega)\right] \tag{3.1}$$

so that, eliminating the transfer function

$$\Psi^{sn}_{yy}(\omega) = \Psi^n_{yy}(\omega)\left[1 + \frac{\Psi^s_{xx}(\omega)}{\Psi^n_{xx}(\omega)}\right] \tag{3.2}$$

$\Psi^{sn}_{yy}(\omega)$ and $\Psi^n_{yy}(\omega)$ are measured quantities and $\Psi^s_{xx}(\omega)$ is a known perturbation. Thus by performing the two experiments outlined above, one may be able to infer from the results the shape of the input noise power density spectrum, $\Psi^n_{xx}(\omega)$, and establish the shape of the unknown driving force.

2. Output Noise

A point, unloaded, nuclear reactor is now to be characterized by a linear system with a white noise driving force such that the input power density spectrum is a constant, $\Psi_{nn}(\omega) = C$. We can normalize the problem by assigning the value 1 to C.

In a measurement of the output noise from a reactor some of the neutrons which we measure may be source neutrons or other neutrons which have been previously characterized as part of the assumed white noise input. This effect is taken into account by assuming that some of the noise which is measured has not been operated on by the reactor transfer function. The system under consideration is shown in Figure 3.2 where n(t) is the assumed noise source, G(t) is the reactor's Green's Function, $y_s(t)$ is that portion of the noise which has been operated on by G(t), portions of n(t) are shown driving both output and input and y(t) is the measured output which includes both $y_s(t)$ and $n_2(t)$.

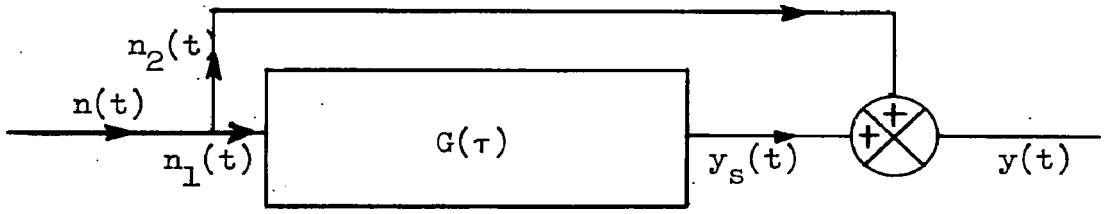


Figure 3.2 Noise Measurement Block Diagram.

It has been shown in Chapter II that the power density spectrum of the output noise of a linear system is proportional to the square of the modulus of the transfer function so that, in this case,

$$\Psi_{y_s y_s}(\omega) = \left|T(\omega)\right|^2 \Psi_{n_1 n_1}(\omega) \qquad (3.3)$$
$$= \left|T(\omega)\right|^2$$

since we have assumed $n_1(t)$ is white noise and $\Psi_{n_1 n_1}(\omega) = 1$.

The measured output, y(t), is equal to the sum $y_s(t) + n_2(t)$. It is then necessary to find the power density spectrum of y(t).

The autocorrelation function of y(t) may be written

$$\psi_{yy}(\tau) = \lim_{T\to\infty} \frac{1}{2T}\int_{-T}^{T} y(t)y(t+\tau)dt$$

$$= \lim_{T\to\infty} \frac{1}{2T}\int_{-T}^{T} (y_s(t)+n_2(t))(y_s(t+\tau)+n_2(t+\tau))dt \qquad (3.4)$$

$$= \lim_{T\to\infty} \frac{1}{2T}\int_{-T}^{T} y_s(t)y_s(t+\tau)dt + \lim_{T\to\infty} \frac{1}{2T}\int_{-T}^{T} n_2(t)n_2(t+\tau)dt$$

$$+ \lim_{T\to\infty} \frac{1}{2T}\int_{-T}^{T} n_2(t)y_s(t+\tau)dt + \lim_{T\to\infty} \frac{1}{2T}\int_{-T}^{T} y_s(t)n_2(t+\tau)dt$$

$$= \psi_{y_s y_s}(\tau) + \psi_{n_2 n_2}(\tau) + \psi_{n_2 y_s}(\tau) + \psi_{y_s n_2}(\tau)$$

The above equation shows that the autocorrelation function of y(t) is equal to the autocorrelation function of $y_s(t)$ plus the autocorrelation function of $n_2(t)$ plus the sum of the cross-correlation functions $\psi_{n_2 y_s}(\tau)$ and $\psi_{y_s n_2}(\tau)$.

If it is assumed that $n_2(t)$ and $y_s(t)$ are uncorrelated then

$$\Psi_{n_2 y_s}(\tau) = \lim_{T\to\infty} \frac{1}{2T}\int_{-T}^{T} n_2(t)\, y_s(t+\tau)\, dt$$

$$= \lim_{T\to\infty} \frac{1}{2T}\int_{-T}^{T} n_2(t)\, y_s(t)\, dt \qquad (3.5)$$

$$= \overline{n_2(t)}\ \ \overline{y_s(t)}$$

Since we have already assumed that $\overline{n_2(t)} = 0$, we see that $\Psi_{n_1 y_s}(\tau) = 0$. Likewise, $\Psi_{y_s n_2}(\tau) = 0$. Now Equation (3.4) becomes

$$\Psi_{yy}(\tau) = \Psi_{y_s y_s}(\tau) + \Psi_{n_2 n_2}(\tau) \qquad (3.6)$$

Taking the Fourier Transform, we see that

$$\Psi_{yy}(\omega) = \Psi_{y_s y_s}(\omega) + \Psi_{n_2 n_2}(\omega) \qquad (3.7)$$

And substituting for $\Psi_{n_2 n_2}(\omega)$ and $\Psi_{y_s y_s}(\omega)$, we get

$$\Psi_{yy}(\omega) = 1 + \left| T(\omega) \right|^2 \qquad (3.8)$$

where we have normalized $\Psi_{n_1 n_1}(\omega)$ and $\Psi_{n_2 n_2}(\omega)$ to 1.

The subcritical, point, unloaded reactor transfer function may be written

$$T(i\omega) = \frac{1 - \sum_{j=1}^{n} \frac{i\omega B_j}{i\omega + \lambda_j}}{i\omega\left[\ell + \sum_{j=1}^{n} \frac{\beta_j}{i\omega + \lambda_j}\right] - \rho} = \sum_{j=1}^{n+1} \frac{A_j}{i\omega + \omega_j} \qquad (3.9)$$

where $-\omega_j$ are the roots of the inhour equation, β_j and λ_j are the fraction and decay constant respectively for each delayed neutron precursor, ρ is the reactivity, and n is the number of delayed neutron groups.

Using the above, the power density spectrum is given by

$$\Psi_{yy}(\omega) = 1 + \sum_{j=1}^{n+1} \sum_{k=1}^{n+1} \frac{A_j A_k}{(i\omega+\omega_j)(-i\omega+\omega_k)} \tag{3.10}$$

We have not, as yet, taken into account the average neutron level in the reactor. To do this, we define k to be the average neutron level and introduce the term $k^2\delta(\omega)$ into the power density spectrum .

Using this, the measured power density spectrum is written

$$\Psi_{yy}(\omega) = 1 + k^2\delta(\omega) + \sum_{j=1}^{n+1} \sum_{k=1}^{n+1} \frac{A_j A_k}{(i\omega+\omega_j)(-i\omega+\omega_k)} \tag{3.11}$$

Inverse Fourier transforming, the autocorrelation function becomes

$$\Psi_{yy}(T) = \delta(T) + k^2 + \sum_{j=1}^{n+1} \sum_{k=1}^{n+1} A_j A_k \int_{-\infty}^{\infty} \frac{e^{-i\omega T}}{(i\omega+\omega_j)(-i\omega+\omega_k)} d\omega \tag{3.12}$$

The form of this autocorrelation function agrees with Velez.[24]

The inversion indicated above is straight forward if care is taken in choosing the path of integration in the complex plane so that no positive exponential occurs. The result is

$$\Psi_{yy}(\tau)=\delta(\tau)+k^2+\sum_{j=1}^{n+1}A_j\sum_{k=1}^{n+1}\frac{A_k}{\omega_j+\omega_k}e^{-\omega_j\tau}$$

$$=\delta(\tau)+k^2+\sum_{j=1}^{n+1}A_jB_je^{-\omega_j\tau} \qquad (3.12a)$$

where $$\beta_j=\sum_{k=1}^{n+1}\frac{A_k}{\omega_j+\omega_k}$$

The count rate variance to mean ratio is related to the auto-correlation function by Equation (2.33) repeated below with $\bar{x}$ replaced by k_T.

$$\frac{Var}{Mean}(T)=-kT+\frac{2}{kT}\int_0^T\int_0^{T'}\Psi_{yy}(\tau')\,d\tau''d\tau' \qquad (3.13)$$

Performing the indicated operations the equation for variance to mean ratio becomes

$$\frac{Var}{Mean}(T)=-kT+\frac{2}{KT}\frac{T}{2}+\frac{2}{KT}\left(k^2\frac{T^2}{2}\right)+\frac{2}{k}\sum_{j=1}^{n+1}\frac{A_jB_j}{\omega_j}\left[1-\frac{1-e^{-\omega_jT}}{\omega_jT}\right] \qquad (3.14)$$

$$=\frac{1}{k}+\frac{2}{k}\sum_{j=1}^{n+1}\frac{A_jB_j}{\omega_j}\left[1-\frac{1-e^{-\omega_jT}}{\omega_jT}\right]$$

This is the quantity of interest in the experimental work to be detailed later. The above derivation, although straight-forward, does not make explicit the characteristics of the multiplication processes which contribute to the form of the final equation. The derivation to follow will deal with these multiplication processes and also will show how the detecting system affects the result.

B. Physical Approach

The count-rate variance to mean ratio may be derived by consideration of the multiplication processes in a nuclear reactor without reference to the stochastic process functions defined earlier. Here, no white noise source is hypothesized; the argument follows from basic probabilities to be defined. This derivation takes into account the efficiency of the detector which is used to measure the output noise.

1. Definitions

Consider two time intervals, Δt_1 and Δt_2. An equation for the expected number of neutrons detected in these two non-overlapping intervals will be developed by following the fission chains.

Define:

$p(m,\Delta t_1)$ ≡ probability of m detections in Δt_1

$p(n,\Delta t_2)$ ≡ probability of n detections in Δt_2

$p(m,\Delta t_1;n,\Delta t_2)$ ≡ joint probability of m detections in Δt_1 and n detections in Δt_2

$p(n,\Delta t_2|m,\Delta t_1)$ ≡ conditional probability of n detections in Δt_2 on the hypothesis of m detections in Δt_1

$\langle c(t_1)c(t_2)\Delta t_1\Delta t_2\rangle$ ≡ expected number of counts in Δt_1 and Δt_2

2. Physical Derivation

In order to compute the count-rate variance to mean ratio, the expected number of counts in a pair of intervals of time is first computed. This is done by observing that for small intervals the expected number of counts is approximated by the probability of a count, thus:

$$\lim_{\Delta t_{1,2}\to 0}\langle c(t_1)c(t_2)\Delta t_1\Delta t_2\rangle = \lim_{\Delta t_{1,2}\to 0}\sum_{m,n} mn\,p(m,\Delta t_1;n,\Delta t_2) \tag{3.15}$$

$$= \langle c(t_1)c(t_2)\,dt_1\,dt_2\rangle = p(1,dt_1;1,dt_2)$$

This probability can be separated into two terms, one term representing those events for which the probability of a count in Δt_2 is independent of whether or not a neutron was detected in Δt_1, the second term representing those events for which the probability of a count in Δt_2 depends upon whether or not a neutron was detected in Δt_1

$$p(1, dt_1; 1, dt_2) = p_a(1, dt_1; 1, dt_2) + p_c(1, dt_1; 1, dt_2) \tag{3.16}$$
$$= p(1, dt_1)p(1, dt_2) + p(1, dt_1)p(1, dt_2 / 1, dt_1)$$

The first term is identified as the probability of an "accidental" pair of counts and the second term is identified as the probability of a "coupled" pair of counts.

Accidental pairs of counts arise from the detection of a pair of neutrons which have no common fission as an ancestor; coupled pairs arise from the detection of two neutrons having a common ancestor fission. This will become more evident in the following development.

a) Accidental Pairs

Accidental pairs of counts arise from detection of neutrons which do not belong to a common fission chain. Figure 3.3 illustrates possible events leading to an accidental pair of counts

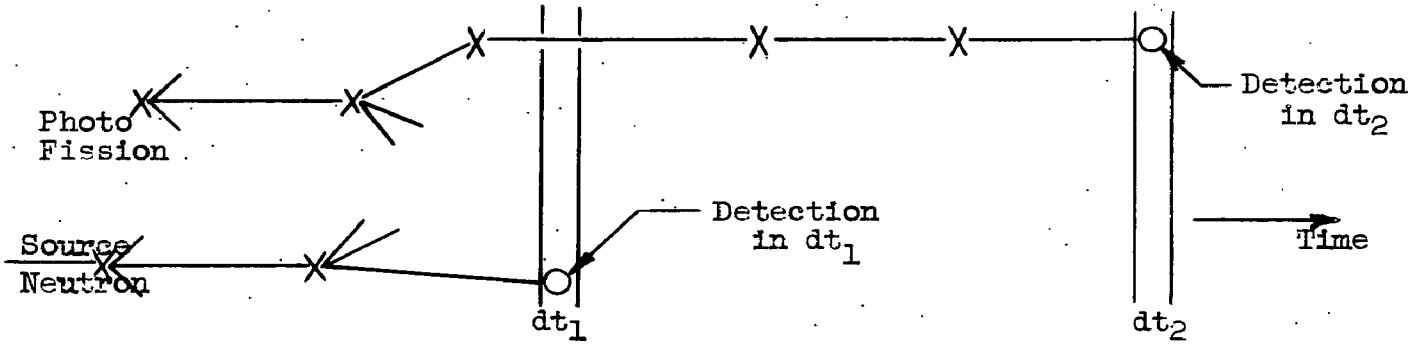


Figure 3.3 Possible Chains for an Accidental Pair of Counts.

To derive an expression for the probability of an accidental pair of counts, define:

F = average fission rate

$$= \int_E \int_{\underline{r}} \Sigma_f(E,\underline{r}) n(E,\underline{r}) v \, d^3\underline{r} \, dE \qquad (3.17)$$

where $n(E,\underline{r})d^3\underline{r}dE \equiv$ the expected number of neutrons in $d^3\underline{r}$ about $\underline{r}$ with energy in dE about E.

$\Sigma_f(E,\underline{r}) \equiv$ the probability per unit path for small paths that a neutron with energy E at space point $\underline{r}$ suffer a collision which induces a fission.

v $\equiv$ neutron speed corresponding to energy E

$\epsilon \equiv$ average counter efficiency

$$= \frac{\int_E \int_{\underline{r}} \Sigma_D(E,\underline{r}) n(E,\underline{r}) v \, d^3\underline{r} \, dE}{\int_E \int_{\underline{r}} \Sigma_f(E,\underline{r}) n(E,\underline{r}) v \, d^3\underline{r} \, dE}$$

where $\Sigma_D \equiv$ the probability per unit path for small paths that a neutron with energy E at space point $\underline{r}$ suffers a collision which results in a detection.

Using these definitions, the probability of a detection in an interval of time dt is

$$p(1, dt) = F \epsilon \, dt \qquad (3.18)$$

Thus, the probability of an accidental pair of counts in dt_1 and dt_2 is given by

$$p(1, dt_1) p(1, dt_2) = F^2 \epsilon^2 dt_1 dt_2 \qquad (3.19)$$

b) Coupled Pairs

Figure 3.4 illustrates the possible ancestry of a coupled pair of counts.

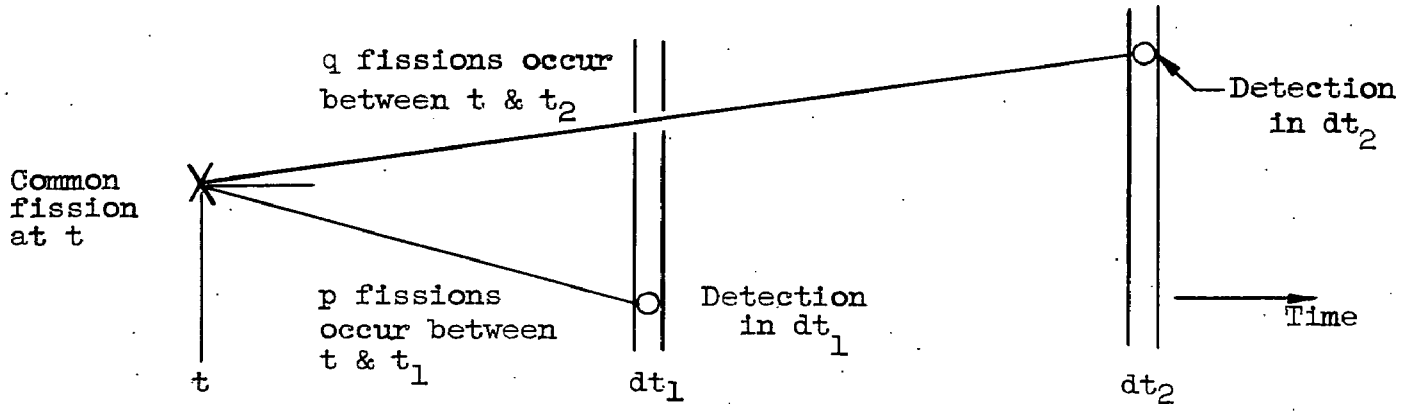


Figure 3.4 Possible Events Leading Up to a Coupled Pair of Counts.

As indicated in Equation (3.16), the quantity

$$p(1, dt_1)\, p(1, dt_2 \mid 1, dt_1)$$

must be computed.

First, $p(1,dt_1)$ can be written as (see Equation (3.18))

$$p(1, dt_1) = F \epsilon\, dt_1 \tag{3.20}$$

To compute $p(1,dt_2|1,dt_1)$, the following quantities are defined:

ν ≡ the number of neutrons emitted in a fission

N_1 ≡ the probability per unit time for small times that a neutron born at time t have a progeny (including itself) in the system at time t_1.

N_2 ≡ the probability per unit time for small times that a neutron born at time t have a progeny (including itself) in the system at time t_2.

Using the above, the probability of one count in dt_1 from a progeny of a fission which emits ν neutrons at time t is

$$\nu F dt N_1 \epsilon dt_1$$

The probability of a count in dt_2 from a progeny of the same fission at time t which produced a detection in dt_1 is

$$(\nu-1)\epsilon N_2 dt_2$$

So, the probability of a pair of counts in dt_1 and dt_2 due to the progeny neutrons of a common fission at time t which emitted ν neutrons is

$$\nu(\nu-1)F\epsilon^2 dt\, N_1 N_2\, dt_1\, dt_2$$

A fission at time t may emit any of several numbers of neutrons; so, considering the average common ancestor fission we average over the ν's. The probability of one detection in dt_1 and one detection in dt_2 due to any common ancestor fission is given by integrating over all past time so that the probability of a coupled pair of counts is written

$$p(1,dt_1)p(1,dt_2\,|\,1,dt_1) = F\epsilon^2(\overline{\nu^2}-\bar{\nu})dt_1 dt_2 \int_{-\infty}^{t_1} N_1 N_2\, dt \qquad (3.21)$$

c) Probability of a Pair of Counts

Equations (3.15), (3.16), (3.19) and (3.21) may be combined to give the expected number of pairs of counts in intervals dt_1 and dt_2 due to both accidental and coupled pairs, yielding:

$$\langle c(t_1)c(t_2)dt_1 dt_2\rangle = p(1,dt_1;1,dt_2) \qquad (3.22)$$

$$= F^2\epsilon^2 dt_1 dt_2 + F\epsilon^2(\overline{\nu^2}-\bar{\nu})dt_1 dt_2 \int_{-\infty}^{t_1} N_1 N_2\, dt$$

It remains to determine N_1 and N_2. From the reactor kinetic equations, let us suppose that

$$N_1 = \sum_{j=1}^{n+1} A_j e^{-\omega_j (t_1 - t)} \qquad N_2 = \sum_{i=1}^{n+1} A_i e^{-\omega_i (t_2 - t)} \tag{3.23}$$

where the A_1 are the numerator terms of the reactor transfer function in the form of Equation (3.9) and $-\omega_1$ are roots of the inhour equation.

At this point, it is not obvious that the expressions (3.23) truly define the required probabilities per unit time. These identifications, however, lead to the same result as the system approach, thus we will conclude that the quantities N_1 and N_2 are properly defined and identified here.

Now, the expected number of counts in dt_1 and dt_2 may be written

$$\langle c(t_1) c(t_2) dt_1 dt_2 \rangle = F^2 \epsilon^2 dt_1 dt_2 + F \epsilon^2 (\bar{\nu}^2 - \bar{\nu}) \int_{t=-\infty}^{t_1} dt_1 dt_2 \sum_{i,j=1}^{n+1} A_i A_j e^{-\omega_j (t_1 - t)} e^{-\omega_i (t_2 - t)} dt \tag{3.24}$$

Doing the integral, we get

$$\langle c(t_1) c(t_2) dt_1 dt_2 \rangle = F^2 \epsilon^2 dt_1 dt_2 + F \epsilon^2 (\bar{\nu}^2 - \bar{\nu}) dt_1 dt_2 \sum_{i,j=1}^{n+1} \frac{A_i A_j}{\omega_j + \omega_j} e^{-\omega_i (t_2 - t_1)} \tag{3.25}$$

Now we do the sum over j, identifying

$$\sum_{j=1}^{n+1} \frac{A_j}{\omega_i + \omega_j} = B_i \tag{3.26}$$

The equation now becomes

$$\langle c(t_1)c(t_2)dt_1dt_2\rangle = F^2\epsilon^2 dt_1dt_2 + F\epsilon^2(\overline{\nu^2}-\bar{\nu})dt_1dt_2\sum_{i=1}^{n+1}A_iB_i e^{-\omega_i(t_2-t_1)} \qquad (3.27)$$

In the experiment, we measure over an interval of length τ which includes t_1 and t_2. If we have c counts in an interval, the number of pairs of counts in the interval is $c(c-1)/2$ and the expected number of pairs of counts is $\overline{c(c-1)}/2$.

The expected number of pairs of counts in an interval of length τ is related to the expected number of pairs of counts in dt_1 and dt_2 by

$$\frac{\overline{c(c-1)}}{2} = \int_{t_2=0}^{\tau}\int_{t_1=0}^{t_2}\langle c(t_1)c(t_2)dt_1dt_2\rangle \qquad (3.28)$$

Applying this relation to Equation (3.27) and doing the integrals, we get

$$\frac{\overline{c(c-1)}}{2} = \frac{F^2\epsilon^2\tau^2}{2} + F\epsilon^2(\overline{\nu^2}-\bar{\nu})\tau\sum_{i=1}^{n+1}\frac{A_iB_i}{\omega_i}\left[1-\frac{1-e^{-\omega_i\tau}}{\omega_i\tau}\right] \qquad (3.29)$$

The term $F\epsilon\tau$ can be identified as $\bar{c}$ so that the above equation may be written

$$\frac{\overline{c^2}-\bar{c}}{2} = \frac{\bar{c}^2}{2} + \bar{c}\,\epsilon(\overline{\nu^2}-\bar{\nu})\sum_{i=1}^{n+1}\frac{A_iB_i}{\omega_i}\left[1-\frac{1-e^{-\omega_i\tau}}{\omega_i\tau}\right] \qquad (3.30)$$

Rearranging terms, the equation becomes:

$$\frac{\overline{c^2}-\bar{c}^2}{\bar{c}}(\tau) = \frac{\text{Var}}{\text{Mean}}(\tau) = 1 + 2\epsilon(\overline{\nu^2}-\bar{\nu})\sum_{i=1}^{n+1}\frac{A_iB_i}{\omega_i}\left[1-\frac{1-e^{-\omega_i\tau}}{\omega_i\tau}\right] \qquad (3.31)$$

where the identification of $\frac{\overline{c^2}-\bar{c}^2}{\bar{c}}(\tau)$ with $\frac{\text{var}}{\text{mean}}(\tau)$ has been made from the definition of variance to mean ratio.

The introduction of the detector into this derivation has introduced the counter efficiency, ϵ, into the equation for variance to mean. Also, the study of the fission chains has introduced the constant $\overline{\nu^2} - \bar{\nu}$ which does not appear in Equation (3.14).

The normalization implicitly assumed in this derivation is not necessarily the same as that assumed in the derivation leading to (3.14) so it may be expected that the two results would differ by a constant factor, which they do.

IV. EQUIPMENT

A. Experimental Setup

Two experimental configurations were used in the experiment. One configuration was used to record data on the tape recorder and the other configuration was used to count pulses over a gate time and record the count on IBM cards. These two configurations are shown in Figures 4.1 and 4.2 The figures are self-explanatory.

Each piece of equipment used is discussed below. Those pieces of equipment which are standard items are discussed briefly with reference to manufacturer's data while the special pieces of equipment are discussed in more detail.

B. Description of Equipment

1. Reactor

The Ford Nuclear Reactor is a one megawatt swimming pool reactor using 90% enriched U^{235} MTR type fuel elements. The critical mass, with a carbon reflector on the vertical faces is approximately 3kg. The reactor is light water moderated and cooled. It is used primarily as a neutron source and as a training reactor.

The detector was placed at the core-face, in the reflector, for each of the experiments. The core configurations during the experiments are shown in Figures 4.3 and 4.4.

2. Detectors

Manufacturer's specifications for the two detectors used are listed below:

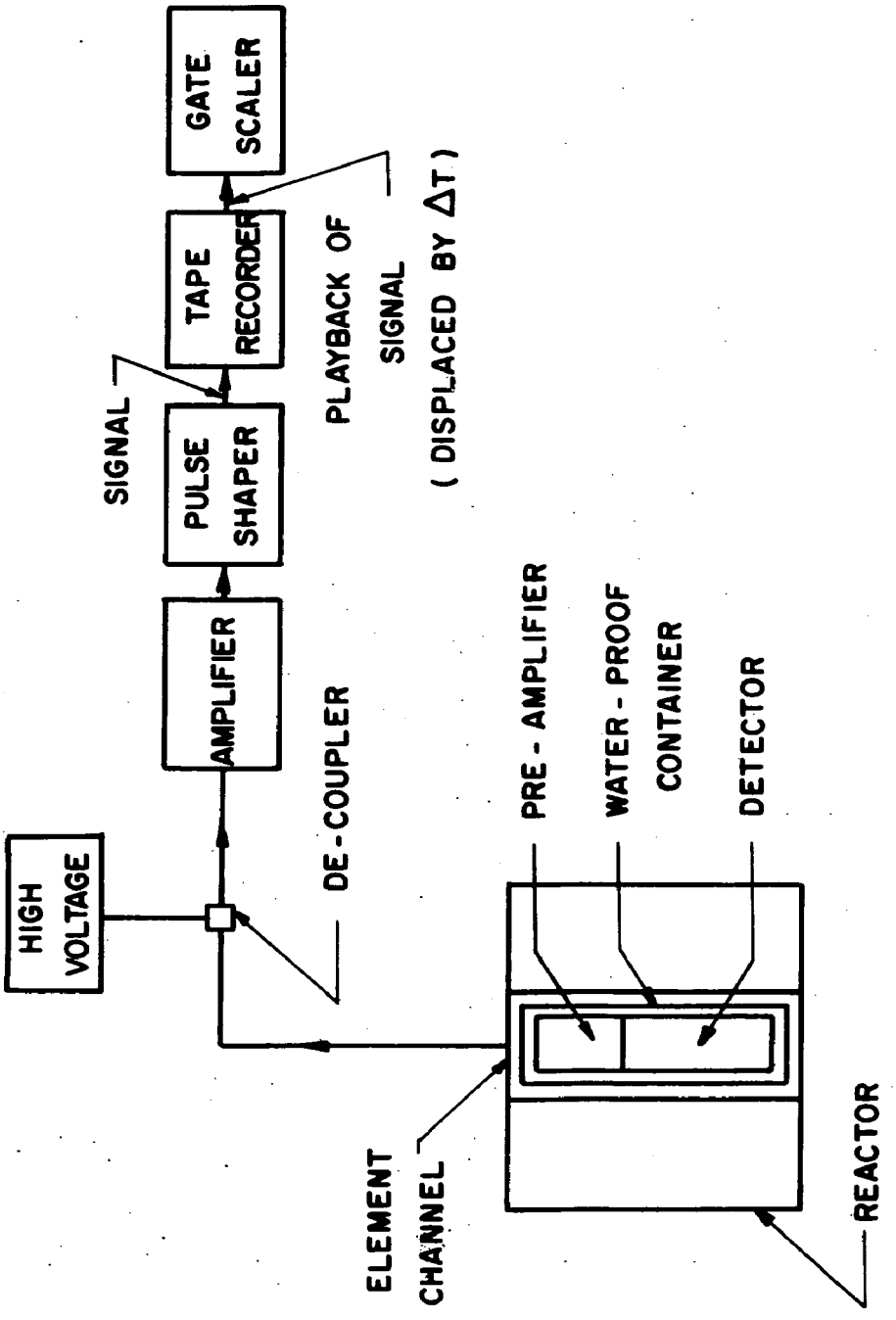


Figure 4.1 Data Taking Configuration.

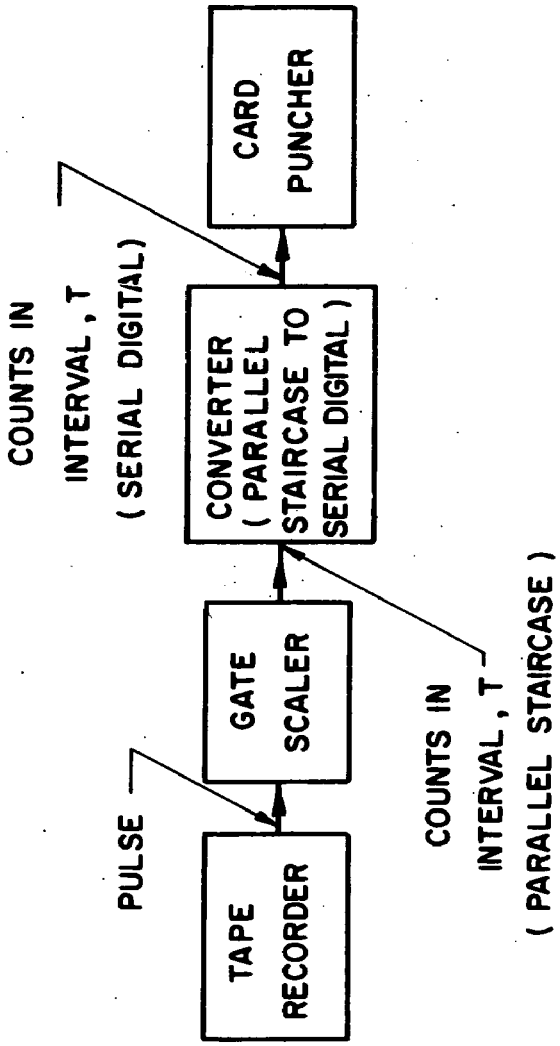


Figure 4.2 Data Transcription Configuration.

KEY:

- EMPTY CHANNEL WITH PLUG
- H — EMPTY CHANNEL WITH SAMPLE HOLDER
- S — MOVABLE P_o-BE SOURCE
- T — DETECTING TUBE
- CARBON REFLECTOR ELEMENT
- FUEL ELEMENT
- SPECIAL ELEMENT WITH CONTROL ROD(CR) OR SHIM ROD(A,B,C)
- Ⓕ FISSION CHAMBER FOR REACTOR INSTRUMENTATION

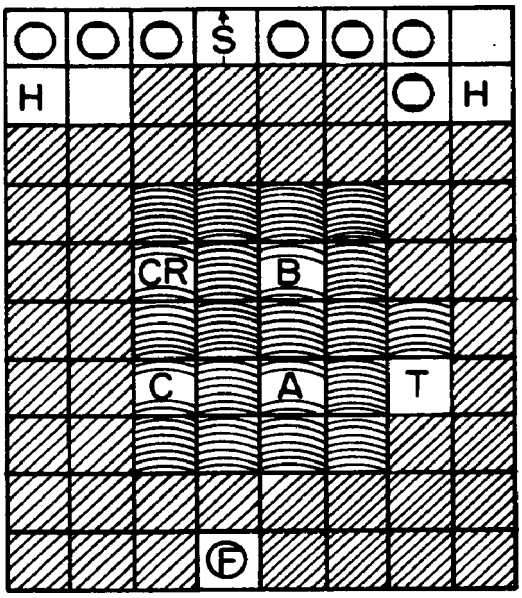


Figure 4.3 Core Configuration for BF_3 Tube Experiments.

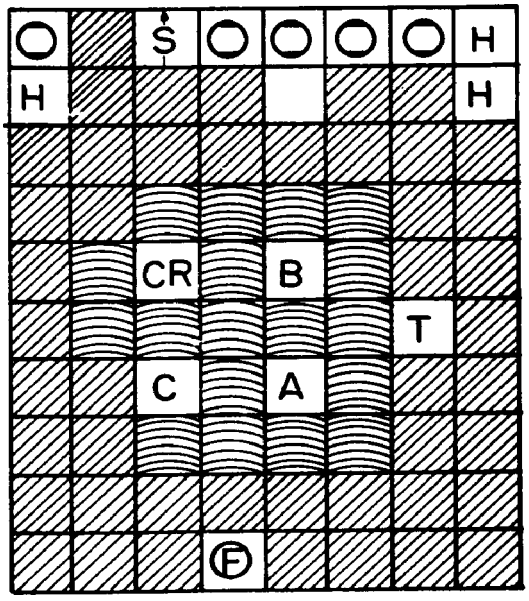


Figure 4.4 Core Configuration for Fission Chamber Experiments.

a) Fission Chamber

Manufacturer	Westinghouse Electric Co.
Model No.	WL-6376
Mechanical data	
overall length	11-7/8"
diameter (max.)	2-3/32"
net weight	1-3/4 lb.
insulating mat'ls	polystyrene and alumina
sensitive length	6"
body mat'l	aluminum
neutron sensitive mat'l	2 mg/cm^2 U_3O_8 fully enriched in U^{235}
filling	A-N_2 at 1 atm.
Operational ratings	
operating voltage (app.)	300 volts
sensitivity	0.7 count/neutron/cm^2
neutron flux range	2.5 to 2.5x10^5 neutrons/cm^2/sec
operating plateau	200 to 800 volts
output	200μ volts, rise time 0.2μ sec

b) BF_3 Tube

Manufacturer	N. Wood Counter Lab.
Model No.	G-10-12
Mechanical data	
overall length	17"
diameter	1"
net weight	not specified
insulating mat'ls	glass
sensitive length	12"
body mat'l	aluminum
neutron sensitive mat'l	enriched BF_3 (96% B^{10})
filling	BF_3 and quenching gas at 40 cm Hg
Operational ratings	
operating voltage (app.)	2000 volts
sensitivity	not specified
neutron flux range	not specified
operating plateau	length of plateau = 300 volts
output	not specified

The detectors were mounted in waterproof cans. The BF_3 tube had its pre-amplifier in its can. The pre-amplifier for the fission chamber was outside of the pool. The BF_3 tube had a lead gamma ray shield, 1/4" thick, wrapped around its water-proof can. The high voltage leads were enclosed in a one inch diameter "Tygon" tube.

3. Pre-Amplifiers

The pre-amplifier used with the BF_3 tube was a transistorized cathode follower with a 15 volt battery as a power supply. This pre-amplifier was used for impedance match; the gain from its input to the end of the twenty foot cable leading to the de-coupler was approximately 0.3. The pre-amplifier was built in a 1" diameter, 6" long aluminum tube with a connector of the BF_3 tube at its input and a connector to the signal cable at its output. No provision was made to turn the pre-amplifier power supply on and off. Operating continuously, the battery life was approximately two weeks.

The pre-amplifier used with the fission chamber was the standard pre-amplifier used with a model 218 linear amplifier. The manufacturer's specifications are given below:

Manufacturer	Baird Atomic Inc.
Model No.	219A
Operating characteristics	
Maximum gain	30
Bandwidth	2mc
Rise time	0.25μ sec max.
Fall time	10μ sec min.
Input polarity	positive or negative
Input impedance	1000 megohm
Linearity	2%

4. Amplifier

The amplifier was used on the delay line bandwidth with the output of the pulse height selector. Therefore, only the specifications corresponding to this operating condition are given:

Mamufacturer	Baird Atomic Inc.
Model	218
Operating characteristics	
Bandwidth	2mc
Rise time	0.2μ sec
Decay time	0.8μ sec

Maximum gain	1600
Input polarity	negative
Input impedance	2000 ohms
Output imedance (PHS)	4700 ohms
Linearity	1%
Amplitude (PHS)	60 volts negative

5. Pulse Shaper

To tape record pulses successfully it was necessary to match the output impedance of the amplifier to the input impedance of the tape recorder and to supply the tape recorder with pulses of optimum shape and size. In order to investigate pulse shape and size a combination one-shot multivibrator, cathode follower circuit with variable height and width output pulses was built. The pulse used to drive the tape recorder was optimized on this pulse shaper with the optimum pulse being a 20 volt, 8μ sec nearly square pulse. The circuit diagram of the pulse shaper is shown in Figure 4.5.

6. Tape Recorder

Manufacturer	Ampex Corp.
Model No.	307
Operating characteristics	
No. of channels	1
Tape speed	60"/sec
Drive	Capstan, friction drive
Wow and flutter	0.1% rms
Tape width	1/4"
Maximum size reel	10 1/2"
Maximum length of tape	3600', 1mil thickness
Bandwidth	80 kc

7. Gate Scaler

Manufacturer	Dymec Corp.
Model No.	2500
Operating characteristics	
Range	1 cps to 100 kc
Accuracy	±1 count, stability of crystal
Stability	1 part in 10^5
Registration	5 places, columnar display, to 99,999

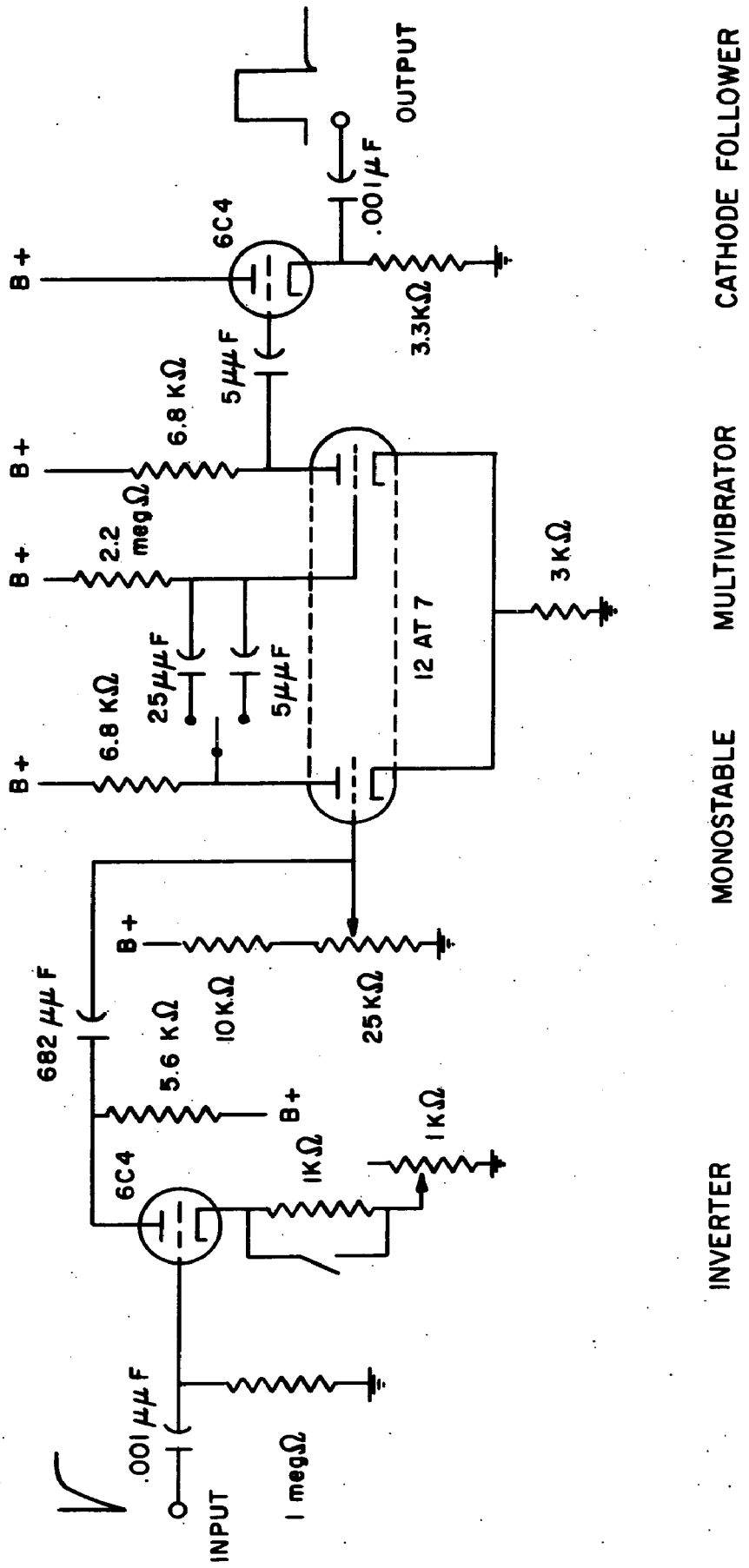


Figure 4.5 Circuit Diagram of Pulse Shaper.

Input requirement	0.2 volts rms min.
Output	bcd (4-line) & single line "staircase"
Input impedance	1 megohm, 50μμf shunt
Gate times	1 millisec to 9.999 sec in ms increments
Display time	variable 0.1 to 10 sec
Self check	counts time base
Power supply	260 watts
Time base frequency	100 kc

Since the gate scaler is a central piece of equipment in this experiment a description of its operation is given here. At the upper right of Figure 4.6 is the digital display counter. This counts and displays in decimal form on 5 registers the number of pulses applied to its input. These pulses come from the tape recorder connected to input A and pass through the signal gate before they reach the input of the display counter.

The opening and closing of the signal gate is controlled by the preset counter. This counter counts the number of pulses applied to its input. The four multiplier rotary switches on the front of the instrument are connected to the present counter in such a manner that the preset counter holds the signal gate circuit closed until it has counted a number of pulses equal to the number set on the multiplier switches. Then the preset counter opens the signal gate circuit, cutting off the flow of pulses to the display counter. The preset counter stays at this "preset count" with the signal gate circuit open until it is reset.

During the experiment, the preset counter counted the internal time base.

The display time circuit shown on the block diagram allows the count on the digital display counter to remain visible for a time after

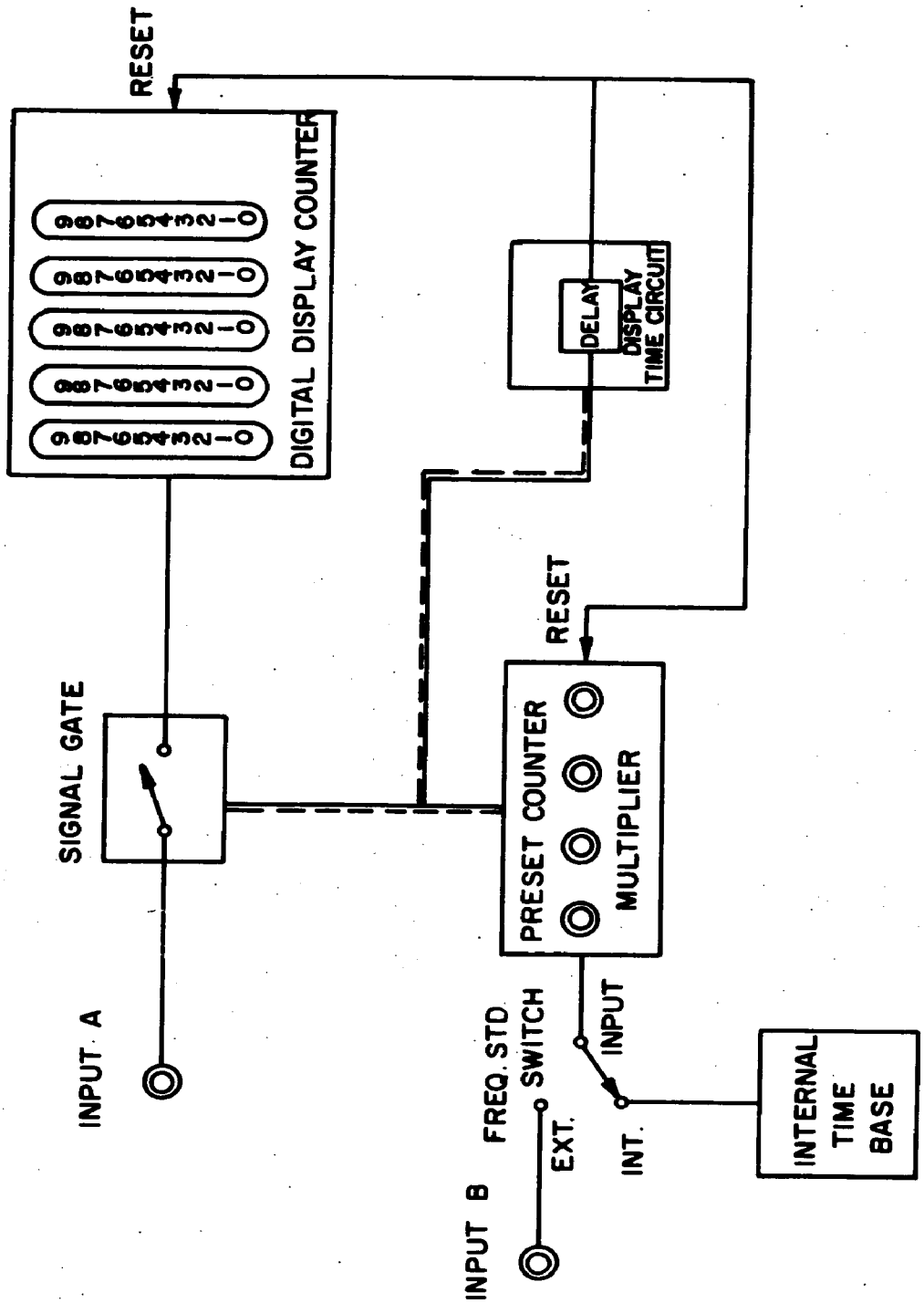


Figure 4.6 Simplified Block Diagram of Gate Scaler.

the preset counter has reached its preset count and the signal gate has been closed. After this "display time" it resets both the display and present counters back to zero and a new count cycle begins.

8. Converter

In order to punch the numbers displayed on the gate scaler onto IBM cards using an IBM-024 card puncher, it was necessary to build a machine to convert the "parallel staircase" output of the gate scaler to the "serial digital" input required by the card puncher. This machine is called the "converter" and its circuit diagrams are shown in Figures 4.7 and 4.8. The operation of the converter is as follows:

a) Initially, the stepping relay is in the no signal position while the gate circuit of the gate scaler is closed and the display scaler is counting.

b) When the scaler displays its count, a signal is sent to the converter which simultaneously resets the stepping relay to position 1 and opens the circuit of the stepping relay wiper so that no signals are admitted to the converter.

c) The signal circuit of the converter is closed and a signal representing zero (140 volts) is admitted. The bank of ten relays converts this voltage into a closed circuit corresponding to the activation of the zero key in the card puncher and a zero is punched. When the card puncher punches the zero, a signal is fed back from it to the converter which makes the stepping relay simultaneously open its signal circuit and step to position 2.

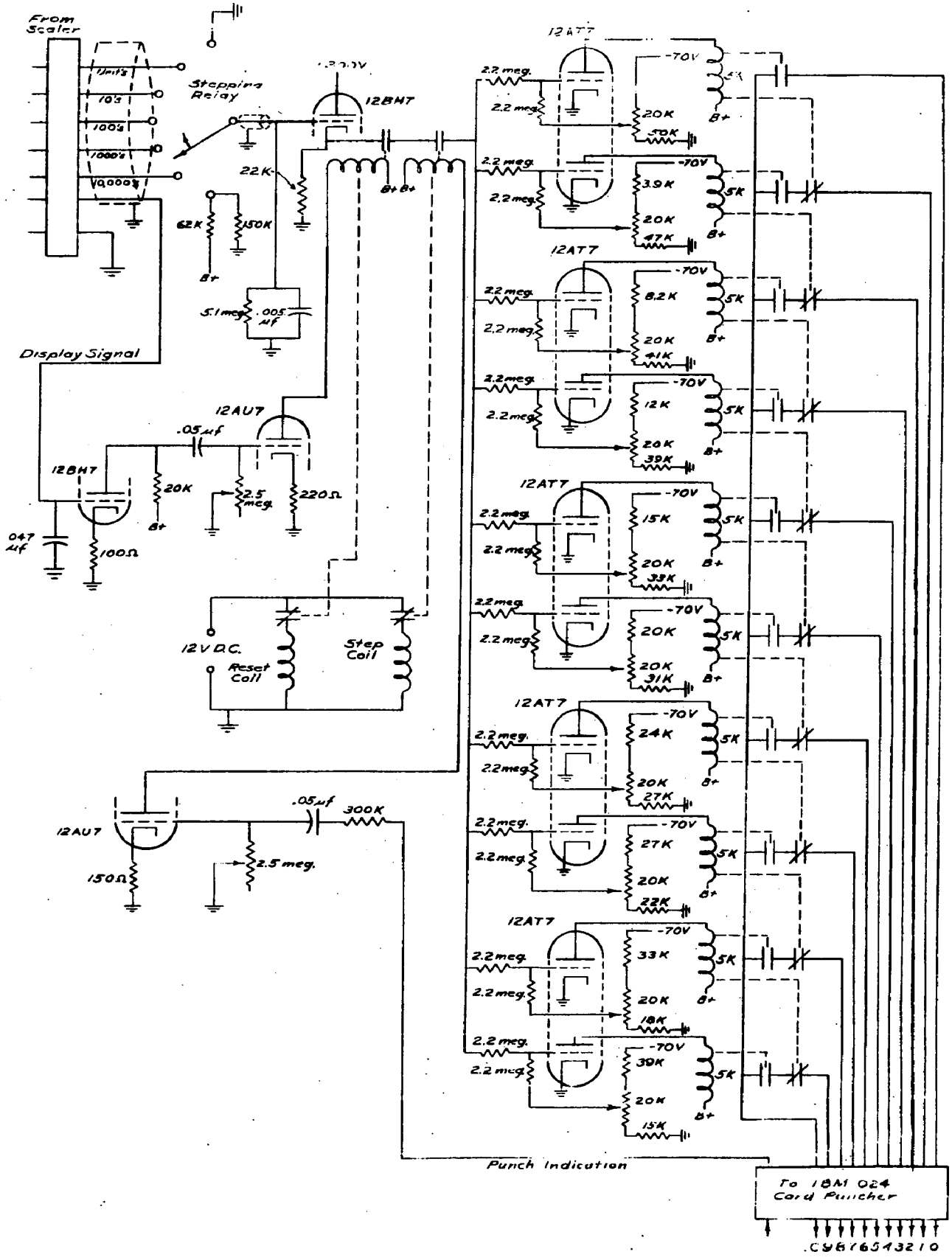


Figure 4.7. Information Converter Parallel "Staircase" to Serial "Digital".

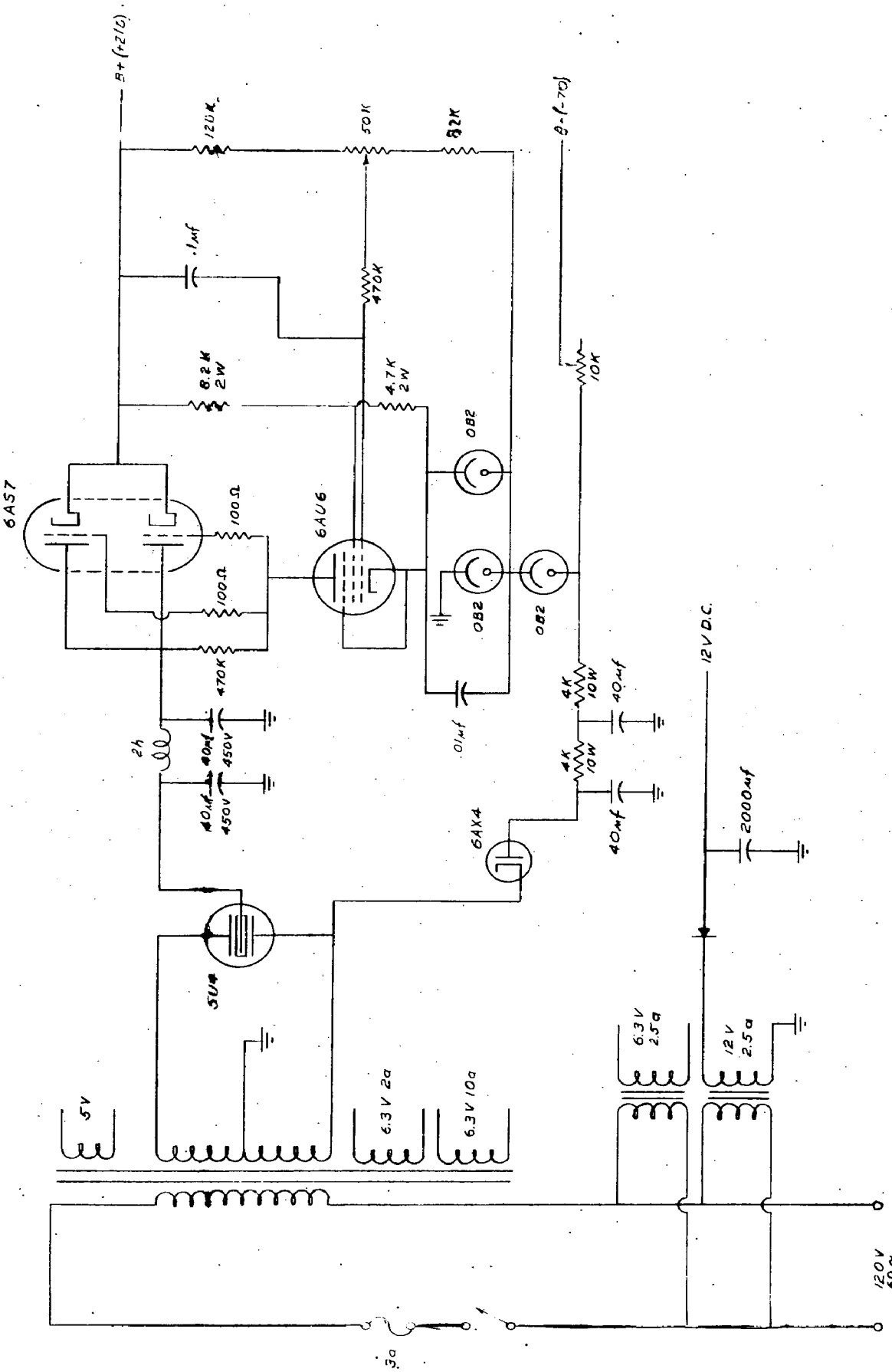


Figure 4.8. Power Supply for Converter.

d) The signal circuit on the stepping relay closes, admitting a voltage corresponding to the i-th digit on the display counter (50v to 140v representing 9 to zero in 10 volt steps). The bank of ten relays translates this voltage into an appropriate closed circuit and the corresponding number is punched. Punching of the number gives a feedback which opens the stepping relay signal circuit and steps it to the next position.

e) Step d) is repeated for i = 1 to 5.

f) When the stepping relay reaches the no-signal position the scaler resets and a new count is begun.

The sequence of events a through f above takes about one second. Every sixth digit punched on an IBM card is a zero. This helps in editing the cards and checking for errors.

9. IBM 024 Card Puncher

The IBM 024 card puncher is designed to be a hand operated key punch with a typewriter keyboard. This typewriter was modified so that the closing of relays could be controlled by the converter instead of by the depressing of keys. This was accomplished by wiring the converter relay contacts in parallel with the keyboard contacts (see Figure 4.7).

Another modification of the card puncher was required to make it release the card after it had punched 72 columns and go on to the next card. This modification consisted of a cam which was mounted on the control drum shaft and used to trip a microswitch which controlled the automatic feed mechanism. When column 72 was punched the microswitch released the present card and entered the next card by means of the IBM 024 card feed mechanism.

C. Operating Characteristics

The operation of the above experimental equipment was routine after several bugs had been worked out. Some trouble was incurred in the stability of the D. C. voltages in the system but this was minimized by using a regulated power supply and occasionally checking bias adjustments.

No relay failure was encountered although some of the relays in the converter operated over two million times.

V. EXPERIMENT

Two significant experimental runs were accomplished on the Ford Nuclear Reactor at the University of Michigan. Data was taken in run #1 using a fission chamber and the data in run #2 was taken using a BF_3 tube. In each of these experiments several tape recordings were made at different reactivities. In Appendix A the reactor parameters and data points for these experiments can be found. This section discusses the experimental conditions which must be met to insure success and the steps which were taken to meet these conditions.

A. Experimental Conditions

In order to perform an experiment to measure nuclear reactor parameters by methods of stochastic processes on a reactor such as the Ford Reactor it is necessary to optimize the experimental technique on several considerations. The competing factors which lead to an optimization are the need for a high efficiency detector with small sensitivity to gamma radiation, the need for putting the detector in a region of low neutron entropy while being limited in count rate by the resolving time of the equipment, and the need to apply point reactor theory to the analysis while locating the detector as close to the reactor as possible.

Recall that the form of the equation for count-rate-variance to mean ratio is

$$\frac{V}{M}(\tau) = 1 + \epsilon \quad \text{(correlated terms)} \qquad (5.1)$$

The first term on the right hand side of Equation (5.1) arises from the accidental pairs of counts as shown in Chapter III. The second

term arises from the coupled pairs. The problems mentioned above arise primarily from the need for the correlated part to be significant compared to one; indicating that ϵ should be as large as possible and that the correlated terms should also be as large as possible. The discussion of experimental conditions leading to large values of ϵ will be discussed under "counter efficiency" and those leading to high values of correlation will be discussed under "correlated terms."

1. Counter Efficiency

In the theoretical development, counter efficiency ϵ, has been defined as the average number of neutrons detected per fission in the reactor. To obtain a ratio of V/M significantly different from one, we need this efficiency to be at least 10^{-8} and preferably of order 10^{-4}. This need for high efficiency immediately suggests using a large counter which will intercept many neutrons, a sensitive detector which will count a large proportion of the neutrons which it intercepts, and placing the counter in a position of high neutron density. Each of these topics is discussed below.

a) Size of Counter

The size of the counter used is limited by the practical dimensions of counters, the available space in which to put a counter, and the requirements for resolving time put upon the instrument. In this experiment, a N. Wood Lab G-10-12 BF_3 tube and a Westinghouse-WL 6376 fission chamber were used. Each of these counters, when enclosed in a waterproof container, was of such a size as to fit into a fuel element channel in the Ford Nuclear Reactor. The size of the counters

was found to be satisfactory in all respects; the dimensions are given under "equipment."

b) Counter Sensitivity

In a reactor which has been operated at high power, high detector sensitivity is especially hard to obtain since, in general, a detector that is sensitive to neutrons is also sensitive to gamma radiation. Thus, the problem of achieving high detector sensitivity is intimately related to the problem of eliminating the gamma background.

The BF_3 tube used was considerably more sensitive to both neutron and gamma radiation than was the fission chamber. For this reason, the BF_3 tube could not be used in the initial experiments in which severe precautions to eliminate gamma ray background were not taken. Using the fission chamber for these experiments, ϵ was small, and thus the correlated parts were not as large as in the later experiments using the BF_3 tube.

To achieve a higher sensitivity, it was necessary to use the BF_3 tube and to take precautions against detecting gamma radiation. This was accomplished by first determining what the effects of a gamma ray background were on the characteristics of the counter, and then taking steps to eliminate these effects. Qualitative measurements of the effect of gamma ray background on the BF_3 tube were made. The effect on the voltage traverse of increased gamma background is to both shorten the length of the plateau and to shift the location of the plateau to a higher voltage. The corresponding effect on the discriminator traverse is to shorten the length of the discriminator "plateau" and to make the slope more steep.

The experimental set-up used to make these measurements is shown in Figure 5.1. The BF_3 tube was kept at a constant distance from the neutron source but moved relative to the gamma-ray source (in this case the shut down reactor).

Observations of pulse-height on the oscilloscope were made simultaneously with the voltage and discriminator traverses. It was observed that with increasing gamma ray intensity the pulse height of the neutron pulses decreased while the pulse height of the gamma pulses appeared to remain approximately constant.

The decrease in pulse height of the neutron pulses is attributed to the lowering of the effective interelectrode voltage by the gamma ray field. This is caused by the fact that the ions produced by the gamma rays provide a space charge opposed to the interelectrode voltage which has the effect of lowering the effective interelectrode voltage resulting in smaller pulses since the gas multiplication of the proportional counter is a strong function of the voltage.

The behavior of the pulses due to gammas appears to be due to competing effects. One would expect the gamma ray pulse height to decrease due to the lowering of the gas multiplication in the proportional region in the same way as the neutron pulse heights decrease. However, an increase in the gamma ray field also gives rise to an increase in simultaneous gamma ray pulses. Apparently in this case, the effective increase in gamma ray pulse height due to simultaneous events is of the same order of magnitude as the decrease in size of gamma ray pulses due to less gas multiplication.

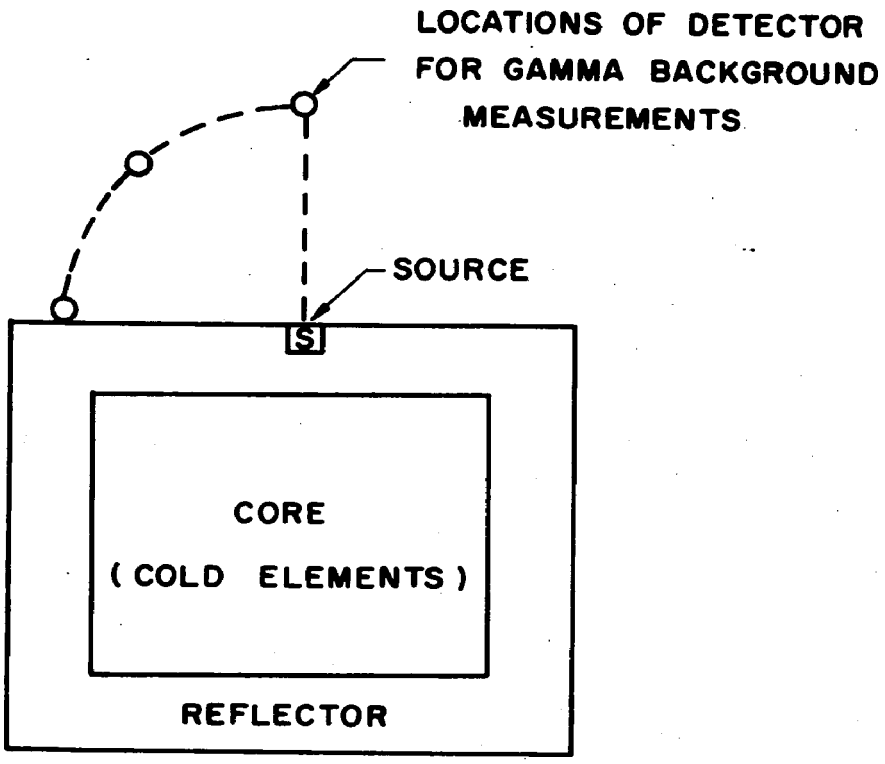


Figure 5.1 Gamma Background Measurement.

One way to minimize this gamma ray effect is to minimize the probability of simultaneous events. This indicates a need for the shortest possible resolving time in the equipment. Again, however, there are competing considerations. To make the resolving time as short as possible one would use the smallest instrument possible. This cannot be done because of the requirement for a large size counter for high efficiency. Thus, the minimum resolving time is determined by the minimum detector size consonant with efficiency considerations. Of course, one may also optimize the detector configuration by placing the electrodes as close together as possible.

In making this type measurement one should always optimize the performance of the BF_3 tube by operating at proper voltage and discriminator values. The foregoing discussion indicates that special attention must be paid to the level of the gamma ray background in determining optimum voltage and pulse height selection since this optimum is strongly effected by the magnitude of the gamma ray background.

The fission chamber used had a low operating voltage, lower sensitivity, and small gas mutiplication and was therefore able to operate in considerably larger gamma-ray fields than the BF_3 tube.

c) Location of Counter

From the standpoint of achieving high counter efficiency it is apparent that with a thermal neutron detector it is most desirable to place the detector in a position of high thermal neutron flux.

2. Correlated Terms

The magnitude of the correlated terms depends strongly upon the number of correlated events. The relative number of correlated events depends upon the operating configuration of the reactor and the location of the detector.

If the reactor is operating at a very large negative reactivity, the multiplication is small. Since the pairs of detections traceable to a common fission are the ones responsible for correlated terms, one would suspect that small multiplication would yield small correlation. This is born out both by the point reactor theory and the relative magnitude of the variance/mean curves taken at different reactivities with the BF_3 tube. Therefore, to achieve a high degree of correlation it is necessary to operate the reactor at very nearly critical.

Although no space dependent model for stochastic processes has yet been found one may make some intuitive guesses about the magnitude of the correlated terms as a function of space. Since the core of the reactor is the source of correlated events, one would expect that the relative number of correlated events detected would decrease as the detector is moved away from the core. Making an analogy to entropy, this is tantamount to saying that the entropy of the neutrons increases with increasing distance from their source. This implies that there is some point of minimum neutron entropy in the core and that entropy increases as we move away from that point.

According to the above arguments, the optimum operating configuration for the experiment is with the reactor nearly critical and the detector close to the core.

B. Equipment Limitations

One must operate within the confines of equipment limitations when meeting the above experimental conditions. The most serious limitations on the experiment are the resolving time and the time base stability. In this experiment, the performance of the system with respect to these two considerations is limited by the tape recorder. The effective resolving time of the tape recorder is approximately 15μ secs and its time base stability (wow and flutter) is such that 0.2% inaccuracies may be expected.

1. Resolving Time

The effects upon the mean number of counts per interval and the variance of the number of counts per interval due to finite resolving time are not the same. The differences are discussed below.

a) Mean Number of Counts Per Interval

The number of events registered in an interval of time must be less than or equal to the true number of events occurring in that interval of time. This is due to the finite resolving time of any physical system. Two extreme cases may be considered with the expectation that real life is represented by some intermediate case. The two cases considered are that of the paralyzable counter and the nonparalyzable counter. For a comparison of these two conditions see Figure 5.2.

The notation used is:

ρ - dead time following occurrence of an event

$\overline{n}$ - mean observed count rate

$\overline{N}$ - mean true count rate

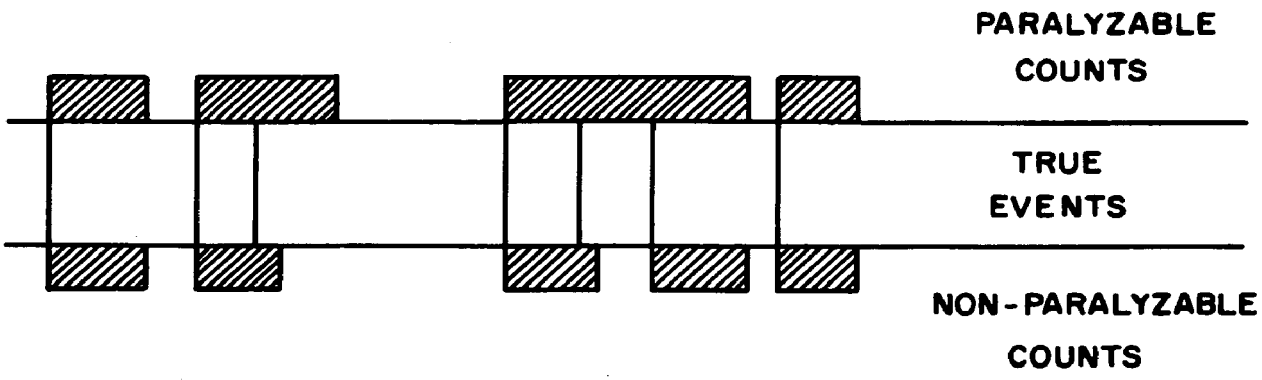


Figure 5.2 Relationship of True Events to Registrated Events in Paralyzable and Non-paralyzable Counters.

1) Paralyzable Counter - The paralyzable situation is defined by a system which is unable to provide a second output pulse unless there is a time interval of at least ρ between two successive true events. For this case the expected mean observed count rate is

$$\overline{n} = \overline{N} e^{-\overline{N}\rho} \tag{5.2}$$

2) Nonparalyzable Counter - The nonparalyzable situation is defined by a system which is unaffected by events occurring during the recovery time, ρ. For this case, the expected mean observed count rate is given approximately by

$$\overline{n} \approx \frac{\overline{N}}{1 + \overline{N}\rho} \tag{5.3}$$

for large $\overline{N}$ and small ρ. A curve showing these effects is shown in Figure 5.3.

b) Variance of Number of Counts Per Interval

The following notation is employed in addition to that used under a).

ψ^2 = variance of measured number of counts in interval

σ^2 = variance of true number of counts in interval

T = length of interval

$\overline{N}T$ = mean number of true events in interval of length T

$\overline{n}T$ = mean number of measured events in interval of length T

1) Paralyzable Counter - Making the assumption that $\overline{N}$ is large, the distribution is normal, and ρ is small, the measured variance is given approximately by

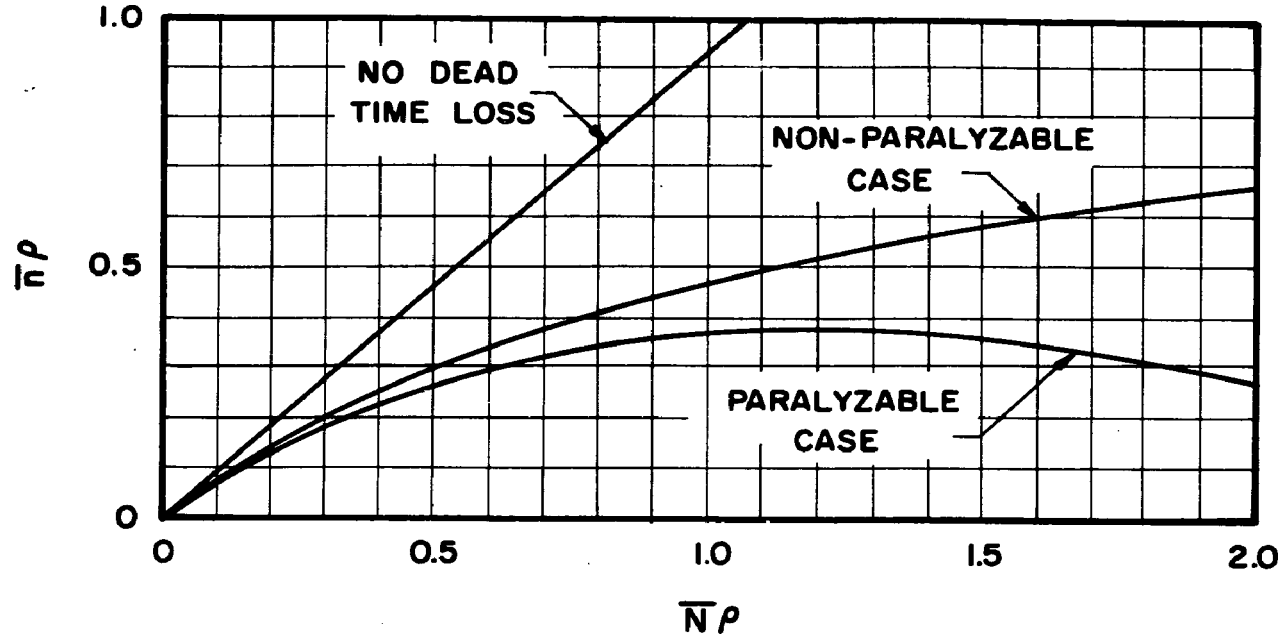


Figure 5.3 Loss in Mean Count Rate Due to Dead Time Losses for Paralyzable and Non-Paralyzable Cases.

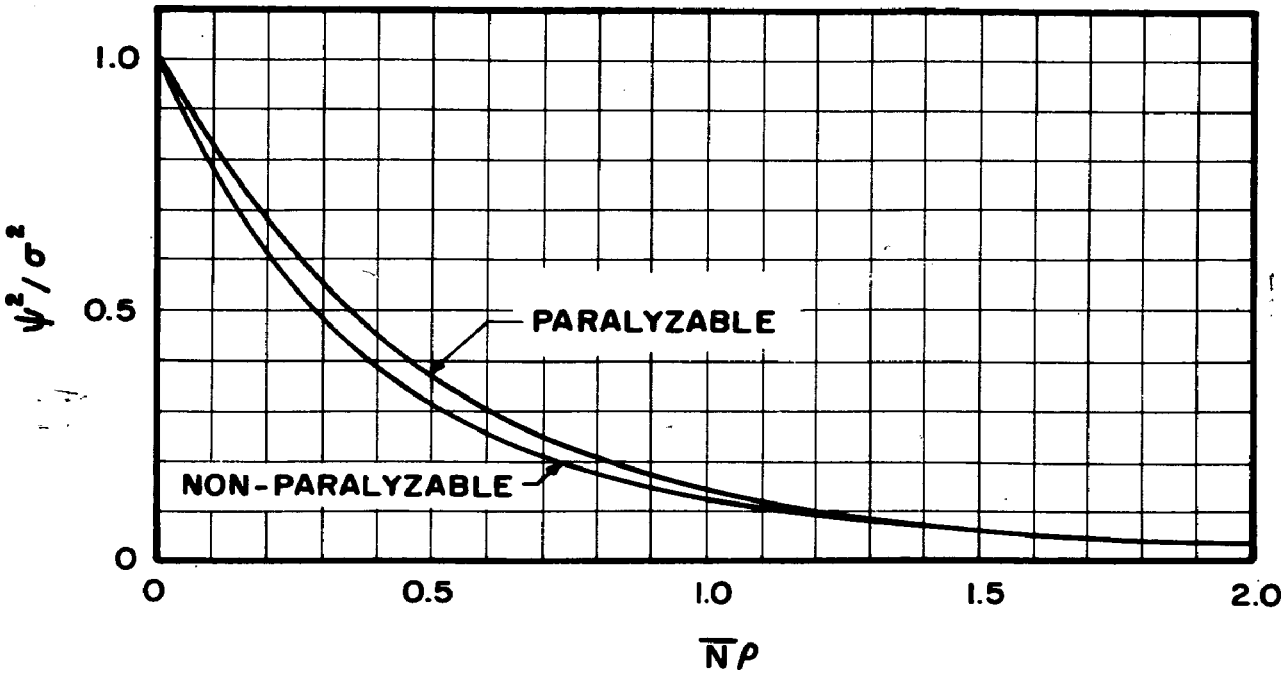


Figure 5.4 Ratio of Observed to True Variance Verses $\overline{N}\rho$ for Paralyzable and Non-Paralyzable Counter.

$$\psi^2 \approx \sigma^2 e^{-2\bar{N}\rho} \tag{5.4}$$

2) Nonparalyzable Counter - Making the same assumptions as in the paralyzable case, the measured variance is given approximately by

$$\psi^2 \approx \frac{\sigma^2}{(1+\bar{N}\rho)^3} \tag{5.5}$$

A curve showing these effects is shown in Figure 5.4.

c) Variance to Mean

Using the above results, the measured ratio of variance to mean for the two cases is:

1) Paralyzable

$$\frac{\psi^2}{\bar{n}T} = \frac{\sigma^2}{\bar{N}T} e^{-\bar{N}\rho} \tag{5.6}$$

2) Nonparalyzable

$$\frac{\psi^2}{\bar{n}T} = \frac{\sigma^2}{\bar{N}T} \frac{1}{(1+\bar{N}\rho)^2} \tag{5.7}$$

A curve showing these effects is shown in Figure 5.5.

Using these results, it is found that the counting losses to the variance to mean ratio limit the counting rate to about 2000 counts per second for a 5% loss in variance to mean. (Paralyzable predicts 3% loss, nonparalyzable predicts 5.5% loss.) In accordance with these results, the average count rate was kept below 2500 CPS whenever possible.

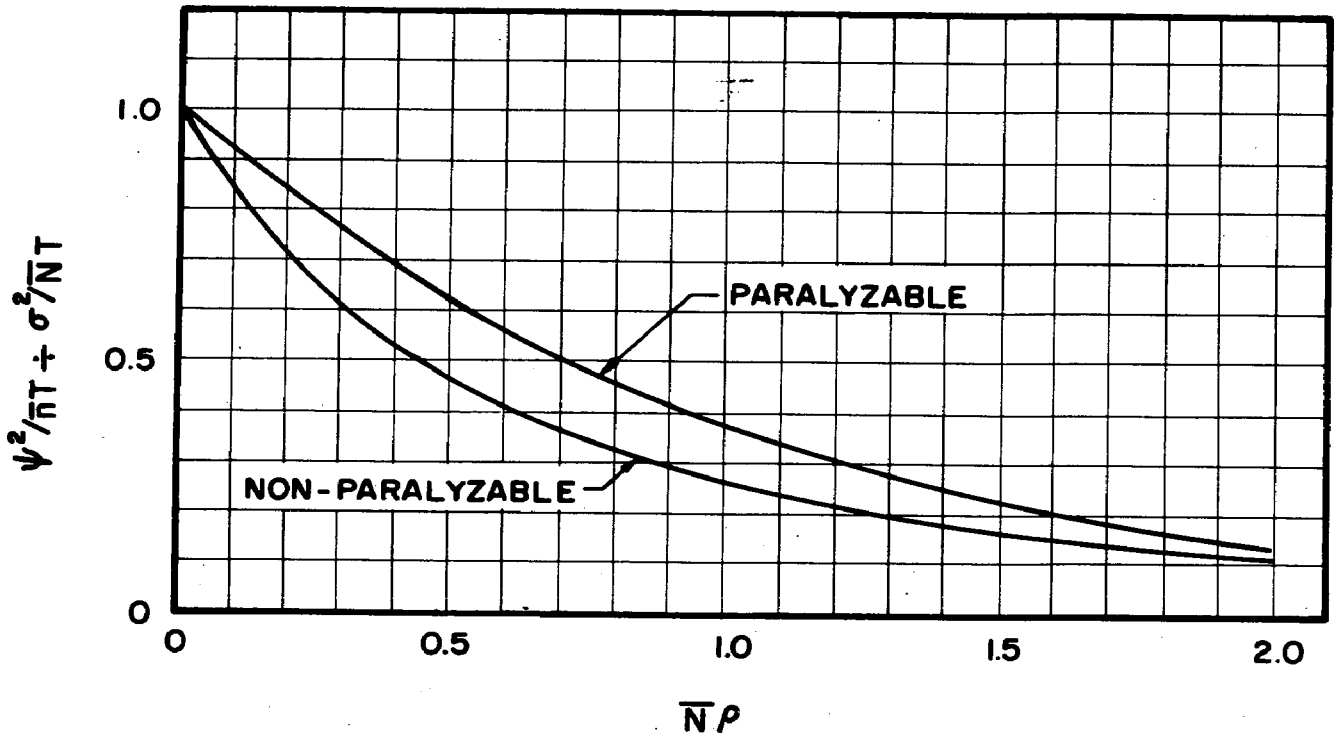


Figure 5.5 Ratio of Measured to True Variance to Mean Ratio Versus $\bar{N}\rho$.

2. Time Base Stability

The stability of the time base used in these measurements was determined by the stability of the tape transport system since it was by far the most unstable factor in the overall time base. The crystal oscillator in the scaler was much more stable. Figure 5.6 shows a sample measurement of the wow and flutter characteristics of the tape recorder. These effects can be analyzed as follows:

If n_i are the number of observed events in a time interval T, then if the time interval varies by an amount ϵT around T, the experimental variance to mean ratio can be written

$$\left(\frac{Var}{Mean}\right)_{expt.} = \frac{p\sum_{i=1}^{p}(n_i \pm \epsilon n_i)^2 - \left|\sum_{i=1}^{p} n_i \pm \sum_{i=1}^{p} \epsilon n_i\right|^2}{p(p-1)} \Bigg/ \frac{1}{p}\sum_{i=1}^{p} n_i \pm \epsilon \frac{1}{p}\sum_{i=1}^{p} n_i \qquad (5.8)$$

where p is the number of intervals measured.

The theoretical variance to mean ratio (taking into account the resolving time but not the time base instability) is

$$\left(\frac{Var}{Mean}\right)_{theory} = \frac{p\sum_{i=1}^{p} n_i^2 - \left|\sum_{i=1}^{p} n_i\right|^2}{p(p-1)} \Bigg/ \frac{1}{p}\sum_{i=1}^{p} n_i \qquad (5.9)$$

Thus expanding $\left(\frac{var}{mean}\right)_{expt.}$ and collecting terms

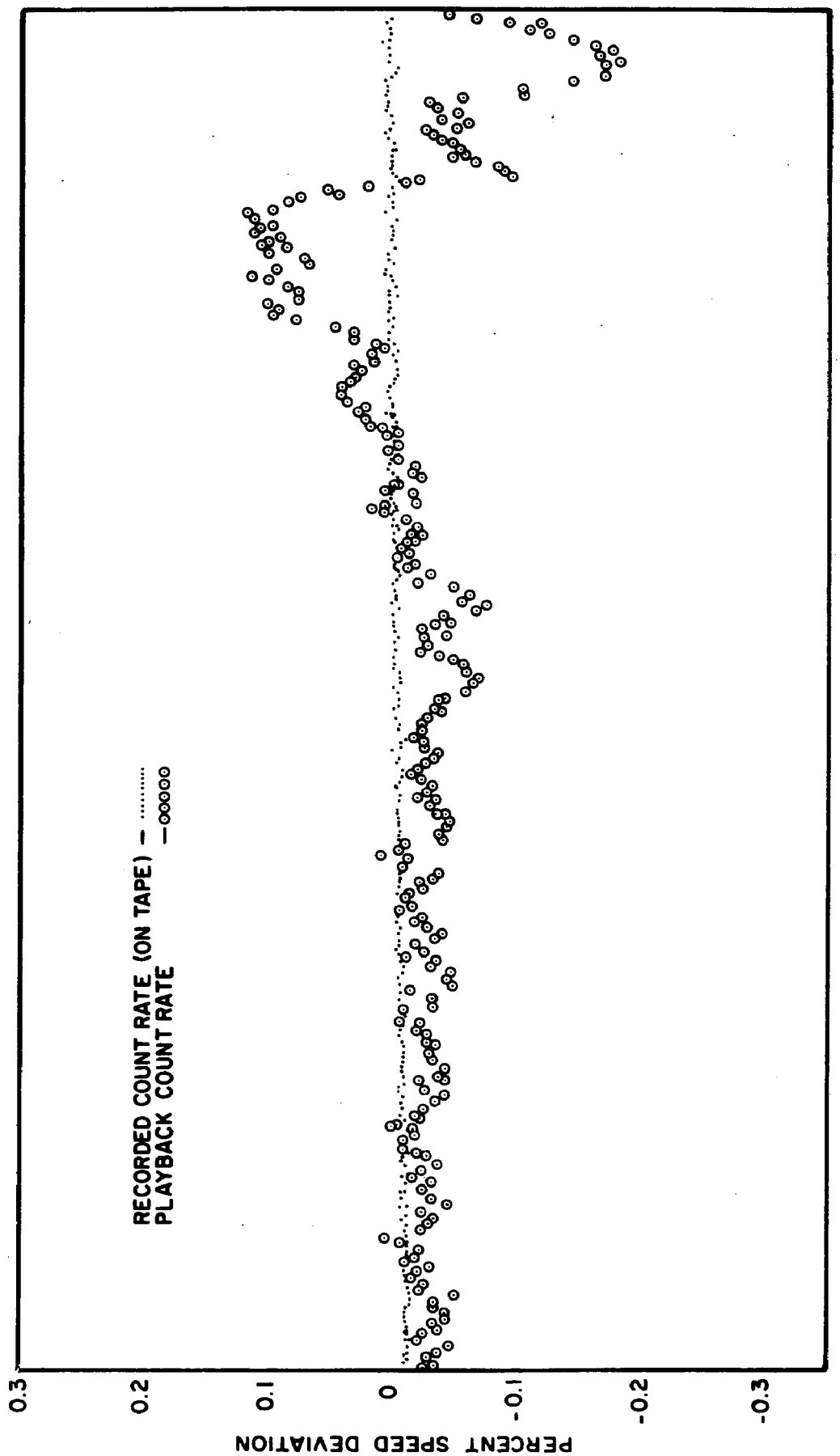


Figure 5.6 Wow and Flutter Measurement on Ampex 307 Tape Recorder.

$$\left(\frac{\text{Var}}{\text{Mean}}\right)_{\text{expt.}} = \frac{1}{1\pm\epsilon}\left(\frac{\text{Var}}{\text{Mean}}\right)_{\text{theory}} \pm \frac{\epsilon}{1+\epsilon}\left(\frac{\text{Var}}{\text{Mean}}\right)_{\text{theory}} + \frac{\epsilon^2}{1\pm\epsilon}\left(\frac{\text{Var}}{\text{Mean}}\right)_{\text{theory}} \tag{5.10}$$

$$= \begin{cases} \dfrac{1+2\epsilon+\epsilon^2}{1+\epsilon}\left(\dfrac{\text{Var}}{\text{Mean}}\right)_{\text{theory}} \Big|_{\text{sign}=+} \\ \dfrac{1-2\epsilon+\epsilon^2}{1-\epsilon}\left(\dfrac{\text{Var}}{\text{Mean}}\right)_{\text{theory}} \Big|_{\text{sign}=-} \end{cases}$$

The rms wow and flutter of the tape recorder was measured to be about 0.2%. The corresponding error from the above is

$$\begin{cases} \dfrac{1+.004+4\times10^{-6}}{1.002} \approx 1.002 \Rightarrow +0.2\% \\ \dfrac{1-.004+4\times10^{-6}}{.998} \approx .998 \Rightarrow -0.2\% \end{cases} \tag{5.11}$$

Thus, the expected variation in $\left(\frac{\text{var}}{\text{mean}}\right)_{\text{expt.}}$ due to time base inaccuracies is approximately 0.2%. Note that second order terms begin to enter the picture when ϵ becomes large.

C. Experimental Procedure

To insure that the reactor was operating in a suitable manner for data taking, the following experimental procedure was adopted. The objects of the procedure are to establish the reactivity during the experiment, obtain an optimum count rate, and make preliminary investigations into the character of the data.

The first step in the procedure is to eliminate the gamma ray background as much as possible. Since the Ford Nuclear Reactor

has been operated at high power for several years, this background can be very large. The major contribution to eliminating the gamma ray background was the unloading of the fuel elements which had been operated at high power and the reloading of the core with fuel elements which had never operated at above approximately ten watts. Further reduction in gamma ray background was achieved by moving the reactor core to the thermal column position where the activity from the structure is much lower since the reactor is seldom operated there and the maximum operating power at the thermal column position had been 100KW.

Not only was the maximum amount of gamma ray background removed, but, in the case of the BF_3 tube, the detector was also shielded with 1/4 inch of lead. The optimum operating voltages were determined as outlined in (5-A).

When the above conditions were met, the control rod was calibrated by the period method. The control rod calibration curves are shown in Figures 5.7 and 5.8. Appendix B contains the data for the control rod calibration in the BF_3 tube experiment. During control rod calibration, care was taken to assure that the reactor power did not rise to extreme levels.

Having the control rod calibrated, criticality was established by establishing a steady state with no (external) source present and at a fairly high level ($\sim$ 10 watts). This steady state was achieved by manipulating shim rods with the control rod at the upper limit. This enabled the control rod to determine the degree of subcriticality at which the measurements were to be taken.

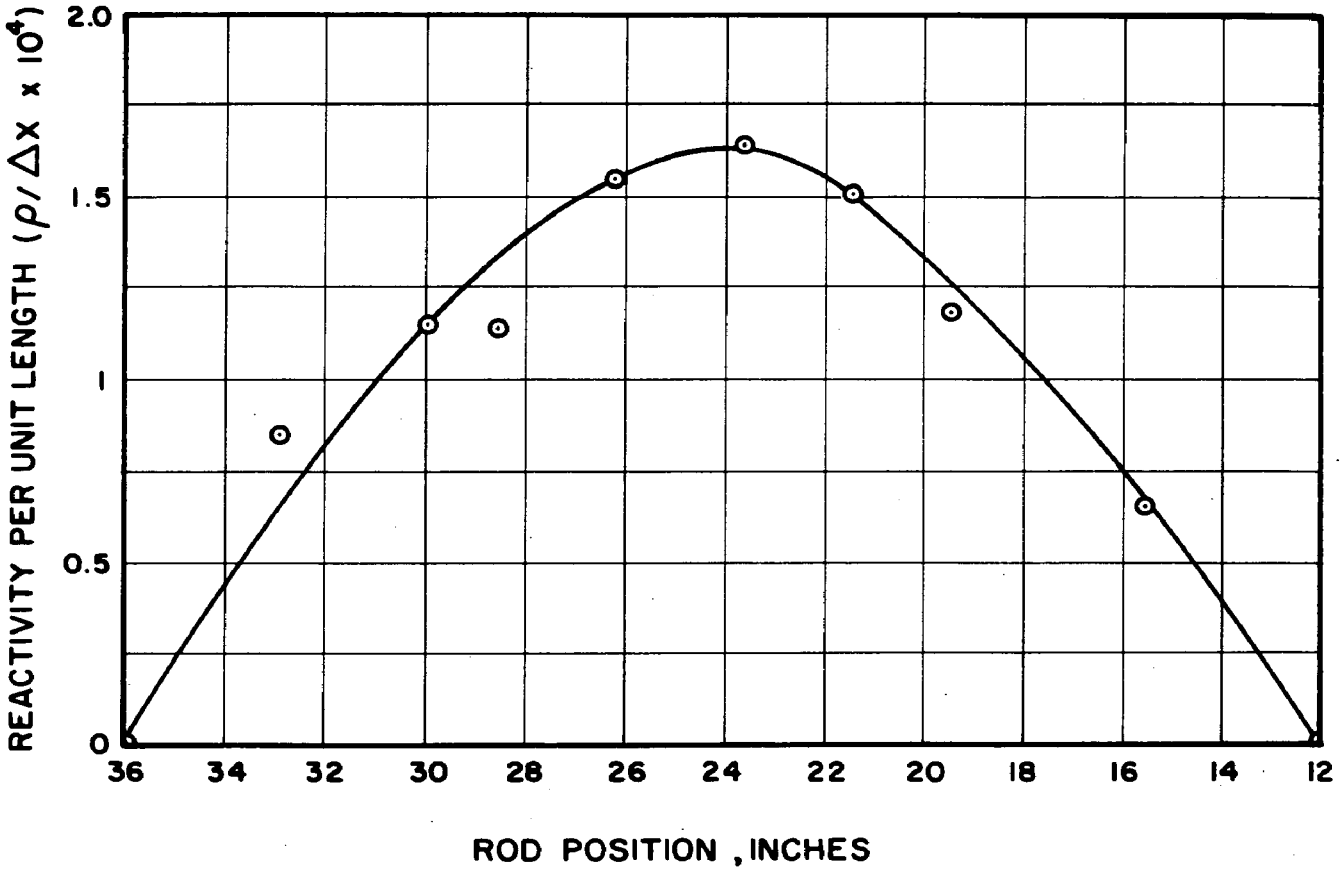


Figure 5.7 Differential Rod Calibration.

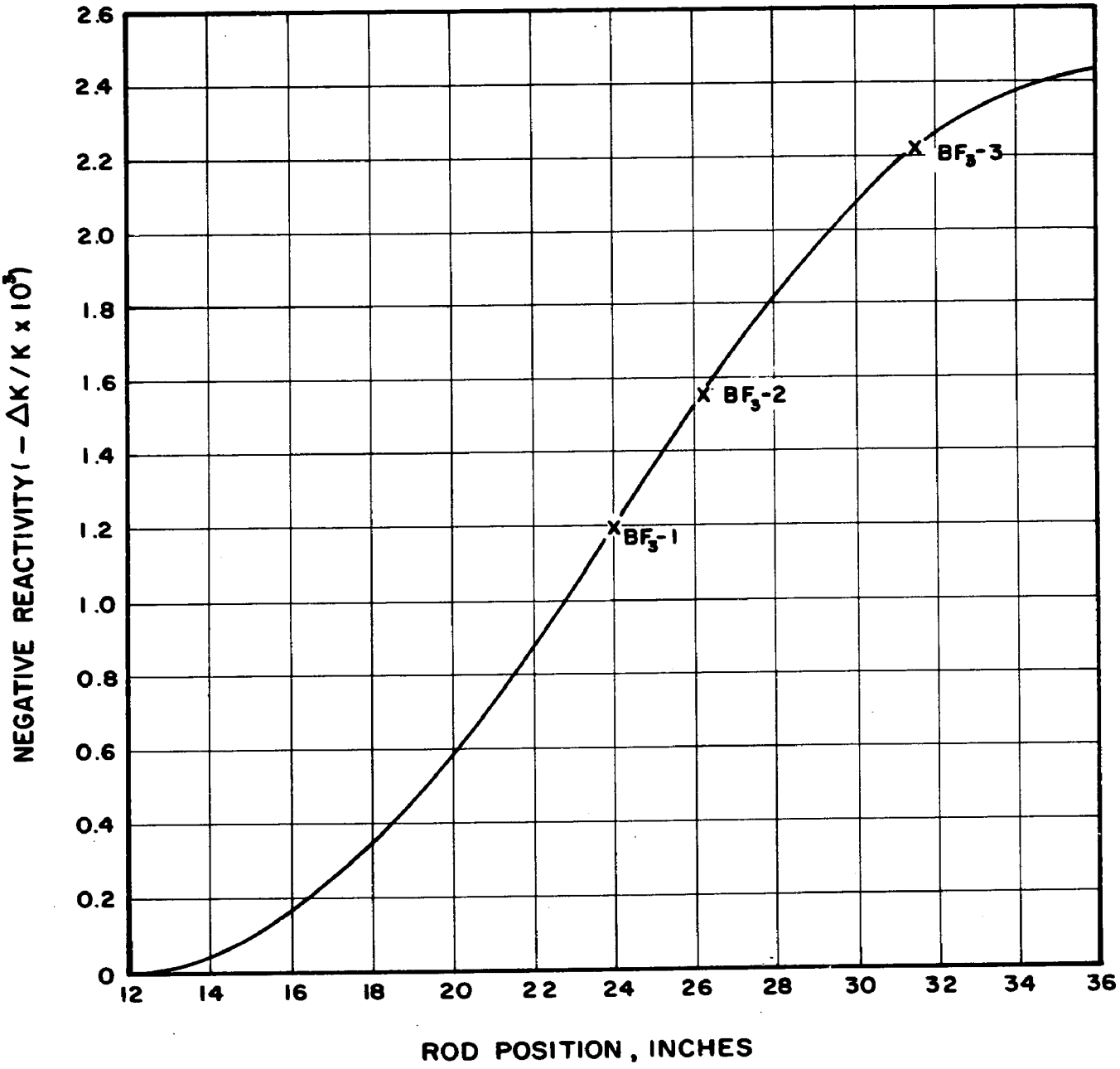


Figure 5.8 Integral Rod Calibration.

Having established criticality, the control rod was driven into the core an amount determined by the initial experimental reactivity which was selected at 50% insertion. The power level of the reactor was allowed to decrease until the detecting instrument was recording at approximately its optimum count rate. At this time, the neutron source was moved closer to the reactor until the count-rate leveled off. (Due to the fact that the source was hung into the pool from a crane, this operation had to be adjusted several times until the proper steady state was reached.) The count rate was monitered for more than thirty minutes in every instance to be certain that a steady state was achieved before any data was taken. At this point, the reactivity was determined, the optimum count rate was achieved, and a subcritical steady state was obtained.

As a final check on the operating condition, a series of fifty gates of 1/2 second duration were counted directly from the scaler. The ratio of variance to mean for this sample was determined using a desk calculator. If this ratio was significantly greater than one, the tape recorder was prepared for recording and a tape recording of reactor noise was then made.

The mechanical drive on the tape recorder tape transport system was warmed up prior to taking data so that the expansion of the friction drive from heating would not shift the time base at playback. The recording heads and drive were cleaned prior to recording.

During recording, the output of the pulse shaper driven by the nonoverloading amplifier was supplying signal to the tape recorder.

The output of the tape recorder was connected to the gate scaler and the gate was set at ten seconds. The number of counts over each of these ten second intervals was recorded by hand for later analysis to be sure that steady state had been achieved and that the distribution of these counts was as expected. Care was taken to be sure that spurious electrical transients were kept to a minimum during the experiment by avoiding use of light switches and not recording during the time when the IBM clocks reset. (The clock setting impulse in the building was suspected of introducing an impulse.)

After the recording was made, the control rod was moved to a new position and the procedure repeated.

The playback of the recorded pulses and subsequent data handling are discussed in Chapter VI.

VI. DATA ANALYSIS

The analysis of the data obtained in the experiment had to be made as efficient as possible since there was a large bulk of data to process. The transcription of data from the tape recording to IBM cards was accomplished in a semi-automatic fashion by modifying an IBM 024 card punch as described in Chapter IV. In this section, the procedure for obtaining the data on IBM cards is discussed under Data Handling and the processing of these cards is discussed under Estimation, theory and practice.

A. Data Handling

The tape recorder functions as a simulated Ford Nuclear Reactor. The tape record is considered to be a representative sample of reactor steady state. The transcription of data from the tape to IBM cards is accomplished by playing the tape recorder to the gate-scaler with the gate set at various gate times. When the gate scaler displays its count, this count is punched on an IBM card as described in Chapter IV. This process is continued until either a group of 600 gates for that gate time are punched or the tape has been run through four times whichever comes first. Harris[13] has shown that this number of measurements leads to satisfactory estimates of variance to mean ratio. For short gate times, the group of 600 gates was punched and for long gate times the tape was run four times and the number of gates punched was less than 600. The reasons for the above criterion were that Harris[13] showed that samples of this size led to an unbiased estimate of variance/mean and it was observed experimentally that larger samples did not significantly reduce

the spread in the data. Increasing the number of gates per data point would not have a large effect on the quality of the data, but would greatly increase the time required to transcribe data.

For the longest gate times, approximately 75 nonoverlapping gates per traverse of the tape could be measured. This number of gates leads to an unbiased estimate of the variance to mean ratio. By re-running the tape some new information is obtained for counts recorded in the gaps where counts were not previously recorded. In this way, a second traverse of the tape adds to the accuracy of the measurement. As the tape is traversed again somewhat more new information is added; however, the returns become less and less significant as the tape is re-run more times for the same gate time. The above criterion balances the small gains from further tape runs against the time required to make these runs.

When a quantity of data was punched, representing a spectrum of gate times and a total number of gates of about 40,000, the cards were edited for double punches and omitted punches on the IBM-101 card sorter. It was found that the average number of cards having such a defect was approximately one per 500 which represents an average number of defects per gate of one per 6,000 since there are twelve pieces of data per card.

After editing, the cards were arranged according to the input format of the calculational program, and the mean, variance, and variance to mean ratio was computed for each gate. These computations are listed in Appendix A.

B. Estimation

1. Estimation of Parameters - Theory

Since the parameters which enter the mathematical model for nuclear reactor stochastic processes enter in a nonlinear fashion, the estimation of these parameters must be accomplished by methods different from standard multiple linear regression. No direct technique exists for handling nonlinear estimation; thus, it is necessary to modify linear regression to deal with the problem. In this section, the method of nonlinear estimation will be developed by a geometrical argument which will then be translated to the analytical development. Having made an estimate of the parameters, it is necessary to assess the validity of these estimates. These procedures are also discussed in this section.

a) Geometrical Development

For identically distributed, independent, Gaussian random variables the "least squares" criterion provides maximum likelihood estimates of parameters. This is the criterion used in the nonlinear estimation procedure to be discussed. Geometrically, the least squares criterion estimates the point on a sub-space generated by the function of interest which is closest to the point in observation space determined by an experiment. This geometrical development is based on work by Box[6].

To illustrate this, consider an experiment for which there are three observations of the dependent variable corresponding to three observations of the single independent variable. This makes the observation space a three space. Consider the function of interest to be one

which has two parameters so that the function sub-space is a sub-surface in this three-dimensional space. (See Figure 6.1)

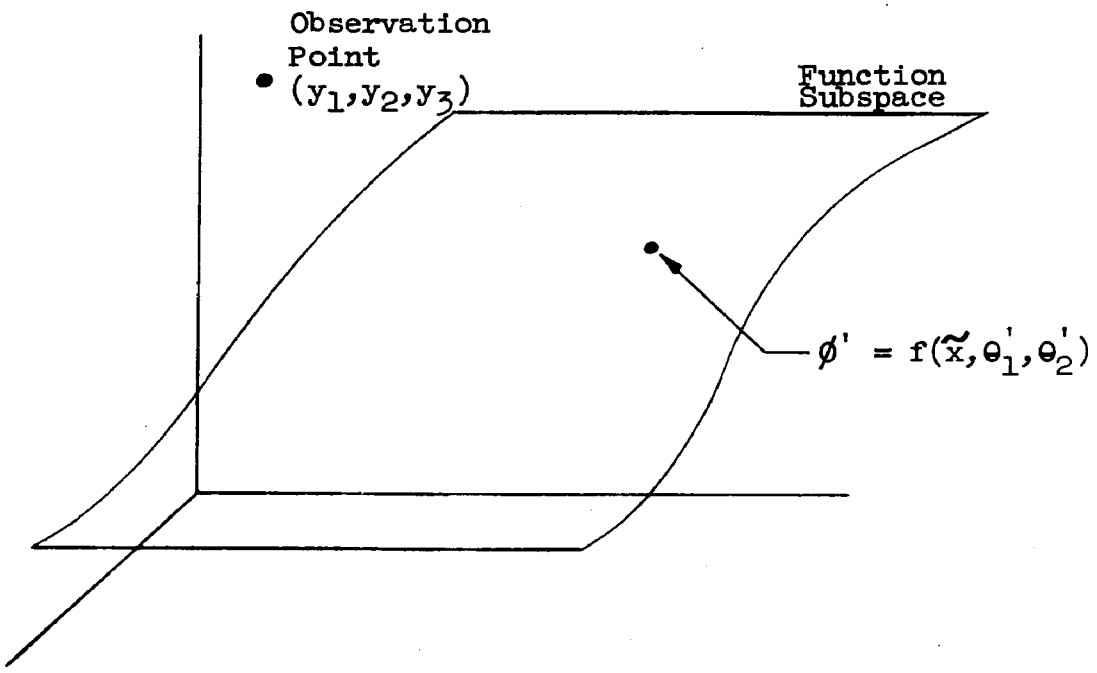


Figure 6.1. Observation Space

The following notation is used:

Function

$$\phi = f(x, \theta_1, \theta_2) \tag{6.1}$$

Observed values of independent variable

$$\tilde{x} = \tilde{x}_1, \tilde{x}_2, \tilde{x}_3 \tag{6.2}$$

Observed values of dependent variable

$$y = y_1, y_2, y_3 \tag{6.3}$$

Parameters

$$\theta=\theta_1,\theta_2 \tag{6.4}$$

Maximum liklihood estimate of parameters

$$\hat{\theta}=\hat{\theta}_1,\hat{\theta}_2 \tag{6.5}$$

Sum of squares

$$S=\sum_{i=1}^{3}(y_i-\phi_i)^2 \tag{6.6}$$

In order to generate the function subsurface, the parameters θ_1 and θ_2 are varied over their possible ranges in parameter space (see Figure 6.2).

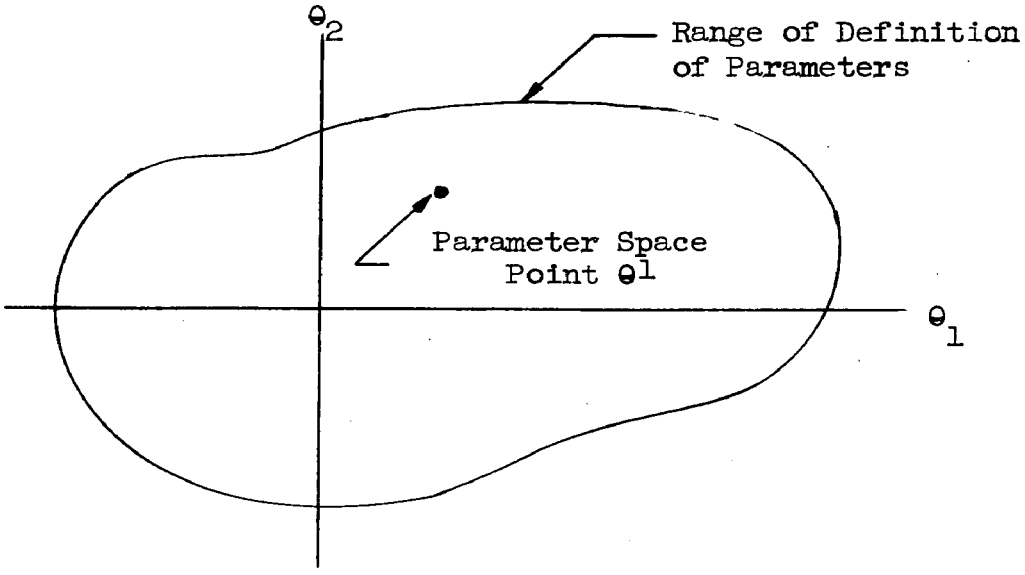


Figure 6.2. Parameter Space

Note that a particular point θ^1 in parameter space maps into a particular point ϕ^1 in the function sub-surface of observation space.

For identically normally distributed random variables, the least-squares criterion minimizes the distance between the observation point y and the function sub-surface ϕ. Thus, a point $\hat{\phi}$ is determined corresponding to $\hat{\theta}$ which are the maximum likelihood estimates of the parameters.

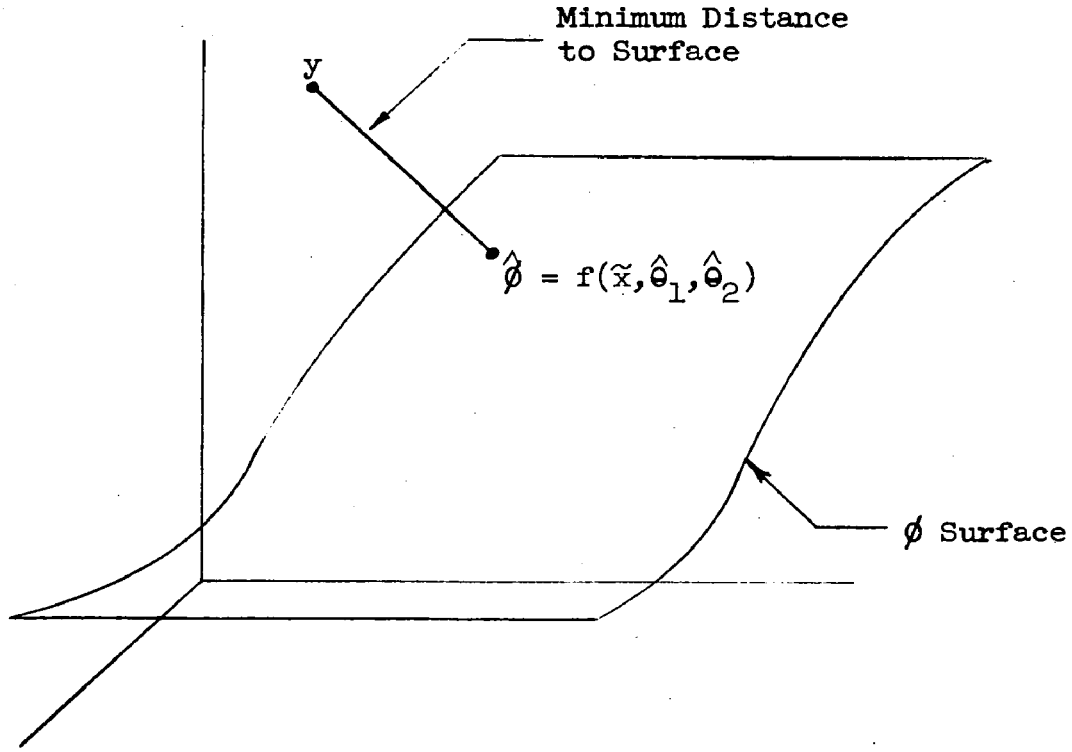


Figure 6.3. Observation Space

The algorithm used to find the points $\hat{\phi}$ and $\hat{\theta}$ is as follows:

1. Select initial parameters θ^o which determines an initial point ϕ^o in the function subsurface (see Figure 6.5).

2. Construct a tangent plane to the function subsurface at the point ϕ^o. (This corresponds to a linearization of the function about the point ϕ^o) (see Figure 6.4).

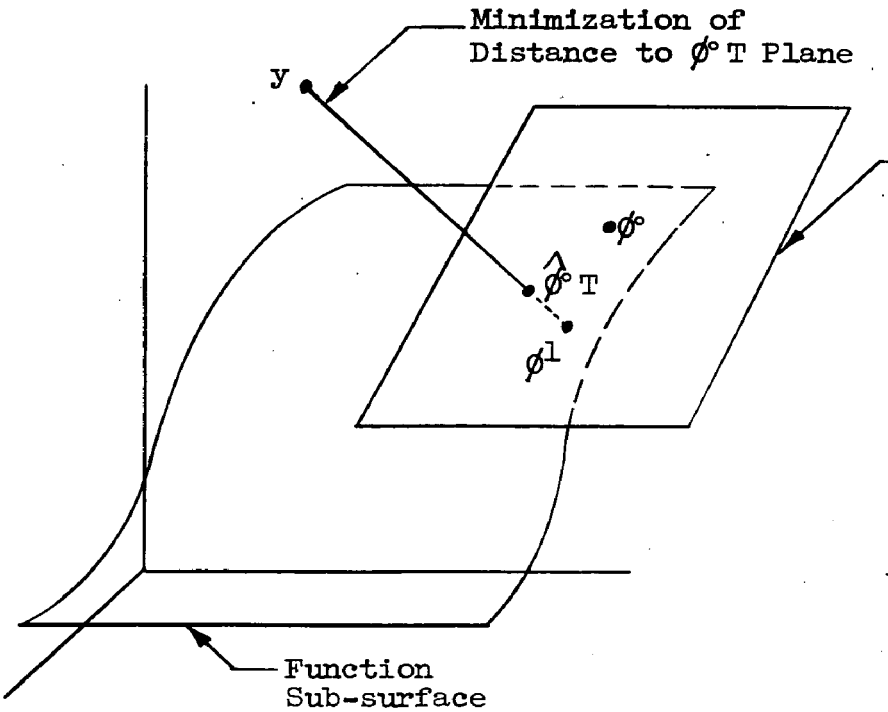


Figure 6.4. Observation Space

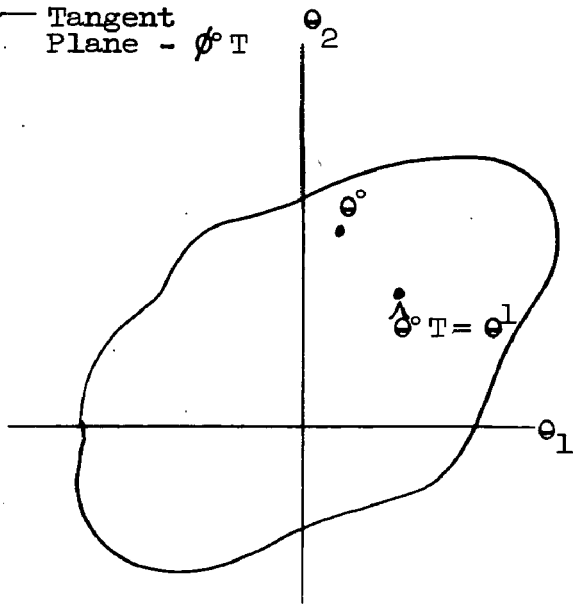


Figure 6.5. Parameter Space

3. Perform a multiple linear regression in the tangent plane ϕ^{oT} to find the point $\hat{\phi}^{oT}$ in the tangent plane which is a minimum distance from y. This determines new values of parameters $\hat{\theta}^{oT}$ in parameter space (see Figure 6.4).

4. Using values of $\hat{\theta}^{oT} = \theta^{1}$, find the corresponding ϕ^{1} in the subsurface. Now repeat setps 2, 3 and 4 replacing all superscripts (i) by (i + 1). Continue this until a convergent θ is determined.

5. Plotting the sum of squares S^{i} against θ^{i} we see that a minimum S is being approached. (see Figure 6.6)

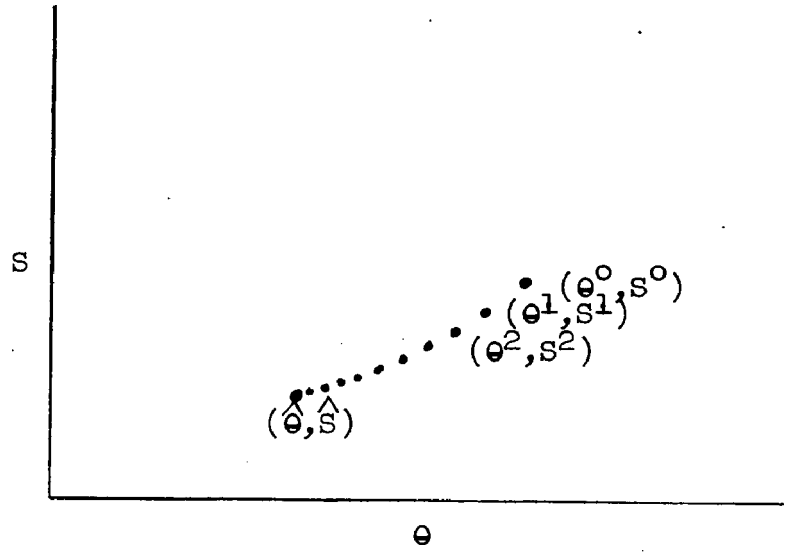


Figure 6.6. Sum of Squares vs. θ

Since the function subsurface may be in general nonlinear, the only claim that may be made for the parameters $\hat{\theta}$ which are computed by the above procedure is that they satisfy a local minimum for the length of the line $\overline{y - \emptyset}$. Certain questions concerning the confidence one may have in the parameters $\hat{\theta}$ determined by the above method must be answered. These are:

1. For a certain degree of confidence, over what range may the parameter estimates vary?

2. What is the relative confidence that can be placed in the determination of several parameters?

3. Is the local minimum sum of squares found by this method the true absolute minimum?

4. How successfully may one use linear methods for answering questions 1, 2 and 3?

The questions raised are answerable by applying methods of statistical analysis discussed below.

1. A confidence region can be determined which defines a contour surrounding the least squares estimates of the parameters. The formulation is based on an approximation to the function ϕ denoted ϕ^T which is linear in the parameters. If the approximation were correct and the errors were independently and identically normally distributed, the confidence region would include the true values of the parameters with a confidence coefficient of $(1 - \alpha)$ where α is the significance level of the Fisher F-distribution at the appropriate degrees of freedom.

The sum of squares on the confidence contour is generated from

$$S = S_m \left(1 + \frac{P}{N-P} F_{P,N-P}(\alpha)\right) \tag{5.7}$$

where S = contour sum of squares

S_m = minimum sum of squares

P = number of parameters

N = number of observations

F = Fisher's F-distribution value

α = significance level

The geometrical significance of this confidence contour is as follows:

Consider the observation space. The value of $\hat{\phi}$ determined by least squares lies in the function subsurface. Construct a tangent plane to this subsurface ϕ^T. Now, any ϕ^T in the tangent plane will be a greater distance from y than $\hat{\phi}^T$. Applying the F-test, the contours at fixed distances from y in the ϕ^T plane are swept out. Call these contours F^T. (see Figure 6.7)

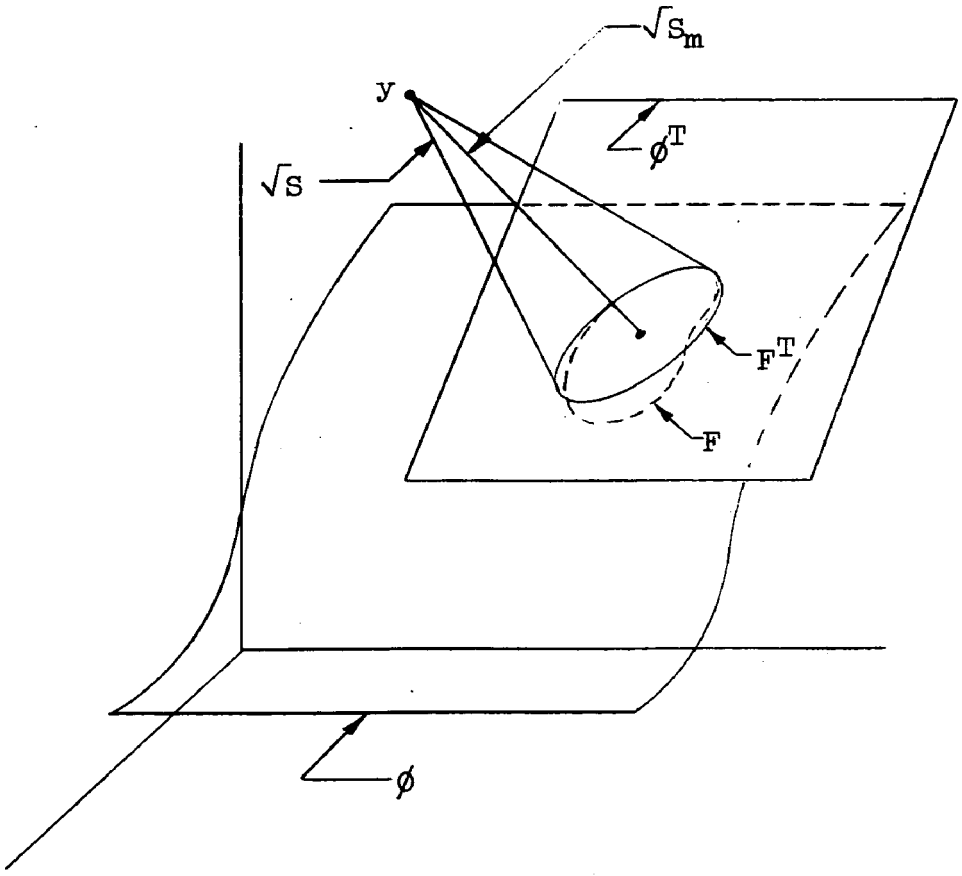


Figure 6.7. Observation Space

This contour also sweeps out a contour in the linearized parameter space θ^T which will be an ellipse. In general, however, the projection of F^T on the function subsurface ϕ, called F, will not be an ellipse, but will be some non-ellipsoidal contour. Likewise, the contour in the linearized parameter space θ^T will be an ellipse, while the contour in parameter space will be non-ellipsoidal (see Figures 6.8 and 6.9).

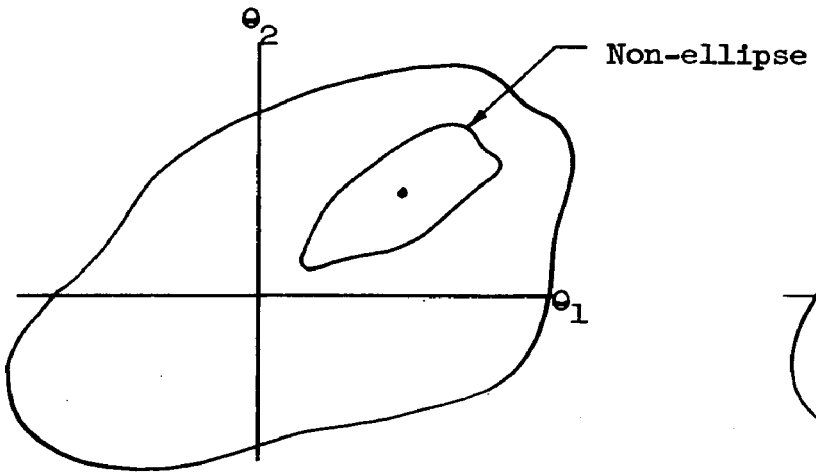


Figure 6.8. Parameter Space

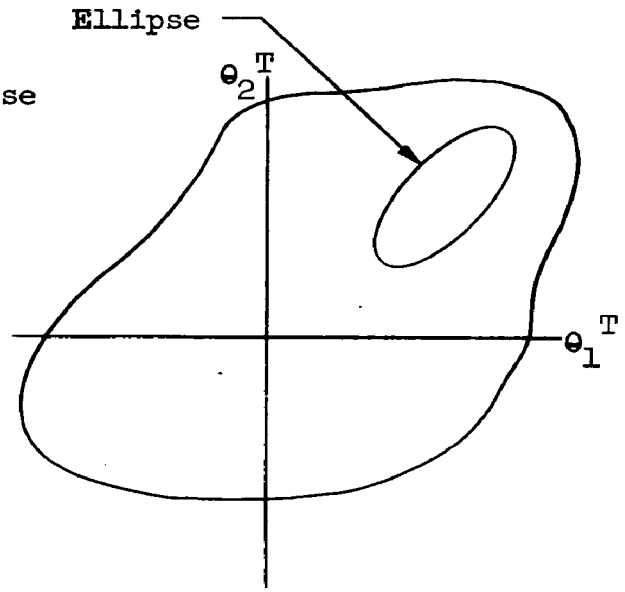


Figure 6.9. Linearized Parameter Space

The contours found in the ϕ^T tangent plane are used to establish the region over which the parameters may be varied for a specified confidence in their estimation.

2. The relative confidence which one can place in the estimation of parameters can be judged by the elongation of the ellipse in normalized, linearized parameter space. That is, all of the parameters are given the same dimension by a normalizing factor so that if the two parameters θ_1 and θ_2 are equally well determined, the confidence contour in linearized parameter space will be a circle. If one parameter or one linear combination of parameters is better determined than another, the contour in parameter space will become elliptical with the poorest determined parameter or linear combination of parameters having the largest projection of the ellipse and the most

well determined parameter or linear combination of parameters having the smallest projection of the ellipse.

3. Determining whether the distance $\sqrt{S_m}$ from y to $\hat{\phi}$ is the true absolute minimum distance from y to the ϕ subsurface is in principle only possible by calculating the sum of squares corresponding to each point on the surface. This task is a near impossibility in most cases, thus alternative methods are employed.

One method of gaining information about other possible minima is to re-do the problem several times, each time starting from a different initial guess of parameters and seeing if we always return to the same minimum; or, if another local minimum is found, the values of the sums of squares are compared to ascertain which is better.

Another method of attacking this problem is to generate larger and larger contours in the tangent ϕ^T plane about the point $\hat{\phi}^T$ and calculate the sum of squares along the projections, F, of these contours on the ϕ subsurface, looking for a sum of squares smaller than $\hat{S}$.

If by several applications of the above tests there is a consistent preference for one minimum, one may infer with some degree of certainty that that is the true minimum.

4. Information may be gained concerning the applicability of linear methods to question 1, 2 and 3 by comparing the contour in parameter space to the elliptical contour in linearized parameter space. If the two contours are fairly similar, one may infer that the function is approximately linear in the parameters in the region of $\hat{\phi}$ and thus these linear methods are (to some approximation) applicable. If the

two contours are highly dissimilar, one is suspect of the linear methods for dealing with questions 1, 2 and 3.

b) Analytical Development

The following will be a fairly terse analytical development of the same problem dealt with in the geometrical development with the exception that now generalizations to k independent variables, n observations and p parameters will be made. In this section, little descriptive material will be included with the thought that the preceding geometrical development sufficiently illuminates the concepts.

Mathematical Model

$$\phi = f(x_1, \ldots x_k ; \theta_1, \ldots \theta_p) \tag{6.8}$$

Experimental Data

Observed values of dependent variable

$$y = \begin{pmatrix} y_1 \\ \vdots \\ y_n \end{pmatrix} \tag{6.9}$$

Corresponding values of independent variables

$$x = \begin{pmatrix} x_{11} \cdots x_{1K} \\ \vdots \\ x_{n1} \cdots x_{nK} \end{pmatrix} \tag{6.10}$$

Computed Values

$$\phi = \begin{pmatrix} f_1 \\ \vdots \\ f_n \end{pmatrix} = \begin{pmatrix} f(x_{11}, \cdots x_{1K} ; \theta_1, \cdots \theta_p) \\ \vdots \\ f(x_{n1}, \cdots x_{nK} ; \theta_1, \cdots \theta_p) \end{pmatrix} \tag{6.11}$$

Algorithm

Linearization by first-order Taylor's expansion

$$f^T=\begin{pmatrix} f_1^T \\ \vdots \\ f_n^T \end{pmatrix}=\begin{pmatrix} f_1^\circ+(\theta_1-\theta_1^\circ)\left(\frac{\partial f_1}{\partial\theta_1}\right)^\circ+\cdots+(\theta_p-\theta_p^\circ)\left(\frac{\partial f_1}{\partial\theta_p}\right)^\circ \\ \vdots \\ f_n^\circ+(\theta_1-\theta_1^\circ)\left(\frac{\partial f_n}{\partial\theta_1}\right)^\circ+\cdots+(\theta_p-\theta_p^\circ)\left(\frac{\partial f_n}{\partial\theta_p}\right)^\circ \end{pmatrix} \tag{6.12}$$

Definitions

$$\theta^\circ=\begin{pmatrix} \theta_1^\circ \\ \theta_p^\circ \end{pmatrix} \tag{6.13}$$

$$f^\circ=\begin{pmatrix} f_1^\circ \\ \vdots \\ f_n^\circ \end{pmatrix} \tag{6.14}$$

$$D_o=\begin{pmatrix} \left(\frac{\partial f_1}{\partial\theta_1}\right)^\circ & \cdots & \left(\frac{\partial f_1}{\partial\theta_p}\right)^\circ \\ \vdots & & \\ \left(\frac{\partial f_n}{\partial\theta_1}\right) & \cdots & \left(\frac{\partial f_n}{\partial\theta_p}\right)^\circ \end{pmatrix} \tag{6.15}$$

$$f^T-f^\circ=D_o(\theta-\theta^\circ) \tag{6.16}$$

OR

$$f^T-f^\circ=D_o\beta^\circ \tag{6.17}$$

Multiple Regression

Fit (f^T-f°) to $(y-f^\circ)$

$$D_o'D_o\beta^\circ=D_o'(y-f^\circ)$$
$$D_o'D_o\beta^\circ=D_o'\omega^\circ$$
$$\beta^\circ=(D_o'D_o)^{-1}D_o'\omega^\circ \tag{6.18}$$

Iteration Formula

$$\theta^{i+1} = \theta^{i} + \left(D_i' D_i\right)^{-1} D_i' \omega^{i} \tag{6.19}$$

2. Estimation of Parameters - Practice

The application of the theory of nonlinear estimation to the problem of estimating the 2n+2 parameters appearing in the point reactor stochastic process model is accomplished with the use of the IBM 704 computer (where n is the number of delayed groups). The program used to perform the indicated operations is a modification of a program written for nonlinear estimation by the mathematics and applications department of International Business Machines Corporation (2, 3, 4, 5).

The function required to be fit to the data is

$$\phi(\tau) = \sum_{i=1}^{n+1} K_i \left[1 - \frac{1 - e^{-\alpha_i \tau}}{\alpha_i \tau} \right] \tag{6.20}$$

Here, the parameters α_i enter nonlinearly and the range of τ is over four decades in time (0.001 sec - 10 sec). The magnitude of the α_i varies by a factor of 10^4.

To aid convergence it is best to make the original parameter estimates as close as possible to the "true values" of the least-squares parameters. To do this, parametric curves function

$$\phi'(\tau) = 1 - \frac{1 - e^{-\alpha\tau}}{\alpha\tau} \tag{6.21}$$

were generated on the '704.' These are plotted on 4-cycle semi-log paper for small τ and large α in Figure (6.10) and on linear paper for large τ and small α in Figure (6.11).

Comparing these curves to the experimental points, the approximate values of the parameters α_i may be estimated along with the approximate values of the K_i's. This estimation procedure is accomplished with the theoretical values of α_i and K_i corresponding to the experimental conditions. That is, for particular Δk, ℓ, ϵ, λ_i, and β_i, particular values of K_i and α_i are determined. Since λ_i's and β_i's are well known, it is certainly most desirable to have the initial estimates of parameters in the range given by theoretical considerations. Using these considerations, a best "eye-fit" to the data can be made for the original parameter estimates.

The algorithm discussed in section VI-B will successfully converge upon the "least squares" parameters as long as the D'D matrix (Equation 5.18) is well conditioned. The conditioning of the matrix is a measure of how near the matrix is to being a singular matrix. If there are approximate linear dependencies existing, the matrix will be nearly singular and the digital computer will have difficulty in matrix inversion. This difficulty was encountered several times, and the regression sum of squares diverged instead of converged for cases where poor conditioning was indicated. To test the conditioning of the moment matrix, D'D, the eigenvalues of the moment matrix were calculated prior to entering the iteration stages of the program. A large ratio of the largest to the smallest eigenvalue was indicative of poor conditioning. The conditioning can be changed by adjusting the parameter estimates,

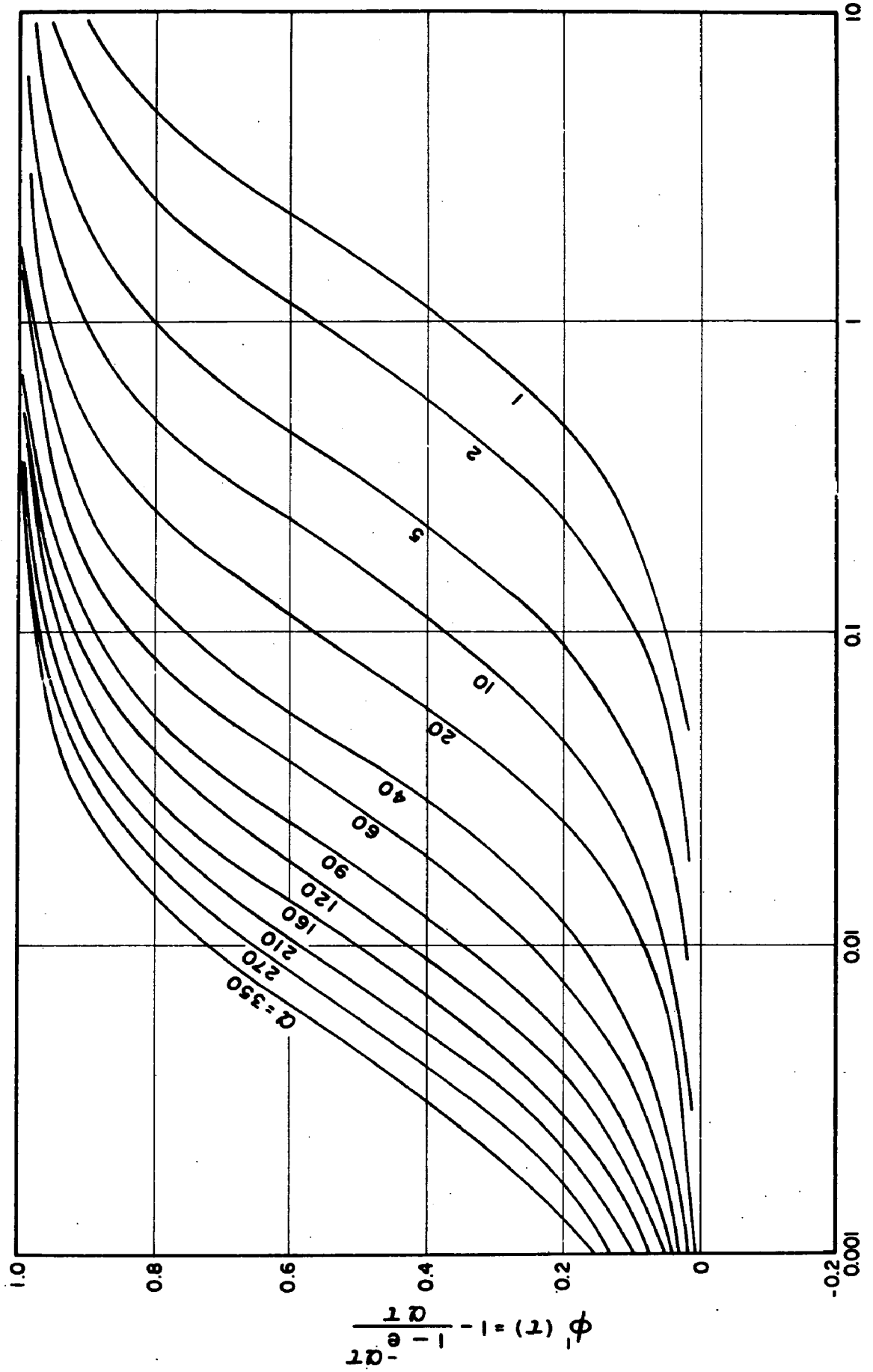


Figure 6.10. Parametric Curves for $\phi^1(\tau)$; $1 \leq \alpha \leq 350$

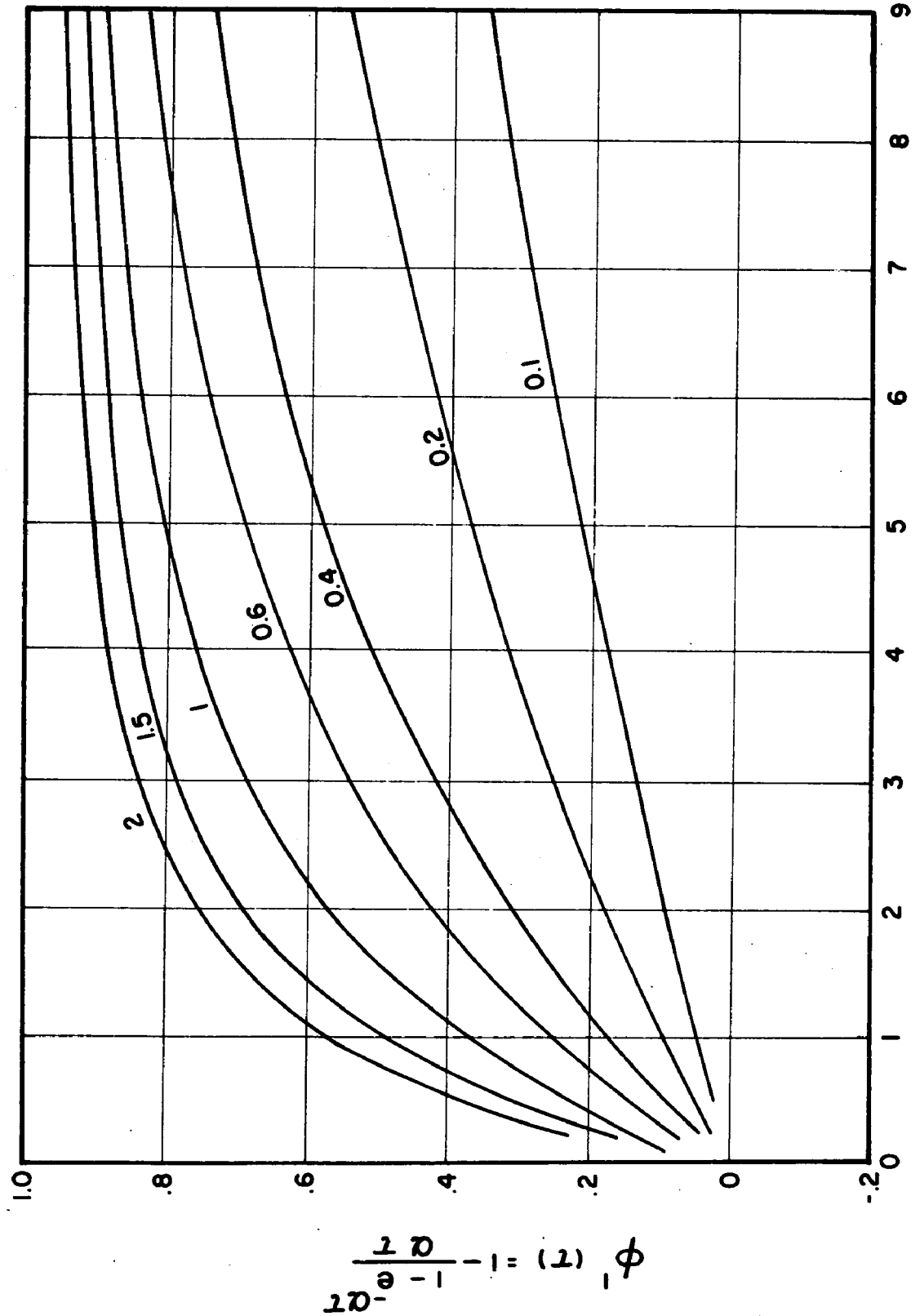


Figure 6.11. Parametric Curves for $\phi^{-1}(\tau)$; $0.1 \leq \alpha \leq 2$

adjusting the size of increments used in finding partial derivatives, and reformulating the functional expression.

Interpolation

A modification of the estimation procedure is termed interpolation. If it is found that iteration is successful in reducing the sum of squares so that the slope is greater than ϵ, we suspect that it will be profitable to continue investigating the function in this direction so we activate "interpolation." The algorithm for interpolation is as follows:

1) Let $\underline{\theta}_0$ and $\underline{\theta}_1$ be the vector values of the parameters before and after iteration respectively. Call the corresponding sums of squares S_0 and S_1. Divide the distance between $\underline{\theta}_0$ and $\underline{\theta}_1$ by two and call this point $\underline{\theta}_{\frac{1}{2}}$ with a sum of squares $S_{\frac{1}{2}}$.

2) $S_{\frac{1}{2}}$ is compared to S_1. a) If $S_{\frac{1}{2}}$ is less than or equal to S_1, the interval $\underline{\theta}_{\frac{1}{2}} - \underline{\theta}_0$ is divided by two and $S_{\frac{1}{4}}$ calculated for $\underline{\theta}_{\frac{1}{4}}$. b) If $S_{\frac{1}{2}}$ is greater than S_1, $\underline{\theta}_2$ is calculated along with S_2.

3) Either procedure a) or b) is followed until the sum of squares increases, in which case a Lagrangian fit to the last three points is made or until it is determined (by the program) that the gain by interpolation is too small, in which case the last $\underline{\theta}$ is kept along with the last S.

The non-linear estimation program follows the general outline given for the theory of nonlinear estimation. The results obtained are listed for each experimental run in the "Results" section showing the parameters estimated, the minimum sum of squares obtained, the confidence regions, the relative confidence in parameters, and the degree of non-linearity in which the parameters enter.

VII. RESULTS

A. Experimental Results

The experimental points obtained for the three runs with the BF_3 tube (designated BF_3-1, BF_3-2, BF_3-3) are shown in Figures (7.1), (7.2) and (7.3). The data from which these points are plotted is tabulated in Appendix A. Figure (7.4) shows the experimental points for the fission chamber run. The data for this run is also tabulated in Appendix A.

The fitted curves which are the least squares fit to the data are shown along with the contribution to these curves from each term of an equivalent two-delay group mathematical model. Note that the contributions of each term are not shown for the fission chamber experiment since theory and experiment were in considerable disagreement on this experiment.

The data and curve for the fission chamber experiment are included here for illustrative purposes. The effect of having a less-sensitive detector is shown clearly by comparing the value of the ordinates for the fission chamber experiment to those for the BF_3 tube experiments. The maximum value of V/M for the fission chamber experiment was not enough different from one to adequately show the effect of correlation. That is, in this experiment, the accidental terms contributed a significantly large amount to the result and thus the estimation of reactor parameters, which are a function of the correlated terms, was insufficiently accurate.

Obviously, a detector which is only slightly less efficient than the fission chamber used would show no correlation at all. Thus,

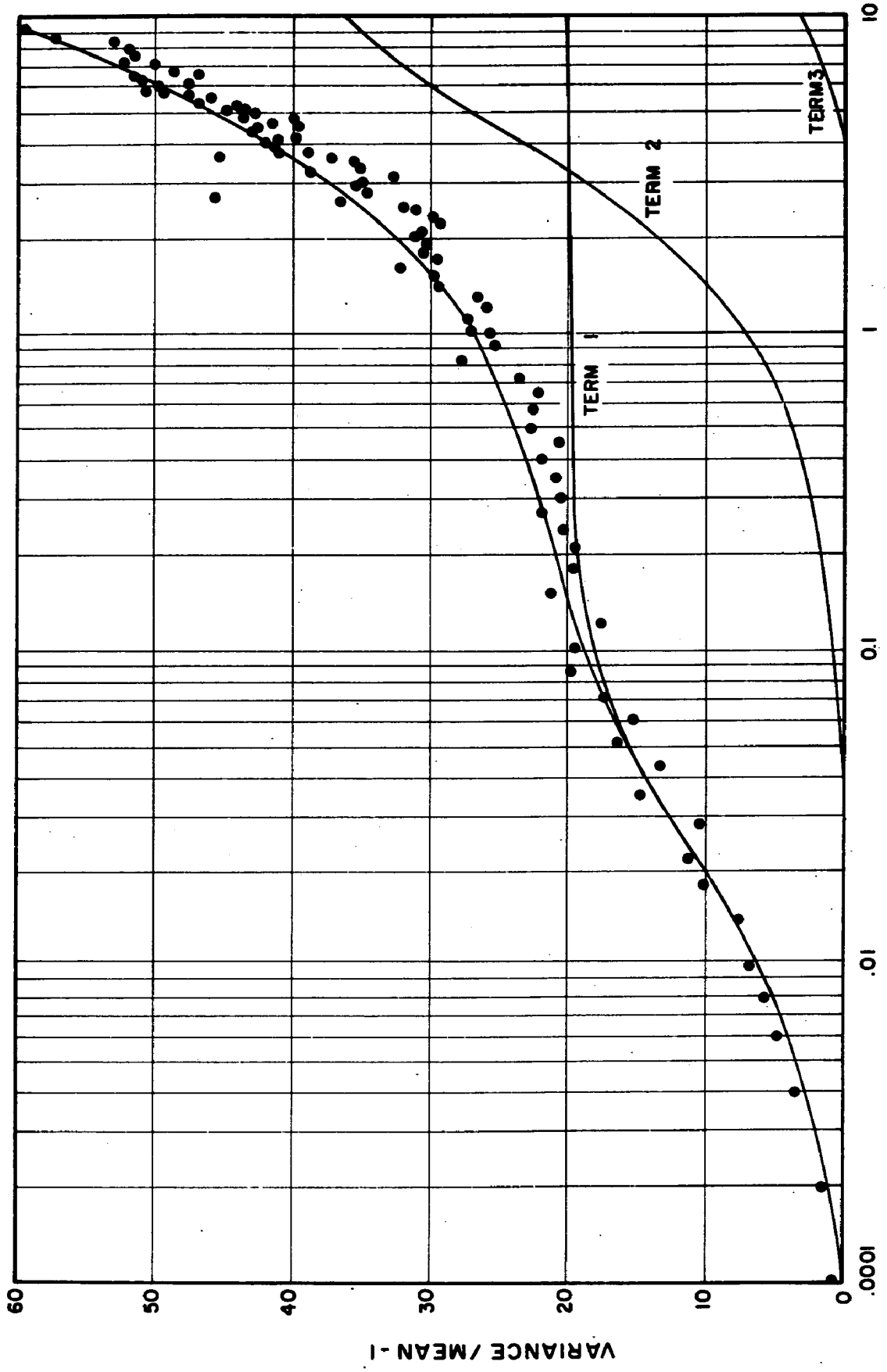


Figure 7.1. Data and Curve Fit
Run: BF_3 - 1

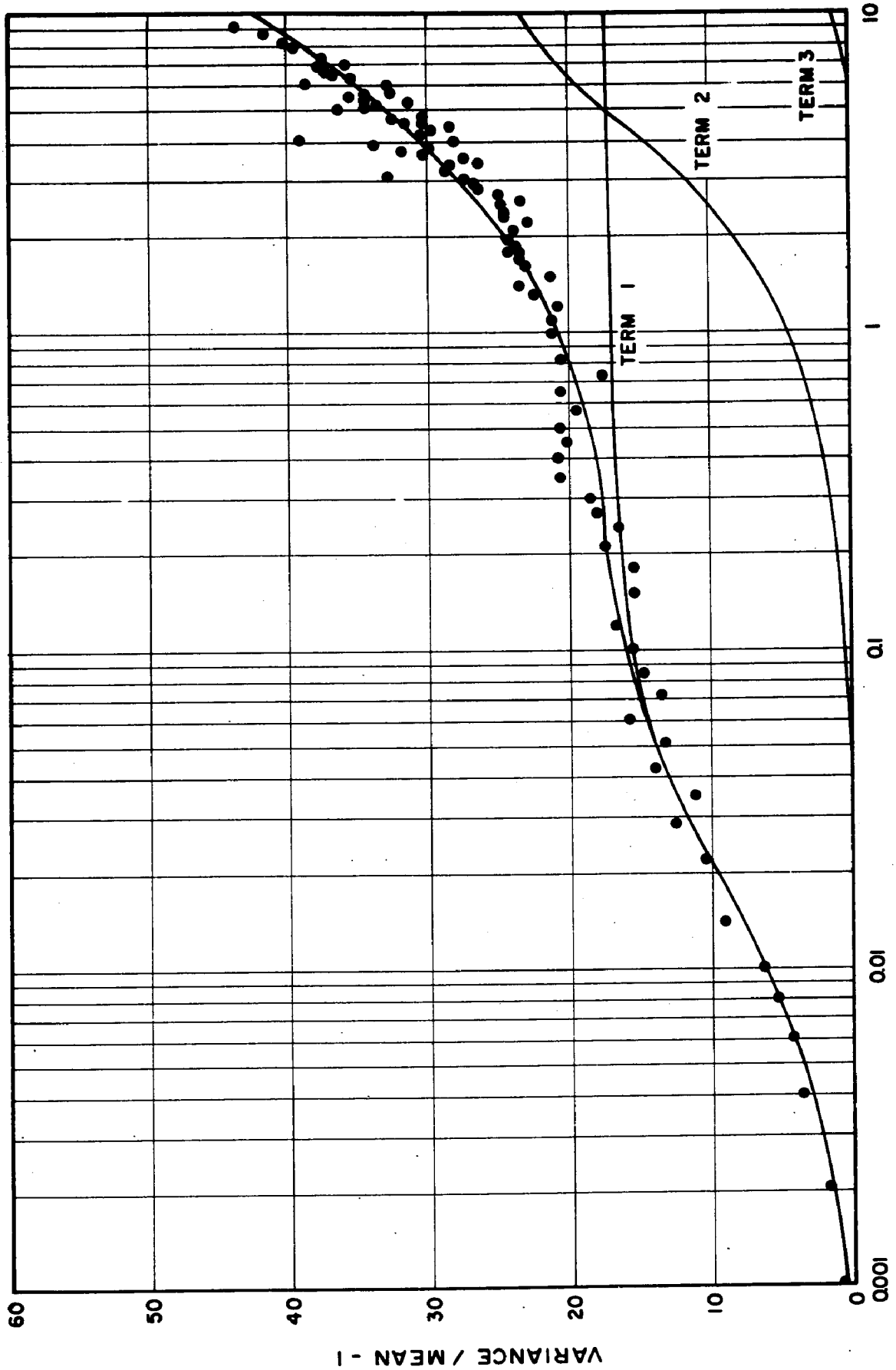


Figure 7.2. Data and Curve Fit
Run: BF_3 -2

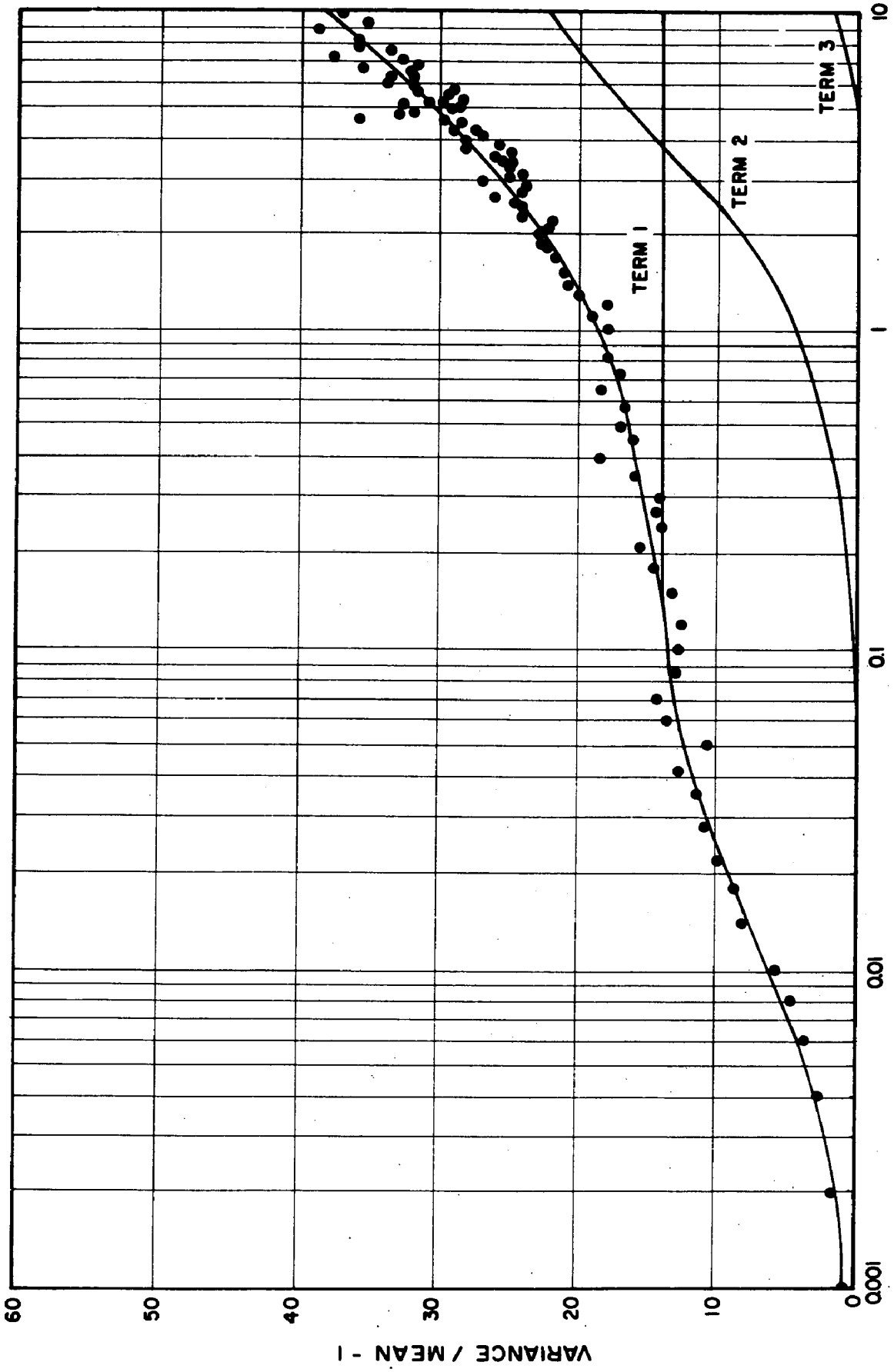


Figure 7.3. Data and Curve Fit
Run: BF_3 -3

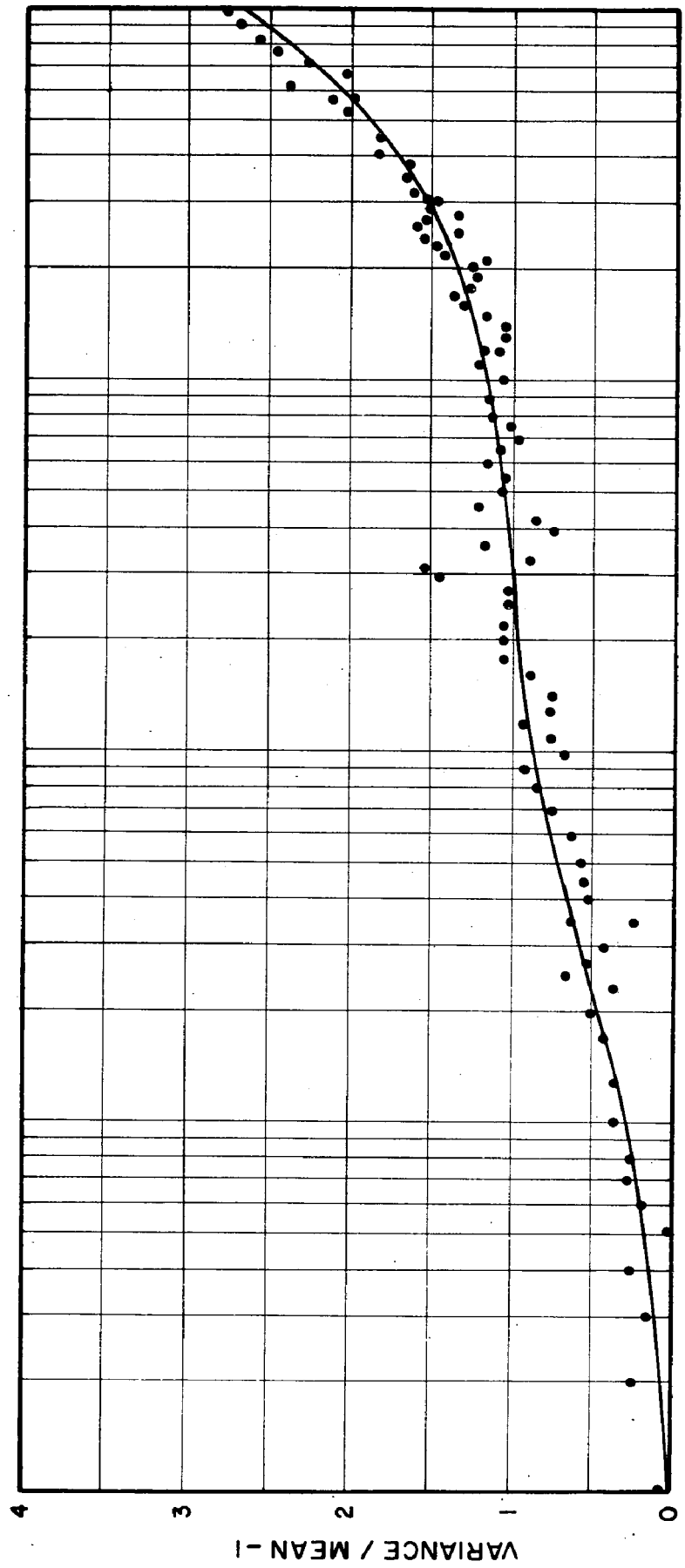


Figure 7.4. Data and Curve Fit
Run: Fission Chamber

the comparison of the results of the fission chamber experiment with the BF_3 tube experiments illustrates the need for a high efficiency detector. The problems associated with using a high efficiency detector are discussed in Chapter V.

The three BF_3- tube runs shown were all accomplished with the reactor operating in the same operating configuration with the exception that the reactivity was changed from run to run. Run # BF_3-1 had the greatest multiplication, BF_3-2 had a somewhat lower multiplication and BF_3-3 had a still lower multiplication.

Figure (7.5) shows a comparison between the fitted curves for these three experiments which illustrates clearly the effect of multiplication on the magnitude of the correlated terms. As the multiplication increases the correlation increases. This is in accordance with the mathematical model.

Note also that as multiplication is increased the curve becomes less flat in the region between where the statistic V/M is being controlled by prompt neutrons and the region where it is being controlled by prompt and delayed neutrons. That is, as multiplication is increased, the prompt and delayed neutron contributions become less distinguishable. This is also in accord with the mathematical model which predicts this behavior.

B. Mathematical Model (general)

The mathematical model developed in Chapter III is rewritten here for convenience (Equation 7.1).

$$\frac{V}{M}(T) = 1 + \sum_{i=1}^{n+1} K_i \left[1 - \frac{1 - e^{-\alpha_i T}}{\alpha_i T} \right] \qquad (7.1)$$

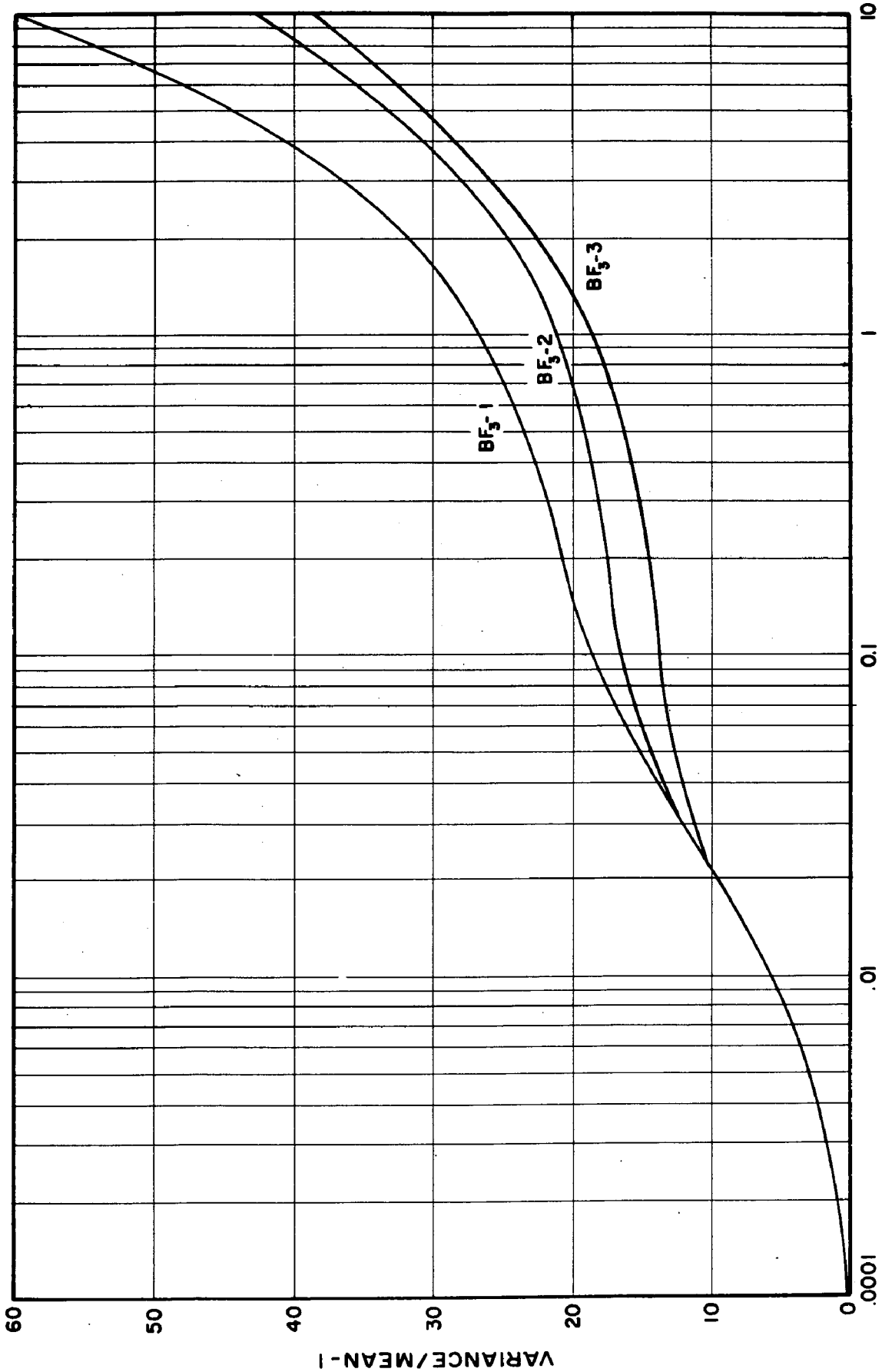


Figure 7.5. Comparison of BF_3 Experiments Fitted Curves

In attempting to estimate the parameters in this model which are best least square estimates it is necessary to employ the techniques of nonlinear estimation which are outlined in Chapter VI. One of the important points which must be decided is what value of n to use.

It was at first decided to use $n = 6$ which is the number of physical delay groups measured by Keepin and Wimett[14] for example. However, when $n = 6$ was used in the mathematical model it was found that either the computation would not converge, or, if it did converge, that the values of the parameters K_i and α_i obtained bore no resemblence to the theoretical parameters. It was found that one of the primary reasons for divergence was that the moment matrix, D'D, used in the regression analysis was poorly conditioned and the algorithm no longer was valid. Erroneous results were produced even when the analysis converged because the data was insufficient to correctly predict fourteen parameters.

Several other values of n were tried. It was found that $n = 3$, 4 or 5 gave the same result as $n = 6$ and were therefore unsatisfactory.

On the other hand, it was found that $n = 1$ converged but that the parameter estimates for the one equivalent delay group were not at all in correspondence with the parameters used in the usual one delay group model. This result is obtained because the one delay group model is not a good approximation to the many group model. Firstly, the one delay group model is not capable of preserving some of the characteristic sums of the six group model. That is, for the usual

one group model

$$\beta = \sum_{i=1}^{6} \beta_i \qquad \lambda\beta \neq \sum_{i=1}^{6} \lambda_i \beta_i$$

$$\frac{\beta}{\lambda} = \sum_{i=1}^{6} \frac{\beta_i}{\lambda_i} \qquad \frac{\beta}{\lambda^2} \neq \sum \frac{\beta_i}{\lambda_i^2} \tag{7.2}$$

where β is the equivalent one group fraction and λ is the equivalent one group decay constant, β_i is the fraction of the $i^{\underline{th}}$ precursor and λ_i is the decay constant of the $i^{\underline{th}}$ percursor. Thus, we see that the mathematics of the one group model are somewhat inadequate.

Also, the one-group model is especially poor in describing reactor behavior in the high frequency (short time) region which is the region in which the measurements were made. We see then, that the one delay group model is incapable of predicting the experimental results, so we are left with only the two group model (n = 2).

All comparisons between theory and experiment which will be given here will use the two group model. For this reason a discussion of this model follows.

C. Mathematical Model (2-group)

The two group model discussed here is based on the work of Skinner and Hetrick[21] and Skinner and Cohen[22]. These authors showed that reduced group constants Ai and Λi which satisfy the

asymptotic behavior of the transfer function must satisfy the relationships

$$\sum_{i=1}^{n} A_i = \sum_{i=1}^{6} a_i \qquad \sum_{i=1}^{n} A_i \Lambda_i = \sum_{i=1}^{6} a_i \lambda_i$$

$$\sum_{i=1}^{n} \frac{A_i}{\Lambda_i} = \sum_{i=1}^{6} \frac{a_i}{\lambda_i} \qquad \sum_{i=1}^{n} \frac{A_i}{\Lambda_i^2} = \sum_{i=1}^{n} \frac{a_i}{\lambda_i^2} \tag{7.3}$$

where Ai and Λi are the relative abundance and decay constant for the i^{th} reduced group; a_i and λ_i are the relative abundance and decay constant for the i^{th} physical delay group.

Obviously Equations(7.3) can be uniquely satisfied by equivalent two group constants since we have four equations and four group constants. If

$$\gamma_0 = \sum_{i=1}^{6} a_i$$

$$\gamma_1 = \sum_{i=1}^{6} a_i \lambda_i \tag{7.4}$$

$$\gamma_{-1} = \sum_{i=1}^{6} \frac{a_i}{\lambda_i}$$

$$\gamma_{-2} = \sum_{i=1}^{6} \frac{a_i}{\lambda_i^2}$$

then the two group constants are given by

$$\Lambda_{1,2} = C \pm \sqrt{C^2 - D}$$

$$A_{1,2} = \frac{1}{2}\left[\gamma_0 \pm \left(\frac{\gamma_1 C - \gamma_0 D}{\sqrt{C^2 - D}}\right)\right] \tag{7.5}$$

where

$$C = \frac{\gamma_1\gamma_{-2} - \gamma_0\gamma_{-1}}{2(\gamma_0\gamma_{-2} - \gamma_{-1}^2)}$$

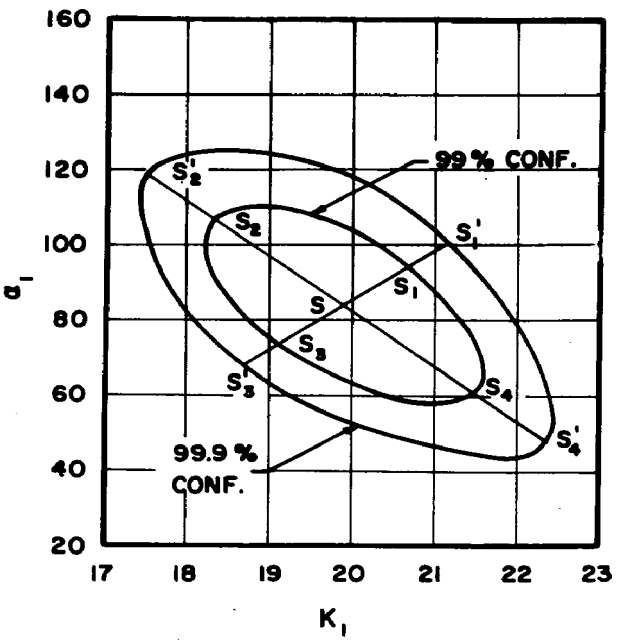
$$D = \frac{\gamma_1\gamma_{-1} - \gamma_0^2}{\gamma_0\gamma_{-2} - \gamma_{-1}^2}$$

For the physical constants of Keepin and Wimett[14], table (7.1), the group constants shown in Table (7.2) were calculated. These group constants lead to values of K_i and α_i in the mathematical model, Equation (7.1), which may be compared with the K_i's and α_i's obtained from the least squares fit to the experimental points.

D. Presentation of Results

Tables (7.3), (7.4) and (7.5) show the comparisons between the experimental results and the theoretical model. Confidence contours as described in Chapter VI are shown for the projections onto the K_1-α_1 and K_2-α_2 planes in Figures (7.6), (7.7) and (7.8) for the three BF_3 tube experiments whose experimental points and fitted curves are shown in Figures (7.1), (7.2) and (7.3) respectively.

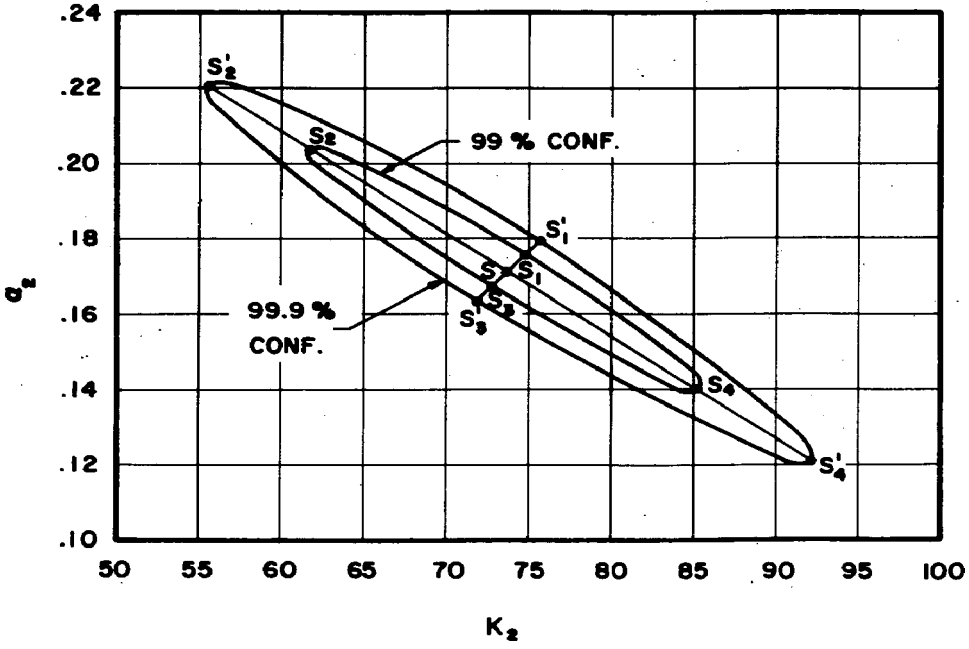
In Tables (7.3), (7.4) and (7.5) the theoretical parameters are shown for two different types of computation. In the first line



Projection on K_1 - α_1 Plane

99%
Contour Sum of Squares
409
Grid Sums of Squares
$S_1 = 408$ $S_2 = 1160$
$S_3 = 410$ $S_4 = 1744$
99.9%
Contour Sum of Squares
459
Grid Sums of Squares
$S_1' = 456$ $S_2' = 4527$
$S_3' = 463$ $S_4' = 10627$

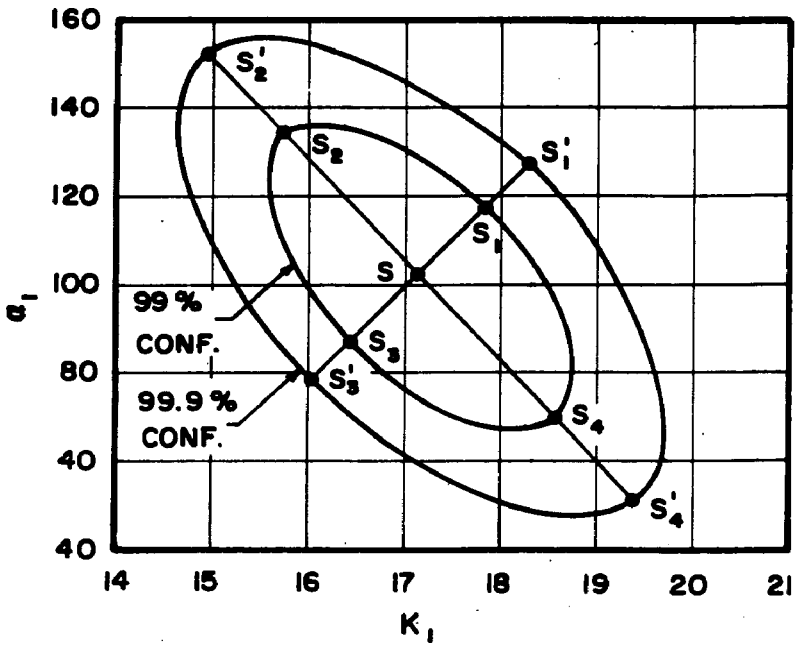
Minimum Sum of Squares
$S = 376$



Projection on K_2 - α_2 Plane

99%
Contour Sum of Squares
409
Grid Sums of Squares
$S_1 = 430$ $S_2 = 409$
$S_3 = 442$ $S_4 = 409$
99.9%
Contour Sum of Squares
459
Grid Sums of Squares
$S_1' = 618$ $S_2' = 460$
$S_3' = 647$ $S_4' = 458$

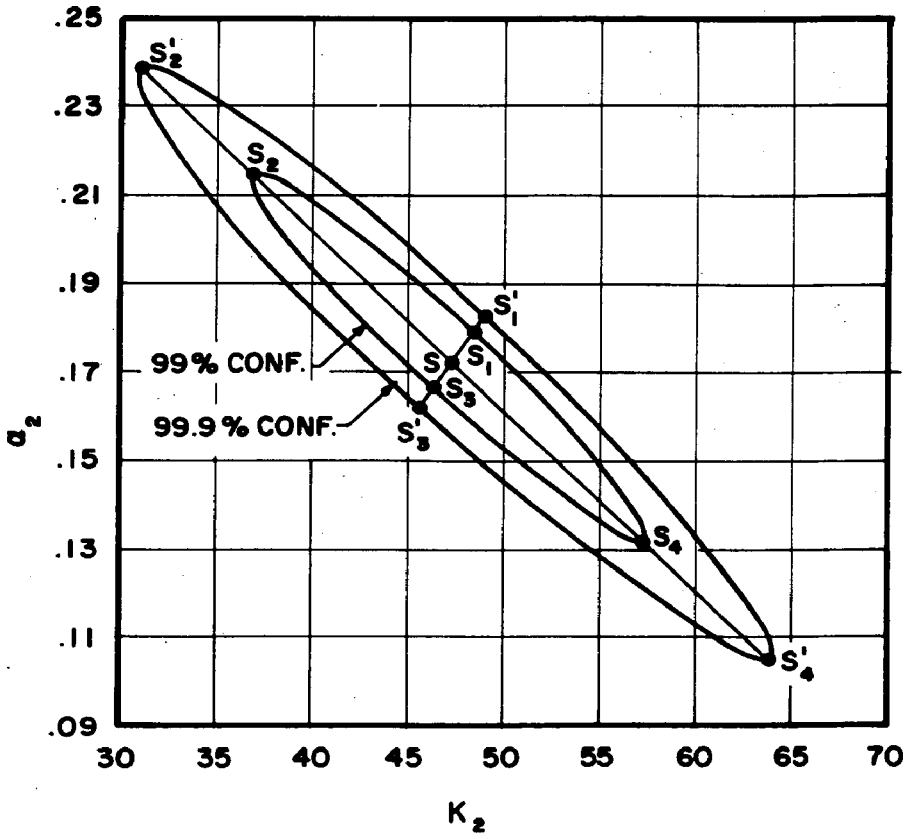
Figure 7.6. Confidence Contours - BF_3 -1



Projection on K_1 - α_1 Plane

99%
Contour Sum of Squares
344
Grid Sums of Squares
$S_1 = 342$ $S_2 = 1157$
$S_3 = 344$ $S_4 = 2135$
99.9%
Contour Sum of Squares
386
Grid Sums of Squares
$S_1' = 383$ $S_2' = 4624$
$S_3' = 391$ $S_4' = 1523$

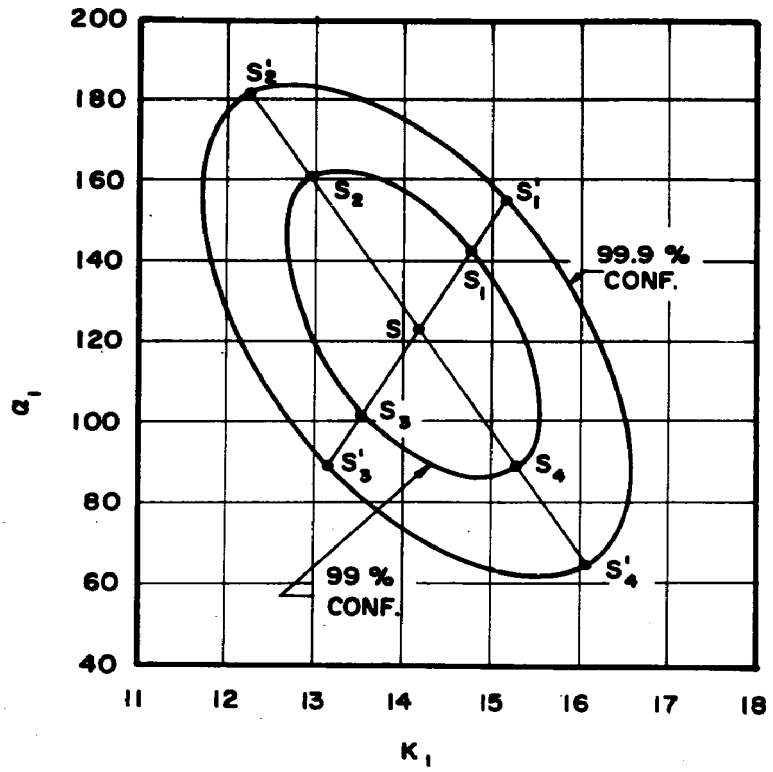
Minimum Sum of Squares
S=315



Projection on K_2 - α_2 Plane

99%
Contour Sum of Squares
344
Grid Sums of Squares
$S_1 = 372$ $S_2 = 344$
$S_3 = 379$ $S_4 = 343$
99.9%
Contour Sum of Squares
386
Grid Sums of Squares
$S_1' = 599$ $S_2' = 387$
$S_3' = 596$ $S_4' = 385$

Figure 7.7 Confidence Contours BF_3-2.



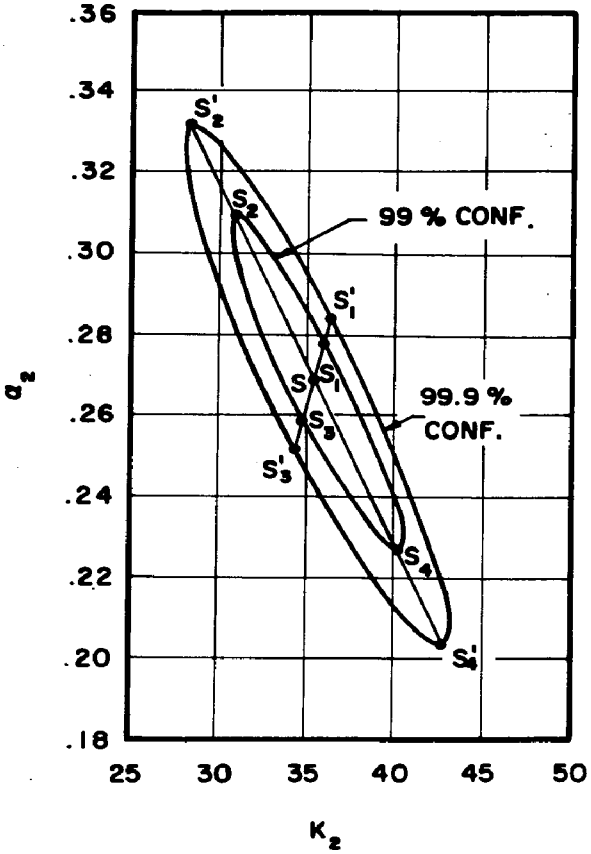
Projection on K_1 - α_1 Plane

99%
Contour Sum of Squares
252
Grid Sums of Squares
S_1 = 251 S_2 = 366
S_3 = 254 S_4 = 482
99.9%
Contour Sum of Squares
283
Grid Sums of Squares

S_1' = 280 S_2' = 881

S_3' = 289 S_4' = 2137

Minimum Sum of Squares S = 231



Projection on K_2 - α_2 Plane

99%
Contour Sum of Squares
252
Grid Sums of Squares
S_1 = 254 S_2 = 252
S_3 = 263 S_4 = 252
99.9%
Contour Sums of Squares
283
Grid Sums of Squares

S_1' = 305 S_2' = 284

S_3' = 344 S_4' = 284

Figure 7 8. Confidence Contours BF_3 -3

TABLE 7.1

PHYSICAL GROUP CONSTANTS (KEEPIN & WIMMETT)

$\lambda_i(sec^{-1})$	β_i	a_i
1.27x10-2	2.47x10-4	.038
3.17x10-2	1.385x10-3	.213
1.15x10-1	1.222x10-3	.188
3.11x10-1	2.646x10-3	.407
1.40	8.32x10-4	.128
3.87	1.69x10-4	.026

TABLE 7.2

REDUCED GROUP CONSTANTS

$\Lambda_i(sec^{-1})$	A_i
0.507	0.663
0.0209	0.337

TABLE 7.3

experiment number	BF_3-1
reactivity	-.172 dollars
detector	BF_3
curve of data and fit	Figure 7.1
minimum sum of squares	376
standard deviation of residuals	2.03
theoretical delay group constants	Table 7.2
mathematical model	Equation (7.1); n=2

PARAMETERS

	K_1	α_1	K_2	α_2	K_3	α_3
theoretical parameters ℓ = 91.6 μ sec	19.92	83.42	96.5	.240	2430	.000126
theoretical parameters ℓ = 80.2 μ sec	19.92	96.3	99	.240	2400	.000126
experimental parameters	19.92	83.91	73.87	.172	> 400	<.002
experimental parameter ranges, 99% confidence	18.3 21.5	60 110	62 86	.138 .204	- -	- -
experimental parameter ranges, 99.9% confidence	17.45 22.4	46 122	55.5 92.5	.120 .223	- -	- -
% diff. expt. and theory ℓ = 91.6 μ sec	0%	0%	23.4%	28.4%	-	-
% diff. expt. and theory ℓ = 80.2 μ sec	0%	13.4%	25.3%	28.4%	-	-

TABLE 7.4

experiment number	BF_3-2
reactivity	-.2400 dollars
detector	BF_3
curve of data and fit	Figure 7.2
minimum sum of squares	315
standard deviation of residuals	1.88
theoretical delay group constants	Table 7.2
mathematical model	Equation(7.1); n = 2

PARAMETERS

	K_1	α_1	K_2	α_2	K_3	α_3
theoretical parameters ℓ = 78.6 μ sec.	17.19	102.76	70.2	.256	1050	.000134
theoretical parameters ℓ = 80.2 μ sec.	17.19	101.9	70.6	.256	1048	.000134
experimental parameters	17.19	102.5	47.19	.173	> 400	< .002
experimental parameter ranges, 99% confidence	15.7 18.7	72 135	37 57	.130 .215	- -	- -
experimental parameter ranges, 99.9% confidence	14.6 19.5	52 154	31.5 64.5	.100 .240	- -	- -
% diff. expt. and theory ℓ = 78.6 μ sec	0%	0%	32.6%	32.4%	-	-
% diff. expt. and theory ℓ = 80.2 μ sec	0%	1%	33.1%	32.4%	-	-

TABLE 7.5

experiment number	BF_3-3
reactivity	-.3400 dollars
detector	BF_3
curve of data and fit	Figure 7.2
minimum sum of squares	231
standard deviation of residuals	1.61
theoretical delay group constants	Table 7.2
mathematical model	Equation (7.1); n = 2

PARAMETERS

	K_1	α_1	K_2	α_2	K_3	α_3
theoretical parameters ℓ = 71.5 μ sec	14.17	122.08	45.7	.277	425	.000148
theoretical parameters ℓ = 80.2 λ sec	14.17	110.1	46.8	.277	409	.000148
experimental parameters	14.17	122.4	35.43	.267	> 400	< .002
experimental parameter ranges, 99% confidence	12.85 15.4	88 161	31 40	.228 .309	- -	- -
experimental parameter ranges, 99.9% confidence	12.15 16.1	64 182	28 43	.203 .332	- -	- -
% diff. expt. and theory ℓ = 71.5 μ sec	0%	0%	22.5%	3.62%	-	-
% diff. expt. and theory ℓ = 80.2 μ sec	0%	9.8%	24.3%	3.62%	-	-

under "parameters" the theoretical parameters were computed by normalizing the value of K_1 to the experimental value and choosing a lifetime, ℓ, which would make α_1 theoretical agree with α_1 experimental. In the second line under "parameters" K_1 was again normalized as above, but the value of α_1 was computed using the average value of prompt lifetime obtained in the experiments.

The material above the "parameter" tables is self-explanatory; it gives reference to the pertinent operating data, experimental data, and statistical data for that experiment.

Note that only qualitative estimates are shown for parameters K_3 and α_3. Note also that no confidence is stated for these estimates. The reason for this becomes apparent by looking at the contribution of the third term to the total V/M curve. Since the contribution of these terms is small, no significant estimates of the parameters could be made. The only conclusion that could be made was that the contribution of this term was only at long times, and the contribution was not large. The parameters governing this third term could be estimated if data was taken for gate times longer than ten seconds.

E. Theory vs. Experiment

The pertinent points concerning the comparison of the model with experimental results can be obtained from the tables and figures mentioned in the previous section.

It is apparent that experiment and theory agree in a qualitative way. However, we see that the model and the experiment may differ by as much as 30% in some parameters and that the differences appear to be more severe in experiments BF_3-1 and BF_3-2 than in BF_3-3.

The reasons for the disagreements observed could be either that more experimental errors occur as the multiplication of the reactor is increased or that the model is less accurate as the multiplication is increased or both. It can be argued that "both" is the correct statement.

1. Experimental Errors

As multiplication increases the $\frac{V}{M}$ ratio increases (Figure 7.5). It is also true that as $\frac{V}{M}$ increases the variance of $\frac{V}{M}$ increases so that to get results with the same certainty at large $\frac{V}{M}$ as those with smaller $\frac{V}{M}$ we need more data. In the experiments shown the amount of data per experiment is constant so we would expect less experimental accuracy for large multiplication.

2. Model Inaccuracies

It has already been observed that the effects of prompt neutrons and delayed neutrons become less distinguishable as criticality is approached. Indeed, the model predicts $\frac{V}{M} \rightarrow \infty$ for all gate times, τ, when $\Delta K \rightarrow 0$. Obviously, if ΔK is very close to zero and $\frac{V}{M}$ is very large everywhere the estimation of individual parameters would be nearly impossible since many possible combinations of parameters would yield the same result. Thus, we expect that the estimation of parameters becomes less accurate as criticality is approached.

It is also true that the model is only a point reactor model and it is suspected that spatial effects become more important as criticality is approached. The reason for this hypothesis is that a larger portion of the events detected are correlated events as the reactor approaches criticality. Correlated events arise from common fissions

(Chapter III) which are spatially distributed in the core. It is apparent that the spatial distribution of the ancestors of accidental events is unimportant since no matter where they originate they are defined to be uncoupled events and give rise to a $\frac{V}{M}$ of 1. It is not at all apparent, however, that the effect of correlated events is independent of the location of the common ancestor fissions. In fact, it is most likely that the spatial distribution of ancestors will make itself felt in the shape of the $\frac{V}{M}$ curve for correlated events. So, since we have more correlation at higher multiplication we might expect stronger spatial effects and thus larger inaccuracies in the point reactor model.

VIII CONCLUSIONS

A. Introduction

Some of the conclusions which may be drawn from the preceding are in disagreement with conclusions made by other investigators in this area. In this section some of the points of agreement and disagreement will be discussed and resolved.

Other conclusions arise from the work reported here and have not been discussed by other authors. These conclusions will be discussed here along with the possible relevance of this experiment to future experiments in this field.

B. Comparison of Conclusions with Preceding Authors

Bennett[1], having derived essentially the same mathematical model that is used here, plotted the model as a function of prompt neutron lifetime. This plot illustrated the effect of delayed neutrons on the shape of the curve. Bennett pointed out that one cannot use the measurement of variance to mean ratio to infer the prompt neutron lifetime of a reactor without taking into account the effect of the delayed neutrons. This measurement supports the above conclusion. It is not in general possible to measure the term controlled by prompt neutrons without also having some contribution from delayed neutrons. Other authors have used prompt neutron theories to find prompt neutron lifetimes by this method without taking delayed neutrons into account.[8,11,16] Obviously their measurements are in error by an amount controlled by the delayed neutron contribution. For reactors with very short lifetimes, one may be able to neglect delayed neutrons with only small errors occurring.

Velez[24] concludes that "theoretical derivation and experimental measurement of the correlation functions can be two independent lines of research, but regarding applications, in the author's opinion, the most urgent need is for experiments to check the formulas already obtained".

The research presented here has been directed toward fulfilling part of this urgent need. With respect to the equations derived by Velez, the work done here has revealed some important information.

1) In the derivation of the autocorrelation function Velez introduced the term "mean time to fission" and defined N_1 as the expected number of neutrons in the system at time t_1 from one ancestor neutron at t. This definition would be satisfactory so long as there is only one class of neutrons (prompt neutrons for example). However, the proper way to define terms in the case where delayed neutrons are important is to include a characteristic time in each group by defining N_1 to be a frequency function as was done here.

Velez's formulation leads to a discrepancy with experiment of a factor of 10^{10} at long gate times using the six delayed group model.

2) Velez illustrates the relative magnitudes of the prompt and delayed terms using a lumped one-group model. This work shows that the one lumped delay group model is quite grossly inaccurate in predicting the results.

Luckow[16] made measurements of the variance to mean ratio for gate times ≤ 1 sec in ZPR IV and ZPR V at Argonne National Laboratory. Data points which did not follow the prompt neutron model were termed "wild points" and the following comment was made concerning them. "These

points have the disconcerting feature of not appearing in every series. Any physical explanation is therefore open to question. ...It is thought that these wild values reflect the contributions of the delayed neutrons for long measuring (not gate) times."

The measurement discussed in this document shows clearly that the "wild points" observed by Luckow were contributions of delayed neutrons. However, the contributions were for long gate times and not measuring times as Luckow suggested. Also, a physical explanation is not very open to question since Luckow's data shows that more "wild points" were seen for experiments performed closer to critical. Using parameters characteristic of ZPR IV and ZPR V it can be shown that the model used here predicts that the delayed neutron effect should be less significant as multiplication is reduced. Thus, the model which includes delayed neutrons is in agreement with Luckow's experiment.

C. Independent Conclusions

This work has corroborated a point reactor mathematical model describing the experimentally observable stochastic processes in nuclear reactors in measurements in which delayed neutrons are important. In Chapter VII comparisons between the model and the experimental results are made which lead to the conclusion that the two-delayed group model is more accurate for more sub-critical situations.

It has been demonstrated that the use of a tape recorder to simulate reactor fluctuations is a desirable alternative to either prolonged reactor operation or a more sophisticated measuring system.

It has been shown that the contributions to the measured variance to mean ratio from all physical delay groups can not be determined by this type of measurement unless a great deal more data is taken.

This experiment has demonstrated the feasibility of measuring nuclear reactor dynamic parameters by stochastic process techniques. The prompt neutron lifetime of the Ford reactor was found to be $80 \pm 10\mu$ sec.

D. Relevance to Future Experiments

In order to significantly extend the amount of information which the experiment will yield it is necessary to have a considerably more sophisticated data taking technique. The extension of the data taking technique to a system with shorter resolving time could be accomplished by using a video tape recorder instead of the audio tape recorder used here. The resolving time of the scaler and other circuitry would also have to be improved, but the tape recorder is the most critical since it is the limiting piece of equipment in the present set-up. Obviously a shorter resolving time leads to higher permissible count rates and better statistics.

A many channel recording and transcription system would also lead to improved measurements.

In order to analyze data at times greater than 10 seconds it would be advisable to eliminate the operation of punching data on IBM cards and arrange for the tape recorded information to be entered into a computer directly.

Future experiments may well be directed at many of the problems raised by this experiment.

One line of investigation would be to refine the measurements in the delayed neutron region and achieve more accurate comparison between the model and the experiment.

Another direction which may be profitable is to investigate further the effect of reactivity on the comparison between theory and experiment. Perhaps further information concerning this phenomenon would yield information which would be valuable in improving the description of the process.

Spatial effects are open for investigation both theoretically and experimentally as are energy dependencies.

Both theoretical and experimental investigation of the assumed white noise source used in the model could be pursued.

APPENDIX A

DATA

Fission Chamber

Number Of Gates	Variance	Mean	Variance/Mean -1	Gate Length (sec)
600	2.3247	2.2567	0.030	.001
600	5.9086	4.7850	0.235	.002
600	8.4899	7.3150	0.161	.003
600	11.394	9.2317	0.234	.004
600	11.565	11.565	0.000	.005
600	16.598	13.892	0.195	.006
600	20.470	16.083	0.273	.007
600	23.138	18.643	0.241	.008
600	31.363	23.195	0.352	.010
588	41.420	30.034	0.379	.013
600	54.768	38.732	0.414	.017
600	68.784	45.778	0.502	.020
576	72.496	53.365	0.358	.023
600	95.633	57.108	0.675	.025
600	93.338	61.685	0.513	.027
600	96.543	68.802	0.403	.030
600	131.22	80.762	0.625	.035
600	139.63	92.320	0.512	.040
588	160.59	103.16	0.557	.045
600	178.61	113.66	0.572	.050
600	224.17	137.38	0.632	.060
600	280.58	159.85	0.755	.070
600	337.13	184.04	0.832	.080
600	397.81	208.40	0.909	.090
600	387.60	229.07	0.692	.100
600	442.82	252.88	0.751	.110
576	540.12	277.30	0.948	.120
600	531.26	300.37	0.769	.130
600	564.63	321.21	0.758	.140
600	697.94	368.67	0.893	.160
600	862.78	414.25	1.083	.180
600	956.48	460.29	1.078	.200
600	1055.10	506.34	1.084	.220
600	1158.30	566.48	1.047	.250
600	1264.80	620.76	1.038	.270
600	1682.80	684.72	1.458	.300
600	1821.00	716.43	1.542	.310
516	1441.10	760.43	0.895	.330
552	1815.70	831.36	1.184	.360
600	1574.70	895.84	0.758	.390
600	1803.50	969.41	0.860	.420
600	2330.80	1059.40	1.200	.460
600	2371.00	1145.60	1.070	.500
600	2573.60	1265.70	1.033	.550
600	2967.00	1367.30	1.170	.600

Number Of Gates	Variance	Mean	Variance/Mean -1	Gate Length (sec)
600	3134.6	1497.7	1.093	.650
600	3147.1	1602.6	0.964	.700
600	3510.8	1732.9	1.026	.750
600	3910.3	1830.2	1.136	.800
600	4466.5	2052.3	1.176	.900
600	4684.0	2282.8	1.052	1.000
600	5598.9	2531.8	1.211	1.100
600	5752.6	2745.4	1.095	1.200
600	6078.8	2991.9	1.032	1.300
588	6657.0	3223.3	1.065	1.400
600	7508.6	3423.3	1.193	1.500
600	8532.4	3685.9	1.315	1.600
600	9173.6	3877.6	1.366	1.700
600	9350.8	4114.0	1.273	1.800
588	9735.8	4370.9	1.227	1.900
600	10271.	4561.1	1.252	2.000
552	10516.	4832.4	1.176	2.100
600	12287.	5068.7	1.424	2.200
504	13206.	5285.3	1.499	2.300
600	14280.	5525.3	1.584	2.400
540	13488.	5742.8	1.349	2.500
600	15620.	5987.8	1.609	2.600
588	15788.	6210.7	1.542	2.700
600	15015.	6447.3	1.329	2.800
576	16852.	6664.6	1.529	2.900
600	17102.	6842.6	1.499	3.000
588	18199.	7129.3	1.553	3.100
600	19672.	7362.2	1.621	3.200
576	21599.	8064.7	1.678	3.500
552	23196.	8743.9	1.653	3.800
420	27044.	9436.2	1.866	4.100
432	29551.	10359.0	1.853	4.500
420	36993.	12208.0	2.030	5.300
384	40839.	13127.0	2.111	5.700
432	48433.	14278.0	2.392	6.200
408	46535.	15409.0	2.020	6.700
324	54427.	16581.0	2.282	7.200
336	61749.	17715.0	2.486	7.700
300	69394.	19333.0	2.589	8.400
288	77055.	20947.0	2.678	9.100
324	86785.	22995.0	2.774	9.999

BF_3 -1

Number Of Gates	Variance	Mean	Variance/Mean -1	Gate Length (sec)
588	4.9011	2.5068	0.955	.001
600	12.533	4.8883	1.564	.002
600	45.120	10.147	3.447	.004
600	86.058	14.825	4.805	.006
600	134.77	19.715	5.836	.008
600	189.67	24.022	6.896	.010
600	301.96	34.132	7.847	.014
600	480.88	43.310	10.10	.018
600	659.67	53.867	11.25	.022
588	760.84	66.364	10.46	.028
600	1389.1	87.670	14.84	.035
576	1508.6	105.87	13.25	.043
600	2169.0	125.06	16.34	.051
588	2353.2	146.44	15.07	.060
576	3253.3	176.28	17.46	.071
600	4418.0	211.80	19.86	.085
564	4869.8	239.17	19.36	.100
588	5473.2	295.09	17.55	.120
600	8091.3	366.82	21.06	.150
588	9093.4	441.59	19.59	.180
588	10367.	507.79	19.42	.210
600	12206.	577.50	20.14	.240
600	15013.	663.22	21.64	.270
600	15568.	727.82	20.39	.300
588	18786.	854.58	20.98	.350
600	22247.	971.07	21.91	.400
588	23901.	1104.2	20.65	.450
600	28821.	1217.9	22.67	.500
600	32336	1386.6	22.32	.570
600	36428.	1580.5	22.05	.650
600	43152.	1769.7	23.38	.730
600	57275.	2009.5	27.50	.820
600	57696.	2219.0	25.00	.910
588	65869.	2452.9	25.85	1.000
600	75979.	2701.2	27.13	1.100
600	79018.	2948.9	25.80	1.200
600	87347.	3181.0	26.46	1.300
600	103392.	3443.4	29.02	1.400
588	113116.	3686.2	29.69	1.500
600	129516.	3935.3	31.91	1.600
588	126016.	4165.6	29.25	1.700
600	138212.	4419.1	30.28	1.800
600	144516.	4648.9	30.09	1.900
588	157357.	4919.4	30.99	2.000
600	162904.	5184.1	30.42	2.100
600	163083.	5415.2	29.12	2.200
600	173056	5655.9	29.60	2.300
516	188159.	5912.2	30.83	2.400
564	201228.	6131.8	31.82	2.500
600	239031.	6381.5	36.46	2.600
600	308080.	6643.4	45.37	2.700
600	243236.	6887.1	34.32	2.800

Number Of Gates	Variance	Mean	Variance/Mean -1	Gate Length (sec)
600	256914.	7116.5	35.10	2.900
564	263306.	7328.8	34.93	3.000
552	255058.	7597.4	32.57	3.100
540	308993.	7854.2	38.34	3.200
504	288741.	8081.4	34.73	3.300
528	302654.	8372.8	35.15	3.400
516	348975.	8594.0	39.61	3.500
516	411817.	8909.1	45.22	3.600
468	360856.	9120.0	38.57	3.700
504	392816.	9335.3	41.08	3.800
528	406665.	9616.5	41.29	3.900
468	420116.	9883.0	41.51	4.000
492	423017.	10089.	40.93	4.100
492	414984.	10322.	39.21	4.200
468	461338.	10542.	42.77	4.300
432	474295.	10880.	42.59	4.400
468	448443.	11089.	39.44	4.500
480	477901.	11300.	41.29	4.600
456	472160.	11547.	39.89	4.700
444	521301.	11767.	43.30	4.800
444	523476.	12038.	42.48	4.900
456	542311.	12288.	43.13	5.000
408	569815.	12540.	44.44	5.100
432	572401.	12760.	43.86	5.200
420	620139.	13042.	46.55	5.300
396	633293.	13265.	46.74	5.400
396	632115.	13562.	45.61	5.500
396	664113.	13783.	47.18	5.610
384	708852.	14070.	49.38	5.730
372	742006.	14437.	50.40	5.860
372	743248.	14720.	49.49	6.000
372	726245.	15123.	47.02	6.150
360	804746.	15500.	50.91	6.310
348	812204.	15889.	50.11	6.480
336	779075.	16363.	46.61	6.660
336	831676.	16815.	48.46	6.850
324	878255.	17322.	49.70	7.050
312	949975.	17908.	52.05	7.300
312	978582.	18682.	51.38	7.600
288	1028044.	19515.	51.68	7.950
288	1105216.	20494.	52.93	8.350
276	1254602.	21606.	57.07	8.800
264	1377585.	22853.	59.38	9.300
228	1447419.	24506.	58.06	9.999

BF_3-2

Number Of Gates	Variance	Mean	Variance/Mean -1	Gate Length (sec)
600	3.3148	1.7900	0.852	.001
600	10.611	3.7167	1.855	.002
600	34.793	7.3083	3.573	.004
600	55.046	10.548	4.218	.006
588	89.388	13.995	5.387	.008
600	137.06	18.288	6.494	.010
600	242.75	24.138	9.057	.014
588	436.58	38.660	10.298	.022
576	683.82	50.384	12.57	.028
396	747.29	61.192	11.21	.035
600	1129.2	75.733	13.91	.043
588	1295.8	91.535	13.16	.051
564	1845.1	109.99	15.77	.060
600	1850.5	128.23	13.43	.071
600	2400.6	150.22	14.98	.085
600	2944.6	176.70	15.66	.100
600	3806.3	212.31	16.93	.120
600	4452.4	269.86	15.50	.150
600	5213.0	315.02	15.55	.180
600	6952.6	374.90	17.55	.210
600	7377.5	417.20	16.68	.240
600	9263.8	486.55	18.04	.270
600	10304.	534.98	18.26	.300
600	13573.	620.16	20.89	.350
588	15655.	715.36	20.88	.400
600	17004.	802.08	20.20	.450
600	19195.	889.00	20.59	.500
600	20660.	1015.6	19.34	.570
552	25468.	1170.0	20.77	.650
564	23948.	1289.7	17.57	.730
600	31296.	1458.1	20.46	.820
600	39549.	1785.1	21.16	1.000
600	43228.	1961.0	21.04	1.100
600	46434.	2136.6	20.73	1.200
600	53864.	2300.7	22.41	1.300
600	60738.	2486.2	23.43	1.400
600	59089.	2678.1	21.06	1.500
600	69003.	2860.2	23.12	1.600
600	73716.	3027.4	23.35	1.700
600	80749.	3215.2	24.11	1.800
576	84476.	3398.5	23.86	1.900
576	89383.	3557.1	24.13	2.000
540	93176.	3739.9	23.91	2.100
576	93526.	3910.9	22.91	2.200
540	102877.	4105.0	24.06	2.300
564	109487.	4281.4	24.57	2.400
600	114406.	4441.4	24.76	2.500
600	112030.	4636.9	23.16	2.600
600	125097.	4814.9	24.98	2.700
576	135841.	4977.3	26.29	2.800

Number Of Gates	Variance	Mean	Variance/Mean -1	Gate Length (sec)
564	142163.	5159.3	26.56	2.900
564	149663.	5334.4	27.06	3.000
600	187881.	5545.8	32.88	3.100
600	162620.	5701.3	27.52	3.200
600	166985	5880.9	27.39	3.300
588	165495.	6073.0	26.25	3.400
576	176659.	6228.8	27.36	3.500
564	200534.	6410.9	30.28	3.600
564	216027.	6580.8	31.83	3.700
552	208740.	6768.8	29.84	3.800
528	242743.	6963.9	33.86	3.900
528	206264.	7106.8	28.02	4.000
468	292097.	7300.5	39.01	4.100
480	234248.	7475.3	30.34	4.200
444	234228.	7637.7	29.67	4.300
420	228560.	7841.9	28.15	4.400
408	260018.	8017.4	31.43	4.500
468	254538.	8179.5	30.12	4.600
432	279849.	8382.9	32.38	4.700
444	266729.	8537.3	30.24	4.800
408	290489.	8719.4	32.32	4.900
420	331803.	8929.3	36.16	5.000
444	320039.	9084.5	34.23	5.100
420	320904.	9272.0	33.61	5.200
420	303987.	9450.0	31.17	5.300
408	341436.	9633.4	34.44	5.400
384	356519.	9806.0	35.36	5.500
360	351485.	9976.6	34.23	5.610
360	341815.	10191.0	32.54	5.730
384	349885.	10445.0	32.50	5.860
324	421929.	10678.0	38.51	6.000
348	410246.	11253.0	35.46	6.310
348	436353.	11552.0	36.77	6.480
336	452038.	11864.0	37.10	6.660
336	469225.	12200.0	37.46	6.850
324	459810.	12563.0	35.60	7.050
324	497646.	13003.0	37.27	7.300
300	529836.	13548.0	38.11	7.600
288	574739.	14175.0	39.55	7.950
264	611611.	14903.0	40.05	8.350
264	668707.	15682.0	41.64	8.800
252	741850.	16583.0	43.73	9.300
228	658282.	17794.0	35.99	9.999

BF_3-3

Number Of Gates	Variance	Mean	Variance/Mean -1	Gate Length (sec)
600	44.2748	2.1750	0.965	.001
600	10.543	4.0817	1.583	.002
600	29.470	8.5467	2.448	.004
588	59.195	13.162	3.498	.006
600	95.520	16.978	4.636	.008
600	141.10	21.083	5.693	.010
600	277.09	30.397	8.116	.014
600	365.18	38.120	8.578	.018
600	506.71	46.545	9.886	.022
600	718.80	61.168	10.75	.028
600	897.33	73.052	11.28	.035
600	1233.2	90.205	12.67	.043
600	1224.4	105.89	10.56	.051
588	1852.5	127.76	13.50	.060
600	2216.6	147.68	14.01	.071
600	2458.9	175.81	12.99	.085
600	2879.9	211.21	21.64	.100
600	3416.8	254.22	12.44	.120
600	4486.9	319.33	13.05	.150
600	5707.2	374.30	14.25	.180
600	7224.4	444.05	15.27	.210
600	7557.7	506.87	13.91	.240
576	8554.0	565.98	14.11	.270
576	9603.9	633.73	14.15	.300
588	12416.	733.43	15.93	.350
600	16240.	845.53	18.21	.400
600	16126.	949.06	15.99	.450
600	18782.	1052.1	16.85	.500
600	21144.	1206.6	16.52	.570
600	25991.	1359.8	18.11	.650
564	27626.	1536.9	16.98	.730
588	32119.	1723.9	17.63	.820
600	39106.	2104.6	17.58	1.000
600	45314.	2313.3	18.59	1.100
600	47028.	2521.2	17.65	1.200
600	57538.	2741.5	19.99	1.300
588	63610.	2940.1	20.64	1.400
600	69048.	3163.7	20.83	1.500
600	80198.	3565.6	21.49	1.700
600	87746.	3788.7	22.16	1.800
600	94826.	3999.1	22.71	1.900
588	99989.	4205.8	22.77	2.000
600	101119.	4417.3	21.89	2.100
564	99918.	4620.4	20.63	2.200
564	120631.	4848.5	23.88	2.300
600	125558.	5044.3	23.89	2.400
600	133882.	5270.8	24.40	2.500
600	146853.	5470.0	25.85	2.600
600	140980.	5698.8	23.74	2.700
600	143798.	5888.8	23.42	2.800

Number Of Gates	Variance	Mean	Variance/Mean -1	Gate Length (sec)
600	169132.	6081.5	26.81	2.900
564	162910.	6326.5	24.75	3.000
600	161667.	6526.4	23.77	3.100
600	173704.	6727.0	24.82	3.200
564	180121.	6958.2	24.89	3.300
552	187628.	7154.7	25.22	3.400
516	197352.	7363.6	25.80	3.500
540	192995.	7583.1	24.45	3.600
528	224183.	7773.6	27.84	3.700
468	210592.	8015.8	25.27	3.800
456	236398.	8212.2	27.79	3.900
480	237680.	8618.1	26.58	4.100
444	248552.	8848.0	27.09	4.200
456	272048.	9072.6	28.99	4.300
468	269963.	9281.9	28.08	4.400
480	288333.	9475.7	29.43	4.500
456	353850.	9729.8	35.37	4.600
432	332909.	9933.0	32.52	4.700
420	382351.	10151.0	36.67	4.800
456	303159.	10314.0	28.39	4.900
432	305533.	10532.0	28.01	5.000
432	358595.	10757.0	32.34	5.100
408	334156.	10948.0	29.52	5.200
420	350528.	11153.0	30.43	5.300
420	327887.	11349.0	27.89	5.400
396	372725.	11580.0	31.19	5.500
384	354685.	11803.0	29.05	5.610
396	359175.	12060.0	28.78	5.730
372	402668.	12332.0	31.65	5.860
384	433353.	12624.0	33.33	6.000
372	440865.	12940.0	33.07	6.150
360	436544.	13289.0	31.85	6.310
360	449541.	13631.0	31.98	6.480
312	505731.	14000.0	35.12	6.660
324	461988.	14412.0	31.05	6.850
324	494748.	14836.0	32.35	7.050
324	589045.	15380.0	37.30	7.300
312	542913.	15950.0	33.04	7.600
300	609144.	16758.0	35.35	7.950
288	641285.	17575.0	35.49	8.350
276	727448.	18513.0	38.29	8.800
264	703853.	19592.0	34.93	9.300
252	795052.	21055.0	36.76	9.999

APPENDIX B

CONTROL ROD CALIBRATION

Pos. No.	Position Rod A"	Position Rod B"	Position Rod C"	Position CR Initial "	Position CR Final "	Period T sec.	Reactivity	Position Increment		Average Position
1	13 83	13.62	13.98	35-7/16	30-3/16	189.5 sec	4.41×10^{-4}	5-1/4	$.84 \times 10^{-4}$	32-15/16
2	13.68	13.64	14.60	32-13/16	27-27/64	138.5	5.745×10^{-4}	4-63/64	1.15×10^{-4}	29-29/32
3	14.05	14.05	13.95	30-3/4	26-17/64	162.	5.042×10^{-4}	4-31/64	1.13×10^{-4}	28-1/2
4	14.19	14.09	14.25	28-7/8	23-7/16	87.3	8.28×10^{-4}	5-7/16	1.53×10^{-4}	26-1/8
5	14.43	14.38	14.39	25-15/32	21-5/8	123.	6.33×10^{-4}	3-27/32	1.645×10^{-4}	23-35/64
6	14.38	14.85	14.44	23-27/64	19-9/32	125.	6.247×10^{-4}	4-9/64	1.510×10^{-4}	21-11/32
7	14.90	14.11	15.10	22-3/16	16-15/16	127.	6.17×10^{-4}	5-1/4	1.175×10^{-4}	19-9/16
8	14.90	14.81	14.95	18-15/16	12	188.	4.44×10^{-4}	6-15/16	$.64 \times 10^{-4}$	15-15/32

BIBLIOGRAPHY

1. Bennett, E. F. "The Rice Formulation of Pile Noise," Nuclear Science and Engineering, 8, (1960) 53.

2. Box, G. E. P. Some Notes on Non-linear Estimation, Princeton-IBM Mathematics and Applications Department, (1956).

3. Box, G. E. P. Use of Statistical Methods in the Elucidation of Basic Mechanisms, Statistical Techniques Research Group Report No. 7, Princeton-IBM Mathematics and Applications Department, October, 1957.

4. Box, G. E. P. and Lucas, H. L. Design of Experiments in Non-linear Situation, Statistical Techniques Research Group Report No. 15, Princeton-IBM Mathematics and Applications Department, June, 1958.

5. Box, G. E. P. and Coutie, G. A. Application of Digital Computers in the Exploration of Functional Relationships, Amer. Inst. Electr. Engrs., Proc., 103 B Suppl. No. 1, (1956) 100-107.

6. Box, G. E. P. Forecasting by Generalized Regression Methods, Princeton-IBM Mathematics and Applications Department, June, 1959.

7. Brownrigg, W. G. L. and Littler, D. J. "Pile Modulation and Statistical Fluctuation in Piles," AERE N/R 476, Harwell, 1950.

8. Cohn, C. E. Determination of Reactor Kinetic Parameters by Pile Noise Analysis, Nuclear Science and Engineering, 5, (1959) 331.

9. Courant, E. D. and Wallace, P. R. "Fluctuations of the Number of Neutrons in a Pile," Phys. Rev., 72, (1947) 1038.

10. Feiner, F., Frost, R. T., and Hurwitz, H., Pile Oscillator Techniques and Error Analysis of Oscillator Measurements, KAPL 1703, 1956.

11. Feynman, R. P., DeHoffman, F., and Serber, R. "Dispersion of Neutron Emission in U-235 Fission, J. Nuclear Energy, 3, (1956) 64.

12. Frisch, O. R., and Littler, D. J. "Pile Modulation and Statistical Fluctuations in Piles," Phil. Mag., 45 (1949) 360.

13. Harris, D. R. The Sampling Estimate of the Parameter Variance/Mean in Reactor Fluctuation Measurements, WAPD-TM-157 (1958).

14. Keepin, G. R., Wimett, T. F., and Zeigler, Delayed Neutrons from Fissionable Isotopes of Uranium, Plutonium, and Thorium, Report LA-2118 (1957).

15. Laning, J. H., and Battin, R. H. Random Processes in Automatic Control, New York: McGraw-Hill, 1956.

16. Luckow, W. K. "The Evaluation of Nuclear Reactor Parameters from Measurements of Neutron Statistics," University of Michigan, Industry Program. IP-270 (1958).

17. Moore, M. N. On the Determination of Reactor Transfer Functions from Measurements at Steady Operation, Nuclear Sci. and Eng. 3, (1958) 387.

18. Moore, M. N. Reactor Transfer Functions: Addendum, Nuclear Sci. and Engineering, 4, (1958) 134.

19. Moore, M. N. The Power Noise Transfer Function of a Reactor, Nuclear Sci. and Engineering, 6, (1959) 448.

20. Newton, C. C., Gould, L. A. and Kaiser, J. F. Analytical Design of Linear Feedback Controls, New York: John Wiley and Sons (1957).

21. Skinner, R. E., and Cohen, E. R. "Reduced Delayed Neutron Group Representations, Nuclear Sci. and Eng., 5, (1959) 291.

22. Skinner, R. E., and Hetrick, D. L. "The Transfer Function of a Water Boiler Reactor", Nuclear Sci. and Eng. 3, (1958) 573.

23. Velez, C. Autocorrelation Functions of Counting Rate in Nuclear Reactors and Their Application to the Design of Reactor Control Instrumentation, Thesis, Univ. of Mich., (1959).

24. Velez, C. Autocorrelation Functions of Counting Rate in Nuclear Reactors, Nuclear Sci. and Eng. 6, (1959) 414.